# IMAGING MASS SPECTROMETRY

**Liam A. McDonnell* and Ron M.A. Heeren***
*FOM Institute for Atomic and Molecular Physics, Kruislaan 407, 1098 SJ, Amsterdam, The Netherlands*

*Received 14 July 2006; received (revised) 11 October 2006; accepted 12 October 2006*

*Published online 30 April 2007 in Wiley InterScience (www.interscience.wiley.com) DOI 10.1002/mas.20124*

*Imaging mass spectrometry combines the chemical specificity and parallel detection of mass spectrometry with microscopic imaging capabilities. The ability to simultaneously obtain images from all analytes detected, from atomic to macromolecular ions, allows the analyst to probe the chemical organization of a sample and to correlate this with physical features. The sensitivity of the ionization step, sample preparation, the spatial resolution, and the speed of the technique are all important parameters that affect the type of information obtained. Recently, significant progress has been made in each of these steps for both secondary ion mass spectrometry (SIMS) and matrix-assisted laser desorption/ionization (MALDI) imaging of biological samples. Examples demonstrating localization of proteins in tumors, a reduction of lamellar phospholipids in the region binding two single celled organisms, and sub-cellular distributions of several biomolecules have all contributed to an increasing upsurge in interest in imaging mass spectrometry. Here we review many of the instrumental developments and methodological approaches responsible for this increased interest, compare and contrast the information provided by SIMS and MALDI imaging, and discuss future possibilities.* © 2007 Wiley Periodicals, Inc., Mass Spec Rev 26:606–643, 2007

**Keywords:** *imaging; SIMS; MALDI; review; imaging mass spectrometry*

## I. INTRODUCTION

It is often said that a picture can say a thousand words; an imaging mass spectrometry data set, containing a picture for each of the hundreds of detected analytes, can be considered an exhibition, with each picture addressing the same subject from a different perspective. The chemical specificity of mass spectrometry; the parallel detection of multiple analytes that allows spatial correlations to be readily recognized; the ability to record the spatial distributions of a wide range of atoms and molecules, including pharmaceuticals, lipids, peptides, proteins, metabolites, and polymers; the ability to perform these analyses on native samples without the requirement of labels; the cross-correlation of these results with images from other analytical techniques; and the continuing improvements in all these aspects are responsible for the ever increasing interest in imaging mass spectrometry. Most commercial vendors now offer imaging capabilities.

The advent of the ionization techniques electrospray ionization (ESI), (Fenn et al., 1989), and matrix-assisted laser desorption/ionization (MALDI) (Karas et al., 1987), as well as high performance time-of-flight (ToF) mass spectrometers (Weickhardt, Moritz, & Grotemeyer, 1996; Guilhaus, Mlynski, & Selby, 1997) combined to permit biomolecules and other macromolecules to be analyzed with high sensitivity and specificity. Today, mass spectrometry-based proteomics is a universal technique for analyzing complex protein samples (Aebersold & Mann, 2003). It is used to identify proteins separated by a wide range of separation techniques including 2-D gel, liquid chromatography, capillary electrophoresis, capillary-isoelectric focusing, molecular scanner gels (Binz et al., 1999; Smith, 2000; Bergquist et al., 2002; Aebersold & Mann, 2003; Manabe, 2003; Loo et al., 2005); to locate and identify post-translational modifications and mutations (Kelleher et al., 1999; Sze et al., 2002; Aebersold & Mann, 2003; Forbes et al., 2004; Kiernan et al., 2004); to investigate protein interactions (Loo, 1997; Heck & van den Heuvel, 2004; Hofstadler, Sannes-Lowery, & Hannis, 2005; Videler et al., 2005); and to quantify protein expressions (Paša-Tolić et al., 1999; Aebersold & Mann, 2003; Nedelkov et al., 2004; Nelson et al., 2004). The 2002 Nobel Prize in chemistry, partly awarded to John Fenn and Koichi Tanaka, recognized the impact of mass spectrometry in modern biological sciences.

Mass spectrometry-based proteomics is applied following isolation of the proteins from cell lysates or tissue samples by biochemical fractionation or affinity selection (Aebersold & Mann, 2003). Different samples and sample preparation procedures have been exploited to apply these techniques to a plethora of biological and pathological problems (Bergquist et al., 2002; Dreger, 2003). Peptides and proteins are the principal actuators in the complex networks present in all living systems. These highly complex networks involve a vast array of mechanisms to ensure good health (Hanahan & Weinberg, 2000): multiple feedback mechanisms ensure proper regulation, the detection and repair of damaged DNA, apoptosis (highly ordered and controlled cell death) prevents malfunctioning cells from adversely affecting the larger system, and the duplication mechanism uses telomeres to prevent uncontrolled growth. All of this cellular machinery uses changes in expression levels, post-translational modifications, ligand- and ion-binding, and proteolytic processing. Furthermore, proteolytic processing and post-translational modifications enable a single protein to participate in many different processes or regulating cycles. For example, these allow the proopiomelanocortin (POMC) precursor protein

Contract grant sponsor: Nederlandse organisatie voor Wetenschappelijk Onderzoek (NWO).

**Correspondence to:* Liam A. McDonnell or Ron M.A. Heeren, FOM Institute for Atomic and Molecular Physics, Kruislaan 407, 1098 SJ Amsterdam, The Netherlands E-mail: liam@amolf.nl; heeren@amolf.nl

to be involved in processes as diverse as adrenal function, skin and hair pigmentation, pain regulation, and food intake (Krude & Grüters, 2000; Pritchard, Turnbull, & White, 2002). The complexity of the networks have resulted in the finding that the peptides and proteins expressed by an organism, and their post-translational modifications, are dependent on a vast array of factors, including environmental, developmental, pathological, and temporal. Clearly the ability to characterize specific biomolecules is crucial for biological, and especially pathological, investigations.

It has long been known that the proteins expressed *within* an organism are dependent on the organ, cell and sub-cellular location, and it has now been established that the spatial distribution of a biomolecule is intrinsically related to its role (Simpson et al., 2000; Kumar et al., 2002). However, a biomolecule can have multiple roles. For example, the POMC-derived peptide MSH, which is implicated in obesity, is located in the pituitary for slower endocrine signaling (Krude & Grüters, 2000), and in neurons for faster neurocrine signaling (Pritchard, Turnbull, & White, 2002). Immunolabeling, as used in the Human Protein Atlas project, is well established for tracing the distribution of peptides and proteins in tissue sections and GFP-derived labeling techniques are now extensively used to study protein dynamics, spatial and temporal, in living systems (Bastiaens & Pepperkok, 2000; Zhang et al., 2002; Phizicky et al., 2003). Despite widespread success, these labeling techniques have several limitations. These include the need to identify the molecules prior to the experiment, the small number of molecules that can be simultaneously investigated in a single measurement, the possible interference of GFP with the protein's normal function, and insensitivity to post-translation modifications and proteolytic processing (Phizicky et al., 2003). This is especially limiting for histopathological investigations as it has been shown that altered post-translational modifications and altered spatial-distributions are associated with many diseases.

To investigate the spatial distribution of specific biomolecules in biological systems and animal models of disease, an increasing number of groups are looking to combine the sensitivity and specificity of mass spectrometry with imaging capabilities. This has included both of the macromolecular ionization techniques, MALDI and ESI, and has provided fresh impetus to secondary ion mass spectrometry (SIMS) imaging. The solution phase aspect of ESI limits its imaging capabilities to sample preparation. Nevertheless, ESI-based high-throughput, high-sensitivity proteomics techniques are currently being exploited to determine the spatial distribution of a large number of proteins within a mouse brain. The mouse brain is divided into an array of $1 \times 1 \times 1$ mm cubes, and each cube subject to a complete proteomics analysis. This will exploit exceptional analytical capabilities to record the spatial distributions of thousands of proteins, and so provide an important 3D protein map of the brain that other techniques can use for comparison. However, this approach is too slow for any comparison between different animals: with $1 \times 1 \times 1$ mm cubes an adult mouse brain would require more than 2,000 proteomics analyses.

MALDI is the method of choice for recording intact protein distributions. MALDI can analyze hundreds of proteins directly from tissue sections, and combining this with spatial coordinates, allows the spatial distributions of these proteins to be determined in parallel, without a label and within practical time-scales (Chaurand, Schwartz, & Caprioli, 2004c). Stoeckli et al. (2001) were the first to demonstrate the utility of MALDI imaging mass spectrometry for pathological studies. The analysis of a human glioblastoma tissue section revealed different proteins to be localized in different areas of the tumor. Figure 1 shows a reproduction of the images. Figure 1a shows an optical image of the tissue section and Figure 1b–d shows the distributions of the three proteins β-Actin, S100A4, and Thymosin β4. The first protein β-Actin is localized in the necrotic areas while Thymosin β4 is concentrated in the proliferating areas. The calcium binding protein S100A4 is localized in the ischemic area between the other two proteins. This result clearly shows the spatial and molecular changes in the proteome that result from disease. This technology is now being applied to investigate the proteome changes associated with many diseases, including Parkinson's (Pierson et al., 2004), Alzheimer's (Rohner, Staab, & Stoeckli, 2004), muscular dystrophy (Touboul et al., 2004b), obesity, and cancer (Chaurand, Schwartz, & Caprioli, 2004b,c).

The success of MALDI imaging mass spectrometry, and the increasing number of its practitioners, has been complemented by an increasing interest in the biological applications of SIMS imaging mass spectrometry. SIMS has traditionally been limited to low mass molecular fragments and atomic ions and high spatial resolution imaging experiments have utilized diagnostic fragments (Van Vaeck, Adriaens, & Gijbels, 1999; Todd et al., 2001; Vickerman & Briggs, 2001; Lechene et al., 2006). This approach has been used to record the distribution of neutron-capture therapy cancer agents in tissues and cells and to study the composition of lipids in cell membranes (Chandra, 2001; Chandra et al., 2002; Ostrowski et al., 2004). As indicated above for the vast majority of biological applications, chemical specificity is key. Modern developments have increased the sensitivity of SIMS for larger molecular ions such that high resolution images of molecules of mass up to $\approx$1,000 amu have been recorded using their molecular ions (McDonnell et al., 2003, 2005, 2006; Sjövall et al., 2003; Nygren et al., 2004; Sjövall, Lausmaa, & Johansson, 2004; Touboul et al., 2004a, 2005; Altelaar et al., 2005, 2006; Sjövall, Johansson, & Lausmaa, 2006). This includes studying the distributions of lipids, vitamins, and pharmaceuticals in tissue and cells. Figure 2 shows a recent example in which high resolution measurements found that vitamin E is preferentially located in the soma-neurite junction of a neurobiological model, *Aplysia californica* (Monroe et al., 2005). This result was interpreted as providing further proof for the active functional role of vitamin E in transport mechanisms and/or cell signaling. Laser ablation inductively coupled plasma mass spectrometry (LA-ICP-MS) has been used for the quantitative analysis of trace elements in hard biological tissue samples such wood, teeth, and shells but is rarely applied to soft tissues and does not provide the molecular information of MALDI and increasingly SIMS, and the subject of this review (Durrant, 1999; Durrant & Ward, 2005).

MALDI imaging and SIMS imaging provide spatial information about different classes of biological compounds. MALDI provides proteomics information and SIMS that of lipids and other surface active species. These imaging techniques are increasingly used to investigate a wide variety of chemical classes within biological systems at tissue and single cell levels.

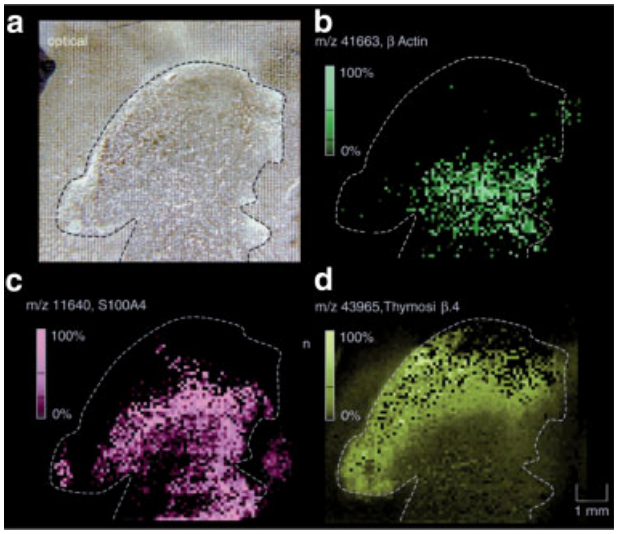


**FIGURE 1.** Protein images from a glioblastoma section. (**a**) Picture of the tissue section mounted on a metal plate, coated with matrix. Images showing the distribution of (**b**) β Actin, (**c**) S100A4, and (**d**) Thymosin β4 within the tissue section. Reprinted with permission from Stoeckli et al. (2001), Copyright 2001 Nature Publishing Group.

The potential of imaging mass spectrometry has long been recognized. The first elemental imaging experiments using SIMS were in the 1960s (Castaing & Slodzian, 1962; Liebl, 1967), and the first molecular imaging experiments using both SIMS and laser desorption were in the 1970s (Benninghoven, 1970; Hillenkamp et al., 1975). These techniques provided excellent elemental and small-molecule analysis capabilities and have been, and continue to be, extensively used in semiconductor research. Widespread biomolecular imaging mass spectrometry had to wait for the advent of MALDI and SIMS methodologies capable of generating biomolecular ions with sufficient sensitivity. Whereas the high mass capabilities of MALDI enabled it to be readily applied for imaging protein distributions within tissue sections (Stoeckli et al., 1999), the principle SIMS application, semi-conductor research, directed its development toward higher spatial resolution rather than higher sensitivity for higher mass molecules. The success of imaging MALDI has begun to steer SIMS developments toward high mass molecules while retaining the high spatial resolution capabilities.

In this review, we discuss all of the components of an imaging mass spectrometry experiment in terms of chemical and spatial information. This includes questions such as ''how is the spatial information obtained?'' ''how does the ionization mechanism influence the results?'' ''what are the limiting factors and how are they being overcome?'' This final question concerns many recent developments that have significantly improved the sensitivity, speed, spatial resolution, and information content of the imaging mass spectrometry experiments.

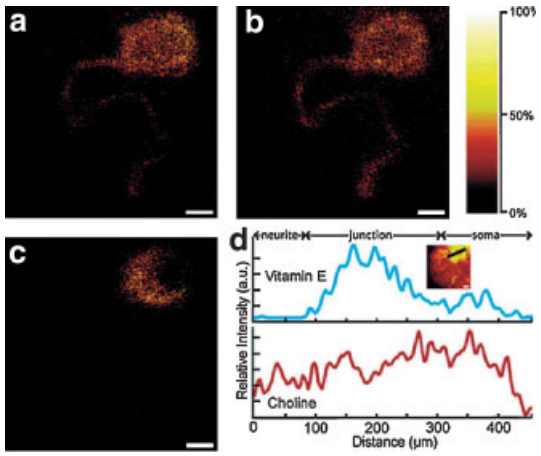


**FIGURE 2.** Images showing the spatial variation of the intensity of specific ions obtained from an isolated neuron. (**a**) Shows the distribution of the choline fragment at $m/z = 86$, a fragment specific to the head group of cellular lipids sphingosine and phosphatidylcholine. (**b**) Shows the distribution of the acyl chain fragment at $m/z$ 69, another ion often claimed to be indicative of cellular membranes. (**c**) Shows the variation of vitamin E using the molecular ion at $m/z$ 430. This image and the line scan shown in (**d**) show vitamin E is localized at the soma-neurite junction. Scale bars are 100 μm. Reprinted with permission from Monroe et al. (2005). Copyright 2005 American Chemical Society.

## II. TECHNIQUES—HOW IS THE SPATIAL INFORMATION OBTAINED?

Imaging mass spectrometry is performed using two different approaches, microprobe and microscope. The difference between these modes pertains to how the spatial information is obtained.

### A. Microprobe

Microprobe is the most common imaging mass spectrometry technique and conceptually the most simple. This is the technique now described in MALDI literature as Imaging Spectrometry Imaging (IMS). Microprobe mode imaging can be described as position-correlated mass spectrometry. Figure 3a shows a schematic of a microprobe experiment. A focused ionization beam is used to analyze a small, localized region of the sample. The resulting mass spectrum is stored along with the spatial coordinates of the spot, as defined by the focus of the ionization beam. A new region is then analyzed and another mass spectrum recorded. This process is repeated until the entire sample area has been examined and mass spectra associated with each location have been obtained. The molecular images are then reconstructed from the individual mass spectra after completion of the experiment. In a microprobe experiment, all spatial information from within the ionization spot is lost.

### B. Microscope

Microscope mode imaging uses ion-optical microscope elements to project the spatial origin of the ions generated at the sample

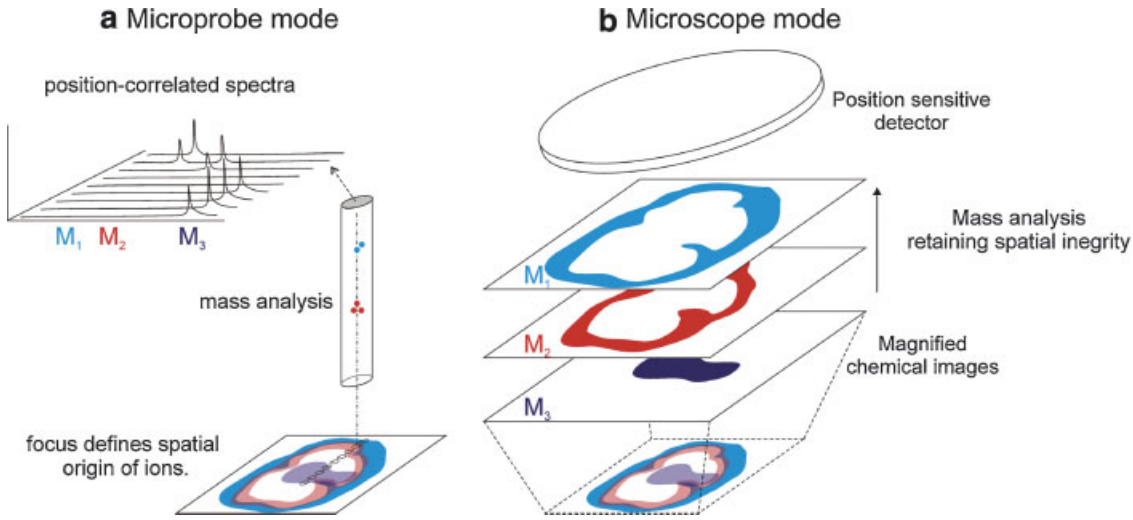


**FIGURE 3.** Schematics illustrating the two approaches in molecular imaging mass spectrometry. (**a**) Microprobe mode imaging records mass spectra from an array of designated positions to construct a molecular image. Using an ion-optical microscope, (**b**) magnified images of mass resolved ion distributions are recorded with a 2D detector. Reprinted with permission from Luxembourg et al. (2004), Copyright 2004 American Chemical Society. [Color figure can be viewed in the online issue, which is available at www.interscience.wiley.com.]

surface onto a position-sensitive detector. Figure 3b shows a schematic of microscope imaging mass spectrometry. With this technique, spatial information is obtained from within the ionization spot and is thus independent of the spot size of the ionizing beam; it is determined by the magnification of the microscope, the quality of the ion optics, and the resolution of the position-sensitive detector. This decoupling allows a much larger area to be examined without having to move the sample (or ionization beam). Larger areas still need to be rastered but the number of positions is greatly reduced. As with all microscopes, the focus a mass spectrometric microscope has a finite depth of vision, which makes sample preparation more critical.

## III. IONIZATION MECHANISMS

Most imaging mass spectrometry experiments now use either MALDI or SIMS (Todd et al., 2001). These two techniques offer different capabilities. MALDI can record the spatial distribution of high mass molecules using the chemically specific molecular ions, however, typical spatial resolutions are approximately 25 μm or more (though 10 μm sources are now available). SIMS is able to provide high spatial resolution images, sub-micron is routine and 50 nm is commercially available (Kleinfeld, Kampf, & Lechene, 2004), however, the molecular ion mass range is much lower than that of MALDI, most imaging experiments use ions of $m/z < 500$. These different capabilities derive from their different ionization mechanisms and the substantially longer history of SIMS as an imaging technique.

An extensive collection of experimental and theoretical publications testifies to the long discussion concerning the mechanisms of both SIMS and MALDI. Here we include a brief summary of the most relevant aspects, for more information, the inquisitive reader is directed to the excellent reviews referred to in the "*Introduction*." Detailed reviews on the development of SIMS and MALDI can be found in several books (Benninghoven, 1987; Vickerman, Brown, & Reed, 1989; Briggs & Seah, 1992; Vickerman & Briggs, 2001b); the proceedings of the biennial SIMS conference; the special issue of the journal Chemical Reviews (Georgiou & Hillenkamp, 2003) concerned with laser ablation of molecular substrates (MALDI) and several other papers (Chabala et al., 1995; Zenobi & Knochenmuss, 1998; Adriaens, Van Vaeck, & Adams, 1999; Van Vaeck, Adriaens, & Gijbels, 1999). A recent publication explains how the physics of large molecule emission is different in MALDI and SIMS, and that this is the reason MALDI can liberate larger molecules (Garrison et al., 2002).

### A. Matrix-Assisted Laser Desorption/Ionization (MALDI)

In MALDI, the matrix is of paramount importance. Application of the matrix solution extracts the molecules from the complex sample, formation of analyte-doped matrix crystals segregates the analytes from detrimental co-factors such as salts (Hanton, Cornelio Clark, & Owens, 1999), and disentangles and isolates the large molecules in a sea of matrix (Delcorte & Garrison, 2003). Ablation of these crystals with a UV laser directs a cooperative motion of the matrix into the vacuum, in which the analyte is entrained (Dreisewerd, 2003). Figure 4a and b shows the results of molecular dynamics simulations below and above the fluence threshold for MALDI. Below threshold, molecules with low binding energies are sublimated from the surface (as in laser desorption). Above threshold, extensive ablation occurs

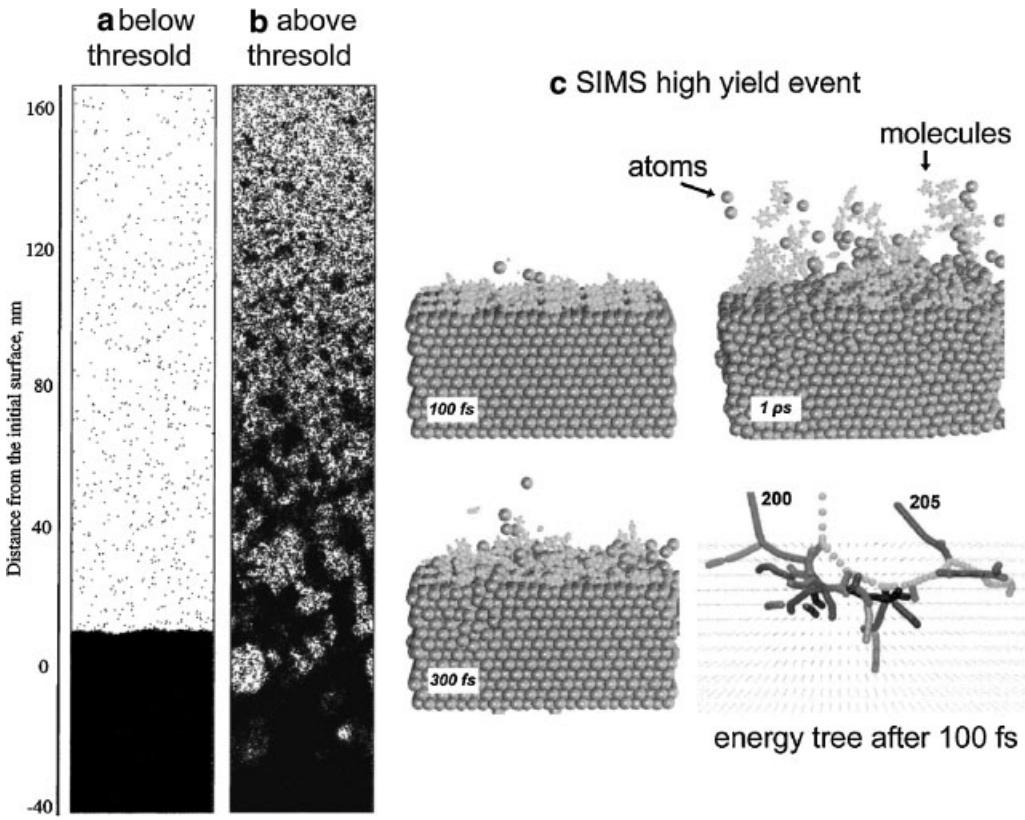


**FIGURE 4.** Molecular dynamics simulations of MALDI and SIMS. (**a**) Below laser fluence threshold molecules are desorbed; above threshold (**b**) a phase explosion of the overheated material occurs leading to ejection of molecules and clusters. (**c**) Shows the evolution of a primary ion impact in SIMS after 100, 300, and 500 fs. The collision tree shows the movement of energetic particles after 100 fs. It is clear that the incident kinetic energy can stay in the near surface region. Figure (a) and (b) are reprinted with permission from Zhigilei and Garrison (2000), Copyright 2000 American Institute of Physics. (c) is reprinted with permission from Delcorte and Garrison (2000), Copyright 2000 American Chemical Society.

ejecting matrix, entrained analyte, and clusters into the gas phase. Evidence for this entrainment mechanism is the near independence of the initial velocity of the analyte ions on the mass of analyte but its dependence on the matrix (Beavis & Chait, 1991; Spengler & Kirsch, 2003; Karas et al., 2003a). Moreover, the clusters of matrix seen in the molecular dynamics simulations have been inferred from experimental results (Karas et al., 2003a; Karas & Krüger, 2003b; Spengler & Kirsch, 2003). Post ionization of these clusters has lead to the conclusion that they form the majority of the material ablated from the sample (Alves, Kalberer, & Zenobi, 2003).

UV–MALDI operates in the so-called thermal confinement regime (Zhigilei et al., 2003a), energy uptake and ablation must compete favorably with energy redistribution throughout the sample. With smaller laser spot sizes, the rate of energy redistribution increases rapidly and a higher laser fluence is required for MALDI to occur (Dreisewerd, 2003). At these higher laser fluences, extensive fragmentation occurs. Caprioli and workers have found that using a laser beam focused to just 7–8 μm diameter leads to a decrease in ion yields of two orders of magnitude compared to a normal, >100 μm, laser spot (Schriver, Chaurand, & Caprioli, 2003) and a high resolution MALDI microprobe at the Environmental Molecular Sciences Laboratory, spot size <500 nm, has found the ''ion density generated per spot or ''pixel'' sampled at a specific location is approximately 0.25% of that garnered from standard MALDI sample spots'' (Beck & Hess). Additionally, high spatial resolution experiments are more sensitive to analyte redistribution during the matrix application step. Electrospray has been used to deposit small crystals, however, this has been found to decrease sensitivity compared to other deposition methods (Schwartz, Reyzer, & Caprioli, 2003). It is for these reasons that the majority of MALDI imaging experiments use large spot sizes; the chemical information is superior to that obtained using smaller spots.

Thus far the discussion about MALDI has primarily concerned, the desorption (ablation) of the analyte-entrained matrix into the gas phase. Equally important is the ionization of the desorbed species as it greatly influences which ions are seen in the mass spectrum. Proton and cation transfer reactions occur throughout the ablated plume, the final products being determined by the relative proton/cation affinities of the species

present in the plume. Breuker et al. (2003) have shown that when enough material is ablated to ensure many collisions within the plume, the analytes observed in the final spectrum are largely under thermodynamic control. Karas and Knochennmus have extensively reviewed the role of these in-plume processes (Karas & Krüger, 2003b; Knochenmuss & Zenobi, 2003). To reduce the amount of cationized peptides and proteins in imaging mass spectrometry of tissue sections, which can complicate spectral assignment as well as lower signal intensities (the ion signal is divided between more peaks), the tissue sections are often desalted by washing in cold ethanol solutions (Schwartz, Reyzer, & Caprioli, 2003). The ion signal dependence on the constituents of the plume can manifest itself as ''ion suppression effects,'' in which the presence of other analytes affects the signal of your analyte(s) of interest. Seeding of tissue sections with some model peptides is normally sufficient to detect whether ion suppression is a complicating factor.

### 1. Choice of Matrix

The multiple roles played by the matrix in the desorption and ionization of large analytes has lead to the optimum choice of matrices for different molecular classes being empirically determined. General recommendations of matrices for each molecular class have been summarized in reviews (Zenobi & Knochenmuss, 1998), by large chemical vendors such as Sigma–Aldrich and are available on the web. For tissue analysis, it has been reported that sinapinic acid provides the best signals for higher molecular weight proteins, whereas α-cyano-4-hydroxycinnamic acid is more suitable for lower molecular weight peptides (Schwartz, Reyzer, & Caprioli, 2003). For higher spatial resolution analysis, in which deposition of the matrix solution has been carefully controlled to minimize spatial relocation, sinapinic acid has been recommended (Kruse & Sweedler, 2003). Finally for MS/MS analysis, it is common to use matrices that produce peptide/protein ions with a high internal energy as this aids the production of structurally informative fragments (Reyzer et al., 2003; Rohner, Staab, & Stoeckli, 2004). Reflecting the importance of sample preparation in imaging mass spectrometry, Section VIII of this review details the multiple steps necessary to obtain mass spectrometric images of biological samples.

## B. Secondary Ion Mass Spectrometry (SIMS)

In SIMS, small spot sizes are routinely obtained using bright point sources, ion beam collimation, and ion-optical focusing lenses. Spot sizes (50 nm) are commercially available and smaller spots have been obtained (Slodzian et al., 1992). Such ultra-high resolution images have only been recorded for atomic ions and low mass molecular fragments, the sensitivity for higher mass ions is too low. The secondary-ion yields decrease rapidly (and non-linearly) with increasing *m/z*. This can be seen in Figure 5, which shows different regions of an SIMS mass spectrum of a mouse brain cross section using $Au_3^+$ primary ions (Touboul et al., 2004a). It is clear that the intensities decrease rapidly with increasing mass.

The impact of a primary ion causes a collision cascade in the solid that turns some of the primary ion kinetic energy back to the surface (Fig. 4c). The kinetic energy deposited near the surface causes those substrate atoms to move and to the release of analyte molecules and ions from the surface. The majority of molecular ions are released from within 10 Å of the sample surface (Delcorte, 2001). Ions and neutrals can be released from the surface as soon as their kinetic energy surpasses the binding energy to the substrate, whether as single atoms, molecules, or as part of a larger cluster.

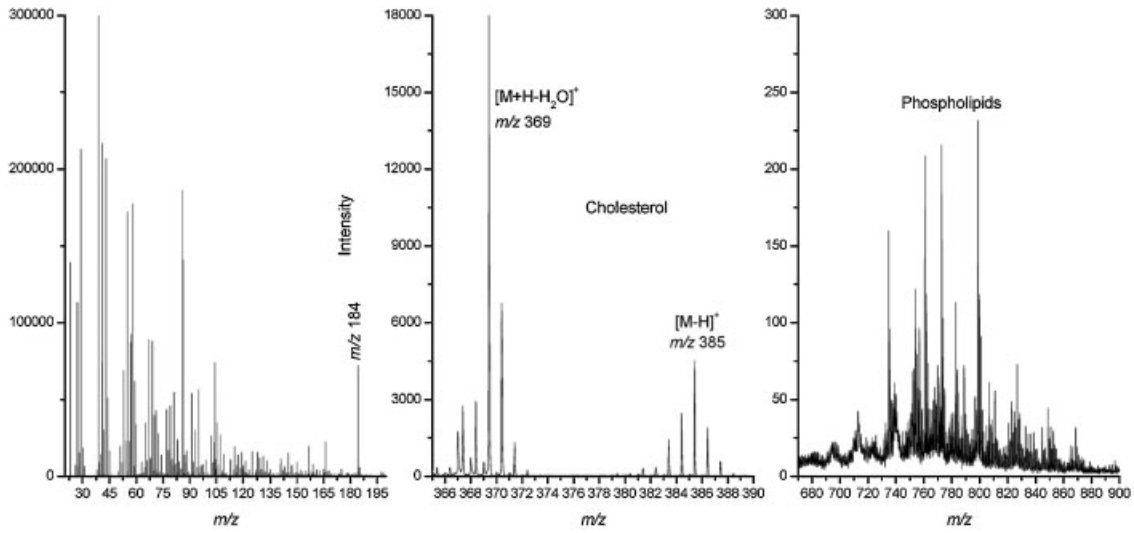


**FIGURE 5.** $Au_3^+$ SIMS mass spectrum in positive ion mode of a mouse brain tissue section. It is clear that the number of counts decreases rapidly with increasing mass. Reprinted with permission from Touboul et al. (2004a), Copyright 2004 American Chemical Society.

Figure 6 shows the energy distribution surrounding a primary ion impact (Delcorte et al., 2000). As can be seen, the distribution is a bell-like curve. Close to the impact point, the high energy of the molecules causes molecules and clusters to fragment (those in direct contact with the primary ion are obliterated). Far from the impact point, the molecules do not posses sufficient energy to overcome the binding energy to the surface. It is only in the region between these extremes where intact molecules are released. The size of this region depends on the identity of the secondary ion, any subsequent processes that can affect the internal energy of the ions (post ionization, see Section VII), the substrate, and the primary ion.

The experimental energy distribution shown in Figure 6 is the average of a very large number of individual impacts of the primary ion on the sample (Delcorte et al., 2000). It has been found that the sputter yields from individual impacts can vary significantly (Rickman, Verkhoturov, & Schweikert, 2004). To investigate the mechanisms of molecular desorption using SIMS, several groups have utilized molecular dynamics simulations (King et al., 1998; Chatterjee et al., 1999; Townes et al., 1999; Nguyen et al., 2000; Delcorte & Garrison, 2000, 2003, 2004; Delcorte et al., 2000; Muramoto & Tamamura, 2002; Postawa et al., 2003, 2004) The release of large intact molecular ions using atomic primary ions was found to be associated with trajectories (collision cascades from individual primary ion impacts) that deposit a lot of energy in the surface region, causing a collective motion of the surface atoms and molecules into the vacuum (Delcorte & Garrison, 2000). Figure 4c shows molecular dynamics results revealing these high yield events. As can be seen in the energy tree, which shows the evolution of the incident kinetic energy of the primary ion, most of the energy stays in the surface region, which leads to ejection of surface molecules and atoms. The success of polyatomic primary ions has been attributed to increased energy in the surface region sputtering more material, a result of the lower penetration depth and overlapping collision cascades of the constituent atoms (Townes et al., 1999; Nguyen et al., 2000; Muramoto & Tamamura, 2002; Postawa et al., 2003, 2004).

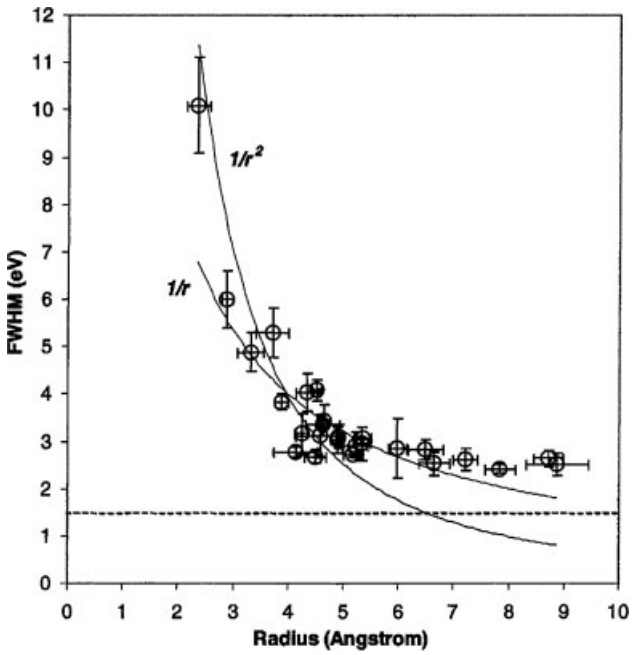


**FIGURE 6.** Correlation between the widths of the kinetic energy distributions and the damage radii for hydrocarbon fragments. This has been shown to mirror the average profile of the energy deposited after a primary ion impact (for polystyrene molecules on a silver substrate using 15 keV $Ga^+$ primary ions). Reprinted from Delcorte et al. (2000), copyright 2000, with permission from Elsevier.

The ejection of larger intact molecules requires a collective motion of the matrix/substrate molecules into the gas phase; entrainment in this matrix permits large molecules to be desorbed into the gas phase while remaining intact. In MALDI, this is ablation of the matrix (Dreisewerd, 2003), in SIMS, collective motion of the substrate (Delcorte & Garrison, 2000) and even ESI can be considered a dynamic collective motion of the solvent into the gas phase (Cech & Enke, 2001; ESI special issue, 2000; Kebarle, 2000; Loo, 1997). The larger the collective motion, the larger the analytes that can be desorbed (Garrison et al., 2002). SIMS has a smaller collective motion and higher molecular internal energy (Luxembourg & Heeren, 2006) than MALDI and ESI, consequently the analytes that can be desorbed are smaller and fragmentation is more extensive.

An important parameter in SIMS is the damage cross-section. This is a measure of the surface area affected by the impact of a single primary ion. The impact of a primary ion damages the molecules close to the point of impact. Re-sampling the damaged areas would provide chemical information about the damaged areas, and not the native surface. To ensure that the chemical information corresponds to the pristine surface, very low primary ion doses are used, $<10^{13}$ ions $cm^{-2}$. Within this regime less than 1% of the top surface layer of atoms (or small molecules) receives a primary ion impact. Statistically, it is unlikely that the same area is sampled twice, thus the mass spectrum provides chemical information about the unchanged (*static*) surface. This type of SIMS is known as static SIMS and the ion dose limit, the static SIMS limit. Nearly all molecular SIMS investigations are performed within the static SIMS limit; the exceptions are recent experiments demonstrating the very low *apparent* damage cross sections associated with polyatomic primary ions (see Section VII). Dynamic SIMS experiments use very high primary ion doses to record the spatial distribution of atoms and small groups such as $CN^-$ (Chabala et al., 1995; Chandra et al., 2002; Lechene et al., 2006). These high ion doses normally prevent the detection of molecular ions. Unless otherwise stated, the SIMS aspects of this review concern the use of static SIMS for biomolecular analysis.

## IV. INSTRUMENTATION

Since its inception, many ionization sources and mass analyzers have been used in imaging mass spectrometry experiments. A systematic evaluation is beyond the scope of this review. Here

an overview of some established instrumentation and their capabilities is presented. Recent instrumental developments are described in more detail in Section VII.

## A. Ionization

### 1. Matrix-Assisted Laser Desorption/Ionization (MALDI)

The influx of much of the new interest in imaging mass spectrometry comes from the biological mass spectrometry community using commercial MALDI–ToF instrumentation. These instruments provide high sensitivity, ease of use, and advanced software capabilities (e.g., direct coupling into protein database search engines). The first imaging capabilities were principally software developments: correlating the spectra with position (microprobe) and extracting the images from the data-cube of position-correlated spectra. More recent instruments allow the laser spot size to be controlled, nevertheless the achievable spot size is limited by the geometry of many MALDI ion sources: the final objective is located too far away for small spots. A well-optimized commercial system that has not been designed for high-resolution imaging has a spot size of approximately 25 μm diameter or larger (Chaurand, Schwartz, & Caprioli, 2004c; Todd et al., 2001). In Section VII, it will be explained how some groups have designed ion sources for high spatial resolution MALDI microprobe imaging.

MALDI imaging experiments are normally performed using either $N_2$ (337 nm) or Nd:YAG (355 nm) lasers. Typical pulse lengths are 3 ns or less (increased sensitivities have been reported using pico-second UV lasers (Vertes et al., 2004)). The fluence or energy density required on the target is dependent on spot size and pulse length; for normal nanosecond lasers and spot-sizes, the threshold fluence is $\approx 100$ J m$^{-2}$ (Dreisewerd, 2003). A recent review includes many of the experimental investigations into MALDI, including laser frequency, pulse length, spot size, and fluence dependence (Dreisewerd, 2003).

### 2. Secondary Ion Mass Spectrometry (SIMS)

The longer history of SIMS as an imaging technique is reflected in the development of imaging-oriented ion sources. Table 1 shows the characteristics of primary ion columns in common use in recent years. The high brightness of the liquid metal ion gun, an increase of $10^4$ over the next brightest ion sources, revolutionized SIMS imaging mass spectrometry. With suitable apertures and focusing ion-optics, these bright point sources can be focused to small spot sizes while retaining sufficient ion current for high-spatial resolution microprobe experiments. LMIGs routinely provide 100 nm spot sizes and smaller, and have been focused to 8 nm for ion beam lithography studies. Chabala et al. (1995) have published an excellent review on the requirements of a high resolution SIMS microprobe for SIMS imaging. Note Chabala's review concerns dynamic SIMS but much of the discussion is applicable to static SIMS imaging.

The small spot sizes necessary for high-resolution microprobe experiments are not necessary if the spatial information is obtained using an ion optical microscope. The first imaging SIMS instrument used sector-based stigmatic ion-optics to obtain 1 μm spatial resolution images (of atomic ions) using a $\approx 0.5$ mm diameter $Ar^+$ primary ion beam (Castaing & Slodzian, 1962). This microscope approach was extended using ToF technology, thus allowing microscope images to be recorded for all secondary ions (Schueler, Sander, & Reed, 1990; Schueler, 1992) and was recently combined with a MALDI ion source to provide high spatial resolution images of higher mass molecules (Luxembourg et al., 2004). The primary needs of a microscope imaging ion

**TABLE 1.**

| Primary ion source | Spot diameter | Current density ($Acm^{-2}$) | Brightness ($Acm^{-2}Sr^{-2}$) | Energy (keV) |
|---|---|---|---|---|
| Electron ionization of gases ($Ar$, $Xe$, $SF_5$) | 50 μm – few mm | $< 10^{-3}$ | $10^{-2}$ | 5-10 |
| Liquid metal ion gun (Ga, In, Au) | > 30 nm | 1 | $10^6$ | 15-30 |
| Surface Ionization (Cs) | > 1 μm | $10^{-1}$ | 500 | 5-10 |

Reproduced with permission from Van Vaeck, Adriaens, and Gijbels (1999), copyright 2004 John Wiley & Sons Limited.

source are uniform sample illumination with the ionization beam and the minimization of aberrations in the flight path of the secondary ions through the magnifying ion optics (Schueler, 1992). In this approach, the spatial information is preserved throughout mass analysis and detection.

### B. Mass Analysis

Table 2 compares some of the performance characteristics of several mass analyzers that have been used for imaging mass spectrometry. Early SIMS instruments were based on scanning MS technologies such as the quadrupole and sector. Sector instruments offer high detection efficiencies for the simultaneous detection of several ions (using several detectors), can operate continuously, and can accommodate high ion densities. The latter two properties make them especially suitable for dynamic SIMS experiments. However, a sector instrument is not suitable for *static* SIMS experiments because it is a scanning instrument: in this mode, a single *m/z* is detected, all other ions are lost. There is simply not enough material in the top few monolayers of a sample to permit such a wasteful approach.

The majority of *static* SIMS and MALDI imaging measurements are performed using ToF mass analyzers. As can be seen in Table 2, the high detection efficiency and parallel detection of ToF analyzers affords them the highest sensitivity. In addition, modern ToF instruments combine this performance with excellent *m/z* resolution, accurate mass capabilities and can operate at high repetition rates. For example, Schueler et al. have reported mass resolution of 15,500 at *m/z* 119 with transmission efficiencies >45% (Schueler, 1992). ToF analyzers dominate MALDI mass spectrometry instrumentation: they are ideally suited to the pulsed nature of the ionization technique. Likewise, the impact of ToF analyzers on SIMS is readily identified in the widespread use of the term ToF–SIMS, which refers to methodologies for performing *static* SIMS and *dynamic* SIMS using ToF analyzers (Vickerman & Briggs, 2001).

Time-of-flight measurements can be performed using linear or orthogonal extraction. The linear geometry, the ions being accelerated directly into the mass analyzer, is more common for imaging mass spectrometry as this typically provides the highest sensitivities. Linear ToF MALDI imaging experiments are often performed using delayed-extraction and a reflectron. It has been found that a short time-delay between firing the laser and extracting the ions can significantly improve the sensitivity and mass resolution of a MALDI experiment (Brown & Lennon, 1995; Vestal, Juhasz, & Martin, 1995). Delayed extraction minimizes the broadening of the analyte's kinetic energy distribution because of collisions with neutrals and partially compensates for this distribution. Delayed extraction is seldom used in SIMS: the kinetic energy distribution of molecular ions is narrower because of the much lower density of particles sputtered from the sample (Garrison et al., 2002). Modern SIMS and MALDI–ToF instruments commonly employ reflectrons (Weickhardt, Moritz, & Grotemeyer, 1996; Cotter, 1999), these ion mirrors improve mass resolution by assuring that ions of the same *m/z* but different kinetic energies arrive at the detector at the same time.

Orthogonal acceleration ToF instruments (Guilhaus, Selby, & Mlynski, 2000) extract the ions generated by the primary ion/laser into the acceleration region of a mass analyzer that performs mass analysis in a direction orthogonal to mass extraction (Fig. 7, left). The advantage of this geometry is that the performance of the mass analyzer (resolution, accuracy) is independent of the ionization step. This property has been exploited to obtain good mass spectra from a primary ion source with poor time-resolution capabilities (Tempez et al., 2004). Ens et al. (2005) have designed a different type of orthogonal ToF instrument: a gas jet and small electric field are used to extract the ions produced by MALDI perpendicular to their desorption direction, (Fig. 7 right). This allows the final laser objective to be situated much closer to the sample, thus allowing smaller laser spots and higher spatial resolution.

Any instrument based on an ion-optical microscope must use a constant extraction field (otherwise the ions would diffuse from their initial position). The TRIFT ion-optical microscope uses three-hemispherical sectors to compensate for kinetic energy variations in the emitted ions, and thus time (mass) and spatial focusing at the detector (Schueler, 1992). The emergence of the liquid metal ion gun, and thus routine high-resolution images at each *m/z*, lead to microprobe imaging becoming the dominant approach.

Some of the above characteristics of ionization sources and mass analyzers can be readily seen in the different designs of imaging mass spectrometers. Figure 8 shows schematics of the NanoSIMS (a), the high-resolution MALDI ToF designed by Spengler et al. (b), the TRIFT ion optical microscope (c), and an archetypal MALDI/SIMS ToF (d). The NanoSIMS shows an

**TABLE 2.** Characteristic performances of different mass analyzers

| Analyzer | Resolution | m/z range | Transmission | Detection | Sensitivity | Rep. rate |
|---|---|---|---|---|---|---|
| Quadrupole | $10^2$-$10^3$ | $10^3$ | 0.01-0.1 | Sequential | 1 | < 1 Hz[#] |
| Sector | $10^4$ | $>10^4$ | 0.1-0.5 | Sequential | 10 | < 1 Hz[#] |
| Time-of-flight | $10^3$-$10^4$ | $10^5$ | 0.5-1.0 | Parallel | $10^4$ | > 10 kHz |

Information for first five column taken from Vickerman (2001).
[#]Final column estimates assume analyzing a wide mass range.

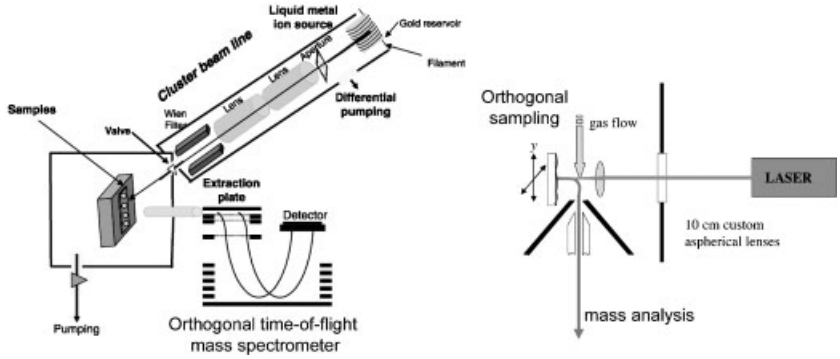


**FIGURE 7.** Orthogonal ToF instruments. The left-hand schematic depicts the experimental set-up of an o-TOFMS instrument using a novel massive gold cluster ion source. The secondary ions are pulsed into the o-TOF analyzer. Reproduced with permission from Tempez et al. (2004), (Copyright 2004 John Wiley & Sons Limited). The right-hand diagram shows an orthogonal MALDI inlet system developed by Ens et al. (2005).

instrumental configuration for high spatial resolution SIMS: the primary ions (yellow beam) and secondary ions (green beam) are controlled by the same ion-optical elements near the sample. This allows perpendicular sample analysis with small spot sizes and high secondary-ion collection efficiency. The magnetic sector allows simultaneous detection of up to seven elements, isotopes, or small molecules (within a narrow mass range) with high detection sensitivity [see Chabala et al., 1995) review for a different experimental configuration]. The high spatial resolution MALDI instrument shown in Figure 8b shares the same high-resolution concept as the NanoSIMS: the ionization beam and extraction of the resulting ions share common elements (Spengler & Hubert, 2002). For this MALDI instrument, the laser objective is hollow, and comprises part of the extraction ion optics. This instrument includes both a linear ToF detector, which allows simultaneous detection of ions of all masses, as well as a reflectron for higher mass resolution.

The ion source of the TRIFT, Figure 8c has a more typical configuration, namely the ionization sources illuminate the sample under an angle. The TRIFT is an SIMS instrument, yet as indicated above, the stigmatic ion optics have now been exploited to record high-resolution MALDI images (Luxembourg et al., 2004, 2005). The TRIFT has a ToF mass analyzer that uses three hemi-spherical electric sectors for time and spatial focusing at its position-sensitive detector. Figure 8d shows the most common design of a MALDI/SIMS ToF instrument. The ionization source illuminates the sample under an angle, and after linear extraction, the ions are analyzed with a reflectron ToF. This configuration allows the latest developments in microprobe analysis and ToF mass analysis to be combined, as well as ensuring high sensitivity by extracting the majority of the secondary/MALDI ions into the mass analyzer. Included in this diagram, but only present in recent MALDI instruments, is the modern development of ToF/ToF tandem mass spectrometry (Medzihradszky et al., 2000). After ToF mass separation, a timed ion-gate is used to select a precursor ion that undergoes CID in a collision cell. This permits tandem-mass spectrometry to be performed at the high repetition rates of a ToF instrument.

It is quite apparent that many different instruments and techniques have been used in imaging mass spectrometry and that these strongly influence the type and quality of the information obtained. In imaging mass spectrometry, resolution is crucial as it defines the chemical specificity of the technique and the scale of spatial information.

## V. RESOLUTION

There are three types of resolution in an imaging mass spectrometry experiment: mass resolution, lateral resolution, and depth resolution.

### A. Mass Resolution

Mass resolution is an important feature because it defines the degree of chemical specificity and, through improving the precision of a mass measurement, helps improve mass accuracy. Accurate mass measurements allow the analyst to make more confident peak assignments. For example, Smith et al. have shown how the percentage of unique tryptic peptides increases with increasing mass accuracy and increasing $m/z$ (Smith, 2000). Accurate mass measurements at low masses are especially powerful as they can be used to obtain the elemental composition of the detected ions.

Early mass spectrometers used mass analyzers that sequentially scanned the mass range, such as quadrupoles and sectors. These instruments typically gave unit mass resolution but, being scanning instruments, their sensitivities are low. The majority of imaging mass spectrometry instruments now use ToF analyzers, which can provide mass resolution in excess of 10,000 and mass accuracies below 20 ppm. The ultra-high mass resolution and mass accuracy of the Fourier transform ion cyclotron resonance mass spectrometer, resolution $>$100,000 and sub part-per-million mass accuracy, is beginning to be developed for imaging mass spectrometry experiments (Maharrey et al., 2004; Taban et al., 2007).

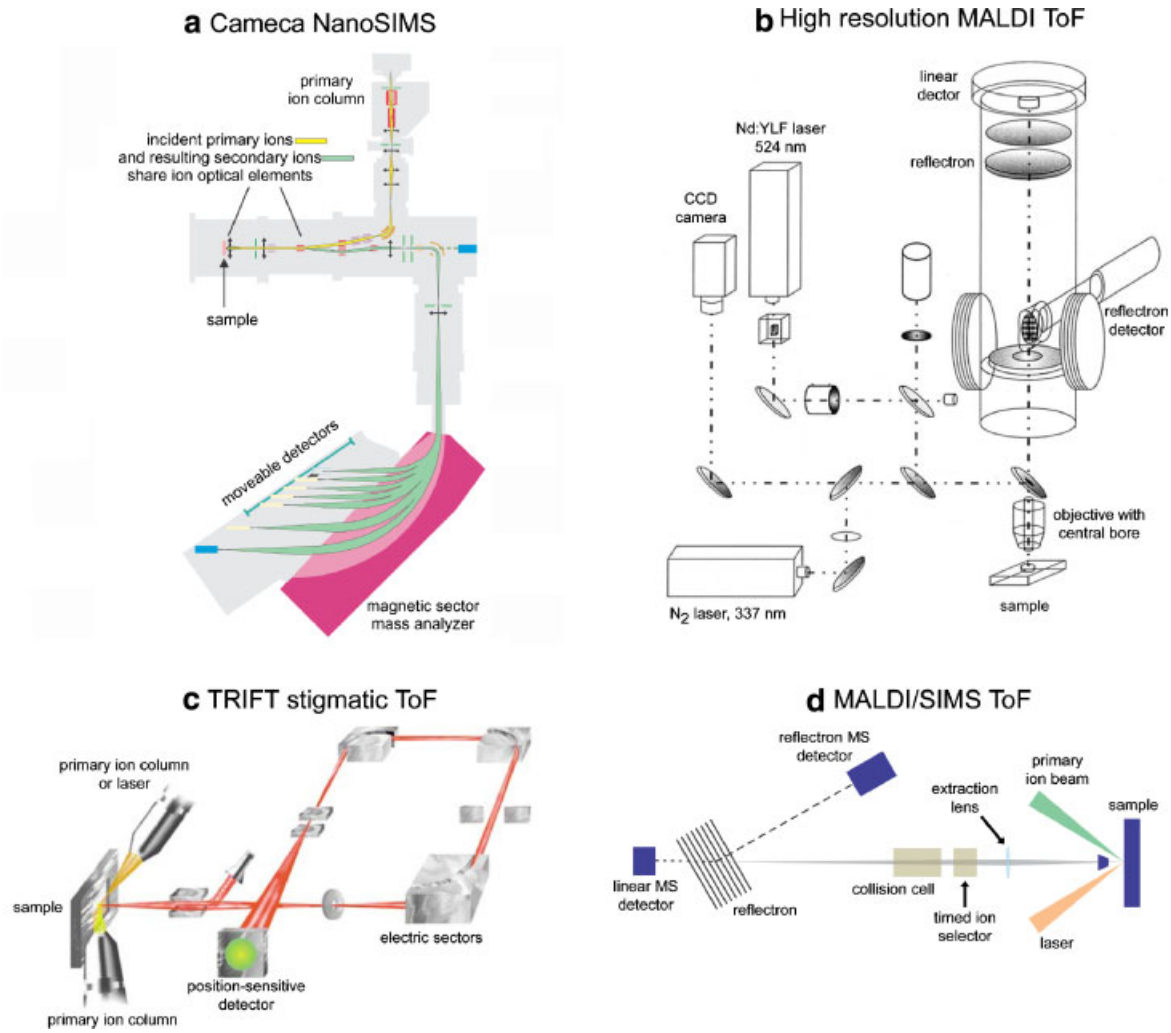


**FIGURE 8.** Examples of instruments used in modern imaging mass spectrometry. (**a**) NanoSIMS, (**b**) the high spatial resolution (highly focused laser) MALDI ToF developed by the group of Bernhard Spengler, (**c**) the TRIFT ToF-SIMS instrument designed by Bruno Schueler including stigmatic ion optics, and (**d**) a schematic of a MALDI/SIMS ToF that includes a reflectron time-focusing device. This schematic also includes the components present in a modern ToF–ToF instrument, namely a timed ion selector and a collision cell. Figure (a) was adapted from the synoptic of the instrument available on the Cameca website (www.cameca.fr); Figure (b) is reprinted from Spengler and Hubert (2002), Copyright 2002, with permission from Elsevier; and figure (c) is adapted from an image contained in the TRIFT IV brochure, which is available from the Physical Electronics website (www.phi.com). [Color figure can be viewed in the online issue, which is available at www.interscience.wiley.com.]

## B. Lateral Resolution (Spatial Resolution)

The Oxford English Dictionary includes two relevant meanings for the word resolution, ''the smallest interval measurable by a telescope or other scientific instrument'' and ''the degree of detail visible in a photographic or television image.'' Similarly, some articles refer to the pixel size as the resolution of the technique (smallest measurable distance) whereas others use the details resolved in the image to calculate an ''experimental spatial resolution.'' The former is easier to specify but omits many crucial factors. The ''experimental spatial resolution,'' or the length scale that can be distinguished, is a convolution of the inherent spatial distribution of the sample, sample preparation, the inherent capabilities of the instrument, and the signal intensity per pixel.

### 1. Sample Preparation

When preparing a sample for a high-resolution study, it is important that the spatial integrity of the sample is retained as much as possible. Any loss of spatial integrity larger than the pixel size will limit the ''experimental spatial resolution.'' For SIMS analyses, biological sample preparation protocols have

been developed that permit high-resolution measurements. Cryomicrotoming and freeze-fracture techniques have been used to prepare tissues and cells (Colliver et al., 1997; Cannon et al., 2000; Cliff et al., 2003). The ratio of $Na^+$ and $K^+$ and their distributions are frequently used to ensure that sample diffusion has not compromised the sample (Grovenor et al., 2006).

Several investigations into sample preparations for imaging MALDI mass spectrometry of tissue sections have been reported (Kruse & Sweedler, 2003; Rubakhin, Greenough, & Sweedler, 2003; Schwartz, Reyzer, & Caprioli, 2003). To minimize analyte migration, the matrix has been applied using the small droplets produced by electrospray ionization (Kruse & Sweedler, 2003). However, it has been reported that this technique leads to lower sensitivity and reproducibility with tissue samples (Schwartz, Reyzer, & Caprioli, 2003). Rather, MALDI is frequently optimized for chemical information, by using large matrix droplets to ensure efficient ionization. For this reason, most MALDI imaging experiments use laser spot sizes $\geq$25 μm. Reflecting its prominent role, Section VIII of this review is dedicated entirely to sample preparation.

## 2. Instrumental Capabilities

The pixel size of an image or the spot size of the ionization beam is often referred to as the resolution. The former is simply determined by the sample area and the number of positions used to analyze the sample. The on-sample spot-size is highly dependent on the light or ion source, the focusing optics, and the geometry of the source.

Modern SIMS imaging mass spectrometers use liquid metal ion guns technologies that routinely provide high spatial resolution capabilities, 100–200 nm (Chabala et al., 1995; Sjövall, Lausmaa, & Johansson, 2004; Brunelle, Touboul, & Laprévote, 2005; Lechene et al., 2006). MALDI imaging mass spectrometry has been performed using sub-micron spots (see Section VII) however, the geometrical requirements of the source components, the lower sensitivities associated with a smaller spot (Beck & Hess; Schriver, Chaurand, & Caprioli, 2003), and electrospray deposition of the matrix (Schwartz, Reyzer, & Caprioli, 2003) have limited such research to academic institutes.

Figure 9 shows the effects of spatial resolution on the information communicated by an image. The image in the upper left shows a matrix-enhanced SIMS image of the distribution of cholesterol in a tissue-section of the brain of the fresh water snail *Lymnaea stagnalis* taken with a pixel size of 600 nm. Subcellular distributions are clearly visible. The other images were obtained by binning these counts into larger ''pixels.'' It is clear that the typical pixel size of MALDI experiments, $\geq$25 μm, shows the global distribution. Nevertheless, the global distributions of proteins and peptides provided by MALDI have never been matched using SIMS.

## 3. Signal Intensity

It is more common that signal intensity is the limiting factor to high-spatial resolution images of high mass molecules. To reliably record the spatial distribution of an analyte, how its concentration varies with position, the image must possess sufficient contrast. For example, it is easier to discern the structure of the tissue shown in the 2.4 μm pixel image of Figure 9 than in the 0.6 μm image. This is because the contrast is greater. The lower contrast, insufficient signal from each pixel, of the 0.6 μm image is sometimes referred to as *sample volume limited*.

In SIMS, the signal intensity of low mass ions far exceeds that of high mass ions, consequently higher resolution images frequently use *characteristic* fragment or isotopically labeled ions. For example, the phosphocholine head group, *m/z* 184, is commonly used to map the distribution of the lipid phosphatidylcholine. Figure 10 shows a high spatial resolution example in which SIMS was used to study membrane fusion between two mating Tetrahymena (Ostrowski et al., 2004). The lower signal intensity of *m/z* 184 in the highly curved area fusing the two cells was interpreted as indicating a lower concentration of the lamellar lipid phosphatidylcholine. In contrast, the hydrocarbon fragment, $C_5H_9^+$, which was asserted to be representative of the total phospholipid content displayed uniform intensity across the mating cells. For the vast majority of biological questions, such fragment ions do not posses sufficient chemical specificity. Indeed the fragment at *m/z* 184 is also produced by sphingomyelin. Recent SIMS developments have concentrated on increasing the yield of intact molecular ions for improved chemical specificity (see Section VII).

MALDI imaging mass spectrometry can provide high yields of intact molecular ions of peptides and proteins, and most applications are now optimized for this chemical information. The mouse brain images shown in Figure 1 clearly show sufficient contrast and resolution to rapidly localize specific proteins within specific physiological and anatomical features. The recent development of MALDI imaging instruments specifically designed for higher resolution, and the recent commercial availability of MALDI imaging mass spectrometry, is likely to lead to swift progress in terms of sensitivity and spatial resolution.

## 4. Time

Each analysis of a small, localized region takes a finite amount of time. To improve lateral resolution by a factor $N$ requires $N^2$ more data points and thus $N^2$ more time. SIMS imaging experiments are fast, with repetition rates exceeding 10 kHz routine. For all but the most demanding experiments, imaging large areas with high spatial resolution, SIMS instruments are fast enough. The repetition rate of MALDI imaging experiments is typically lower than 50 Hz. However, this reflects the fact that MALDI imaging is much younger than SIMS imaging, consequently most systems have been adapted from regular MALDI instruments that were not optimized for speed. This is slowly changing. Modern lasers are available that can operate at more than 5 kHz and have pulse lengths compatible with MALDI (McLean, Russell, & Russell, 2003), modern stage controllers can move the sample-stage in milliseconds and fast non-imaging MALDI experiments have already been performed demonstrating that the high data rates of a fast MALDI experiment can be sustained (McLean, Russell, & Russell, 2003).

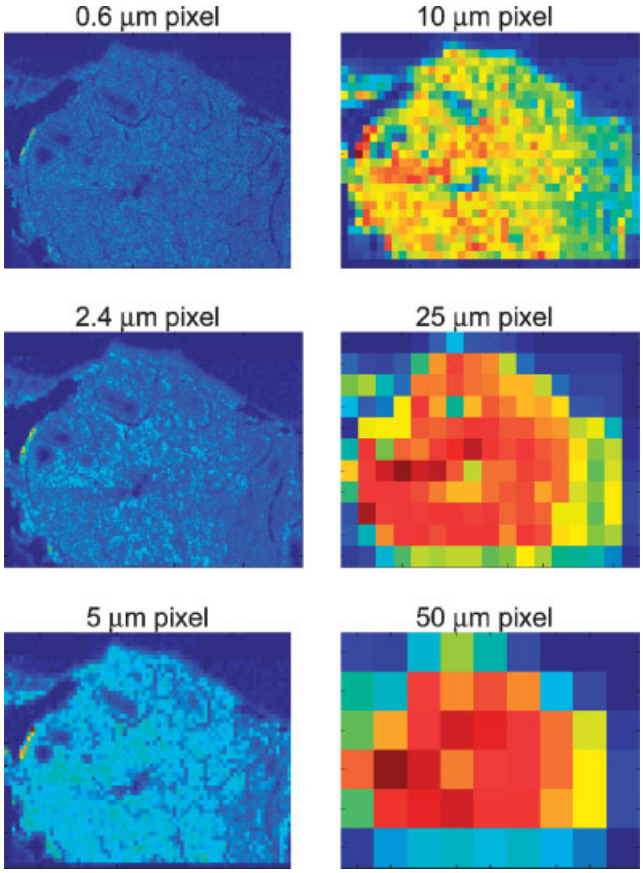


**FIGURE 9.** ME-SIMS images of a tissue section of the parietal ganglion of the pond snail *Lymnaea stagnalis*. The original results were recorded using a pixel size of 0.6 μm. These were binned to approximate the images obtained using a larger pixel size. Original results reported in McDonnell et al. (2005).

## C. Depth Resolution

The impact of an atomic primary ion with a surface sputters material from the top few monolayers. Resampling the same spot provides chemical information about the next few monolayers. By continually sampling a surface, and knowing the rate at which material is sputtered from the surface, SIMS is able to provide depth information. Such an analysis, a depth profile, is normally limited to atoms and very small fragments because of the high ion doses needed to sputter through the sample, and the consequent chemical damage. Recently, it has been demonstrated how the enhanced sputtering of large polyatomic primary ions can limit damage accumulation and thus allow molecular depth profiles (Wucher et al., 2004; Wagner, 2005; Cheng, Wucher, & Winograd, 2006).

The sputtered material is released from the top few monolayers but the collision cascade penetrates deeper into the sample, mixing the lower layers and degrading depth resolution. High-resolution depth profiling experiments use low energy polyatomic primary ion beams to limit their penetration (each atom only has a fraction of the total primary ion energy) and have demonstrated depth resolutions under 1 nm (Wittmaack, 2000; Lee et al., 2005). To combine depth-profiling with high resolution

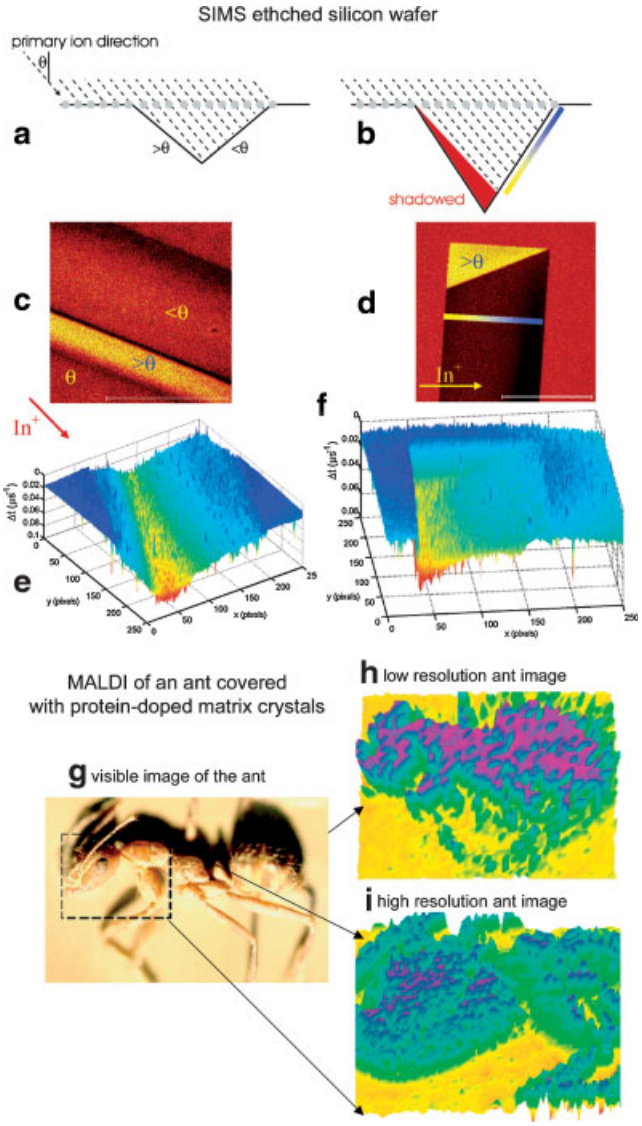


**FIGURE 12.** SIMS and MALDI topography maps. SIMS: (**a**) and (**b**) show schematics of the impact of primary ions with a channel etched into silicon. It is clear that there are three distinct impact angles: normal, larger, and lower, and that the steep sides of the channel in (b) prevent exposure of the ion beam to the inner face. This leads to the different intensities indicated in the Si ion images shown in (**c**) and (**d**), scale bar = 100 μm. The gray circles in (a) and (b) indicate the assumed origins of the secondary ions and are the cause of the projection errors seen in the images. (**e**) and (**f**) show a height map of the channel in which the z-ordinate is the difference in ToF of the matrix ions. These clearly reveal the systematic distortion and shadowing that can occur due to topography. (a) to (f) are reprinted with permission McDonnell et al. (2003), Copyright 2003 American Chemical Society. MALDI: Figure (**g**) shows a picture of an ant that was subsequently coated with a fine layer of the matrix α-cyano-4-hydroxycinnamic acid. (**h**) Shows a low spatial resolution height map of the ant using 150 μm steps and the ToF of the matrix ions (note the entire SIMS images are 150 × 150 μm). (**i**) Shows a higher resolution image of the ant's head using 30 μm steps. Figures (g)–(i) reproduced with permission from Guilliot et al. (1999).

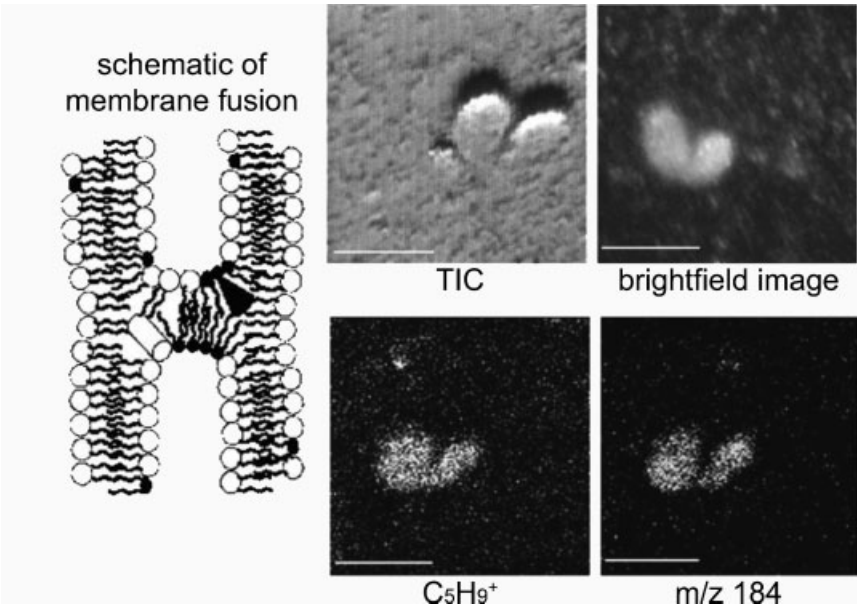


**FIGURE 10.** A schematic of the membrane fusion intermediate structure, the stalk, formed during *Tetrahymena* conjugation. The wavy lines depict the acyl tailgroups of the membrane phospholipids and the white circles represent the headgroup of phosphatidylcholine (PC), a cylinder-shaped lamellar lipid. The black circles represent the headgroup of phosphatidylethanlolamine (PE), a cone-shaped non-lamellar lipid. Membrane fusion sites probably contain a large quantity of cone-shaped lipids, because those lipids fit well into contoured intermediate structures. Total ion current image shows the same structures as the bright field image. The high resolution SIMS images show the distributions of *m/z* 69 assigned as $C_5H_9^+$ and *m/z* 184, an intense fragment due to the headgroup of PC. The *m/z* 69 peaks were interpreted as reflecting the distribution of all lipids and that of *m/z* 184, the distribution of PC. The lower concentration of the lamellar lipid PC in the fused membrane region was explained by these regions containing highly curved membranes. From Ostrowski et al. (2004). Reprinted with permission from AAAS.

imaging capabilities, 3D imaging, some ToF–SIMS instruments employ a dual beam configuration: A high spatial resolution beam for 2D spatial analysis and an intense, low energy, sputter beam for exposing a new surface (the low ion currents required for high spatial resolution are insufficient for depth profiling).

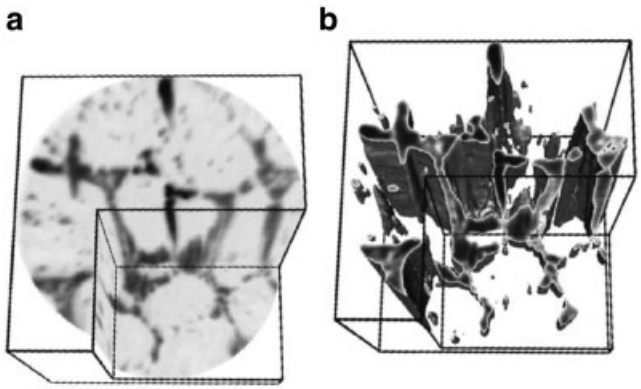


**FIGURE 11.** 3D SIMS analysis of the distribution of vanadium in high-speed steel. Dimensions are 150 × 150 × 10 μm. Left is block view and right an iso-surface view. Reprinted from Hutter et al. (2001), copyright 2001, with permission from Elsevier.

A typical arrangement would be an LMIG as the analysis beam and a DC cesium gun for the sputtering. Provided the proportion of material sputtered by the analysis beam is small compared to the sputtering beam, the depth resolution is determined by the sputtering beam. Figure 11 shows the 3D distribution of vanadium in high-speed steel (Hutter, Nowikow, & Gammer, 2001), clearly demonstrating the level of detail accessible with 3D SIMS imaging. Comparable 3D detail is not yet possible for molecules because of insufficient signal. Molecular depth profiling is normally 1D; all counts from the molecular ion from a specific depth (primary ion dose) are combined to provide enough signal for the depth profile (Wucher et al., 2004; Wagner, 2005; Cheng, Wucher, & Winograd, 2006).

Caprioli and workers recently reported the first 3D MALDI imaging results (Crecelius et al., 2005). In this study, ten 20 μm thick tissue sections, equally spaced throughout a mouse brain, were prepared and analyzed. The resulting depth resolution was 400–500 μm. The depth resolution could have been improved if more sections had been analyzed, however as these 10 sections took several days to analyze, higher resolution was impractical. The improvements in the speed of MALDI experiments (McLean JA, Russell, & Russell, 2003) will enable such 3D imaging to be performed much faster.

These 3D imaging experiments record the distribution throughout the sample. For any imaging technique, the

topography of the sample, its 3D form, is important because of the assumptions implicit in the imaging technique, which can lead to artifacts if not satisfied (McDonnell et al., 2003).

## VI. ARTIFACTS

### A. Topography

In microprobe analysis, the raster used to generate the image, the array of points that define the spatial origin of the ions, is assumed to be flat. When samples contain topography, the real spatial distribution of the analytes is projected onto this 2D array, see Figure 12a and b. In addition to this projection distortion, topography can lead to ionization biases. In SIMS, it is well established that with atomic primary ions the ionization yield is dependent on the angle of impact with the highest intensities being obtained with angles 60–80° from the normal (Vickerman, 2001; Yamada et al., 2001). The high intensity regions in Figure 12c and d clearly show the enhanced ionization yields associated with more grazing angles. The topography map shown in Figure 12e and f, obtained by plotting the ToF of a known molecular ion as a function of its position, allows the analyst to rapidly identify areas prone to bias.

Height maps have also been recorded using MALDI (Guilliot et al., 1999). However, the larger pixels of the MALDI experiment cause its height resolution to be significantly less: small topographical changes are averaged out. Topography-induced ionization biases in MALDI imaging mass spectrometry have not received much attention. In MALDI, once the laser fluence is above the threshold, the ionization yield increases rapidly with increasing fluence before reaching saturation because of increasing fragmentation of the peptide and protein ions (Dreisewerd, 2003). As most experiments are performed near threshold to avoid fragmentation, any topography would affect the fluence and thus the yield. Presumably, it is the flat tissue sections, which are the primary MALDI imaging application, and the low height resolution that has prevented topographical artifacts from receiving much attention. For both SIMS and MALDI, the loss of mass resolution associated with linear ToF analysis of rough samples can be avoided by using orthogonal ToF or ion trap mass analyzers because their mass analysis is independent of the sample surface.

### B. Matrix Effects

In SIMS, the dependence of the ion yield of a given analyte on its chemical environment is commonly referred to as ''matrix effects.'' The stopping power of the substrate influences how much of the initial energy is deposited in the surface region (Urbassek, 2001) and Delcorte has demonstrated that sputtering larger molecules requires significant energy to remain in the near surface region (Delcorte & Garrison, 2000). Consequently, the sputter yield is dependent on the nature of the substrate and the impact angle. However, the biggest matrix effect concerns the ionization of the sputtered species. In addition to the sputter yield varying by approximately one order of magnitude for most samples, electron exchange process between the surface and the departing species make the ionization yield highly sensitive to the electronic nature of the surface. Accordingly, the ion yield is highly dependent on the sample surface (Van Vaeck, Adriaens, & Gijbels, 1999): atomic ionization yields vary between $10^{-3}$ and $10^{-7}$ (Wucher, 2001) and is less than $10^{-3}$ for molecular ions (Lockyer, 2001).

In MALDI, the word matrix is used differently. The matrix is the small organic molecule, typically a small organic acid, added to the sample and is fundamental to the success of the technique (Georgiou & Hillenkamp, 2003). It is not considered to be a complicating artifact, but the liberator: the matrix solution extracts the analytes; the drying matrix untangles the large molecules (Delcorte & Garrison, 2003), incorporates them in the resulting crystals (Horneffer et al., 2001; Horneffer, Reichelt, & Strupat, 2003), and segregates the salts (Hanton, Cornelio Clark, & Owens, 1999; Luxembourg et al., 2003) that are detrimental to sensitivity. Laser desorption of these matrix crystals entrains the large molecules to bring them into the gas phase (Dreisewerd, 2003) and gas-phase chemistry between the matrix and analyte molecules can ionize a large fraction of the entrained analyte molecules (Breuker et al., 2003). The gas-phase chemistry and/or the need for incorporation (close contact) of the analytes (Amado et al., 1997) can lead to ionization biases known as suppression effects (Cohen & Chait, 1996).

The matrix (chemical environment) effects of a SIMS experiment and suppression effects in MALDI should be considered during the interpretation of imaging mass spectrometry results. With care, mass spectrometric images can provide semi-quantitative maps of the distribution of biomolecules and pharmaceuticals, in parallel, using the chemically specific ions and without the need for a label. Semi-quantitative atomic SIMS has been achieved using laser post-ionization (the neutral yield is much less sensitive to the substrate), see Section VII, and with suitable internal standards, quantitative MALDI measurements can be made (Aebersold & Mann, 2003).

### C. Electron Damage

Low energy electrons are used during SIMS analysis of insulators to compensate for the build up of charge because of the primary ion flux. It has been found that prolonged exposure to the electron beam can cause thermal damage (Gilmore & Seah, 2002). The diameter of the electron beam is normally much larger than the area being analyzed by the primary ion beam. Consequently, the sample can be exposed to the electron beam multiple times if neighboring areas are analyzed. Detuning the electron gun to lower fluence is normally sufficient to circumvent this problem.

## VII. DEVELOPMENTS & NEW METHODOLOGIES

Recent developments and new methodologies of imaging mass spectrometry have begun to reduce the impact of some of the above artifacts, as well as increase the sensitivity, speed, and spatial resolution of the experiment. These developments concern all aspects of the experiment, namely ion generation, *m/z* analyzers, and detection.

## A. Ion Generation

### 1. Post-Ionization

It has long been known that only a small fraction of the material desorbed in SIMS and MALDI are ions, typically $10^{-3}$or less, and that the yield of neutral species is also less sensitive to the substrate than the ion yield (Lockyer, 2001). Post-ionization of these neutrals has been thoroughly investigated to improve the speed and quantification of SIMS measurements. The book ''ToF-SIMS: Surface Analysis by Mass Spectrometry'' includes detailed reviews of the development of post-ionization and its applications (Vickerman & Briggs, 2001). In 1992, an International union of pure and applied chemistry (IUPAC) report of atomic trace analysis reported part-per-trillion detection efficiencies and yields exceeding 1%. Recently, the design and initial performance of a new post-ionization instrument was reported that has demonstrated ion yields in excess of 5% and potential yields of 30%, and includes an ultra high resolution LMIG (50 nm spot size) and a high resolution optical microscope (Veryovkin et al., 2004).

The higher atomic yields provided by post-ionization have been exploited for imaging sub-μm particles (Kollmer et al., 2003) and high resolution biological analyses where the distribution of atomic species can address specific questions, for example, biomineralization (Dambach et al., 2004) and the cancer treatment boron neutron capture therapy (Arlinghaus et al., 2004). Laser post-ionization has been applied to laser-desorbed fmoc-derivatized peptides (Edirisinghe et al., 2004), the fmoc group acting as an ionizable tag, as well as small unmodified peptides (Lockyer, 2001). However, molecular post-ionization typically suffer from a high degree of fragmentation, and laser SNMS molecular analysis of biological samples is normally limited to interpreting small fragment ions (Arlinghaus et al., 2004, 2006; Dambach et al., 2004).

Post-ionization in MALDI experiments has principally been used as a method for investigating the desorption/ionization mechanism by separating these two aspects. This has been performed using both direct (Alves, Kalberer, & Zenobi, 2003) and indirect laser post-ionization (Belov, Myatt, & Derrick, 1998), in the latter example, a second laser was used to generate gas-phase sodium ions which then interacted with the desorbed, neutral analyte molecules. In both cases, analyte ions were generated and provide further confirmation of the importance of gas-phase chemistry in the signals obtained using MALDI mass spectrometry.

### 2. Chemical Modification

Two methods have been developed to improve the sensitivity of SIMS measurements: matrix-enhanced SIMS and sample metallization (Nicola, Muddiman, & Hercules, 1996; Wu & Odom, 1996; Hanton, Cornelio Clark, & Owens, 1999; Wittmaack et al., 2000; Luxembourg et al., 2003; Nygren et al., 2004; Adriaensen, Vangaever, & Gijbels, 2004a,b; Adriaensen et al., 2006; Altelaar et al., 2005, 2006; McDonnell et al., 2005, 2006). Matrix-enhanced SIMS (ME-SIMS) uses the sample preparation protocols of MALDI to benefit from the detanglement and chemical ionization aspects of MALDI (Delcorte & Garrison, 2003; Knochenmuss & Zenobi, 2003). Molecular ions of analytes as large as ubiquitin, 8 kDa, and lysozyme, 14 kDa, have been detected with ME-SIMS (Wu & Odom, 1996). For lower mass analytes, <5 kDa, the ME-SIMS spectra frequently resemble those obtained using MALDI, even though ME-SIMS samples much less material (Luxembourg et al., 2003; McDonnell et al., 2005). Recent molecular dynamics simulations of polystyrene in a trimethylbenzene matrix revealed that, along with polystyrene molecules, matrix clusters are also sputtered (Delcorte & Garrison, 2003), mirroring the findings of several MALDI investigations (Karas & Krüger, 2003b; Zhigilei et al., 2003b). Moreover, it was found that the kinetic energy of the molecules released into the gas phase by ME-SIMS is similar to that for MALDI (Delcorte & Garrison, 2003).

ME-SIMS has increased the sensitivity for lower mass molecules such that sub-cellular distributions of cholesterol and small peptides have been recorded, using their chemically specific molecular ions (Altelaar et al., 2005; McDonnell et al., 2005, 2006). Another advantage of ME-SIMS is that the matrix peaks can provide an *in-situ* topographical map of the surface, allowing the user to identify regions prone to topographical artifacts and to deconvolute the loss of mass resolution because of topography from the analyte peaks of interest (McDonnell et al., 2003, 2005). Recently, it was demonstrated that the frozen water matrix, as found in freeze-fractured cellular samples, enhances the ionization of phosphatidylcholine in SIMS (Roddy et al., 2003), and that increased molecular ion yields have been reported following the addition of salts and acids (Delcorte & Bertrand, 2005; Murayama, Komatsu, & Hashimoto, 2005). Fournier and workers recently demonstrated that MALDI imaging of tissue sections is significantly improved by using ionic matrices (Lemaire et al., 2006).

Sample metallization (Meta-SIMS), applying an nm-thick layer of gold or silver to the sample, has been shown to provide increased sensitivities for large analytes as diverse as polymers, dyes, pharmaceutical, fatty acids, lipids, and cholesterol (Delcorte et al., 2003; Nygren et al., 2004; Keune & Boon, 2004a; Adriaensen et al., 2006; Altelaar et al., 2006). In addition, the thin metal layer provides a conductive contact thus effectively converting insulating samples into conducting samples (Scherl et al., 2005), thereby removing the need for charge compensation in SIMS experiments. Figure 13 shows examples of cholesterol images, obtained using the molecular ions, for both ME-SIMS (a) and Meta-SIMS (b). The ME-SIMS results show the optical image (left), a total-ion count image (center), and a cholesterol image (right, $[M+H]^+$) of a section of the parietal ganglion of *Lymnaea stagnalis*. Subcellular distributions are clearly visible. The Meta-SIMS results, Figure 13b, show an optical (left) and cholesterol (right) image of a kidney section of a Male Sprague–Dawley rat. In this case, the cholesterol image was obtained using the silver cationized molecular ions. Without application of the matrix or the thin metal coatings such images were not possible: the sensitivity was insufficient.

The main impediment of sample metallization arises from current difficulties with peak assignment and image interpretation. Many high mass peaks have been obtained from SIMS of gold-coated biological samples, some of which were identified as gold clusters and clusters such as $[M_n + Au_m]^+$ of cholesterol

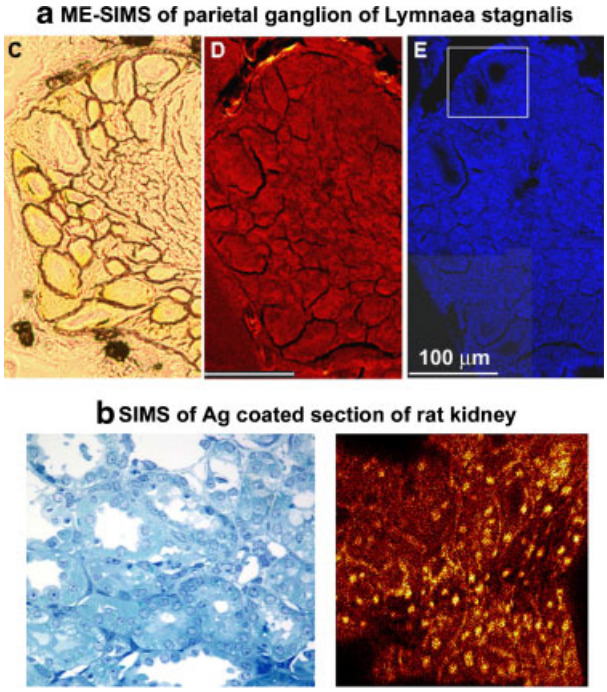


**FIGURE 13.** Examples of SIMS images using chemical modification to improve sensitivity. (**a**) ME-SIMS: Light microscope (**left**), total-ion-count (**center**), and cholesterol (**right**, *m/z* 368.9–371.9) images of the parietal ganglion of the pond snail *Lymnaea stagnalis*. The ME-SIMS images were reconstructed from six separate measurement of 150 × 150 μm, with 10 μm overlap between two consecutive measurements. Adapted from McDonnell et al. (2005), Copyright 2005. John Wiley & Sons Limited. Reproduced with permission. (**b**) Metal-assisted SIMS: Light microscope (**left**) and cholesterol (**right**) images of a kidney section, 1 mm × 1 mm, of a Male Sprague–Dawley rat. Reprinted from Nygren et al. (2004), Copyright 2001, with permission from Elsevier. [Color figure can be viewed in the online issue, which is available at www.interscience.wiley.com.]

(Altelaar et al., 2006). It is likely that some of the unassigned peaks are also gold clusters, which could be identified using the SIMS tandem mass spectrometry capabilities beginning to appear (Todd & Schaaff, 2002) Adriaensen et al. have reported Meta-SIMS ion yields that are time-dependent and do not correspond to the concentrations of the analyte (Adriaensen, Vangaever, & Gijbels, 2004b; Adriaensen et al., 2006). However, the high concentrations used in the latter experiment (1% and 10%) could simply indicate yield saturation and tangling of the larger molecules at the higher concentration.

Gold coating is beginning to find application in MALDI and LDI experiments (Scherl et al., 2005; Altelaar et al., 2006). A thin gold coating has reduced sample charging during mass analysis and thus increased the resolution and sensitivity of MS/MS experiments (Scherl et al., 2005). Other reports have demonstrated how the application of gold nano-particles (McLean, Stumpo, & Russell, 2005) or gold implantation of large gold clusters (Novikov et al., 2004; Tempez et al., 2005) followed by laser desorption can be used to generate peptide and protein ions, in the latter examples from tissue sections.

### *3. New Primary Ions*

Enhanced sputtering by polyatomic primary ions has been known for more than four decades (Grønlund & Moore, 1960; Rol, Fluit, & Kistemaker, 1960). The enhanced yields are produced with a concomitant increase in surface damage, but that the yield enhancement surpasses that of damage (Appelhans & Delmore, 1989). A comprehensive investigation (Blain et al., 1989a,b, 1990) concluded that

- secondary ion yields increase with the velocity of the primary ion
- at the same velocity, the yield increases non-linearly with the number of atoms in the molecule
- the rate of yield increase with velocity increases with the number of atoms
- the yield enhancement is largest for sputtered organic molecular ions and inorganic cluster ions.

These studies and many others have contributed to the now accepted ideas of the lower sputtering depth and overlapping collision cascades depositing more collisional energy in the surface region and thus leading to sputtering of larger molecules. These effects have been the subject of numerous molecular dynamics investigations (Townes et al., 1999; Nguyen et al., 2000; Muramoto & Tamamura, 2002; Postawa et al., 2003; Postawa et al., 2004).

Many polyatomic primary ions have been investigated, Table 3 shows a list of the polyatomic primary ions used to date and their references. The new developments in polyatomic primary ions have been making these sensitivity enhancements compatible with imaging mass spectrometry by designing polyatomic-primary-ion systems that can provide the focused ion beam necessary for high resolution microprobe imaging. These are the gold, bismuth, and $C_{60}^+$ guns (Weibel et al., 2003; Wong et al., 2003; Touboul et al., 2004a; Brunelle, Touboul, & Laprévote, 2005). Figure 14 shows examples of images obtained from tissue sections of mouse brain using a bismuth primary ion beam. The high mass images clearly demonstrate the benefit of polyatomic primary ions for imaging of biological samples. The spatial resolution achievable with the first $C_{60}^+$ ion columns was limited by the spot size, 2–3 μm, but it offers higher yields than gold clusters: a direct comparison revealed $C_{60}^+$ gave 2–3 times more signal (Weibel et al., 2003). Smaller apertures and higher beam energies are now being used to focus it to smaller spots (Xu et al., 2004). Molecule-specific imaging of combinatorial libraries, parallel mass analysis of multiple beads, clearly demonstrated the utility of higher sensitivity SIMS for imaging mass spectrometry: the spatial analysis rapidly allows the analyst to determine if molecular ions originated from the same bead and the higher sensitivity allowed a family of small peptides to be identified and sequenced (Xu et al., 2004).

A tantalizing feature of polyatomic primary ion SIMS is the possibility of obtaining molecular depth profiles, and by extension, recording the 3D distribution of *molecules* in a solid in a single experiment. The build up of molecular damage prevents depth profiling of molecules using atomic primary ions. For some systems, the lower penetration depth of polyatomic

**TABLE 3.** Polyatomic primary ions developed for higher sensitivity SIMS

| Cluster | References |
|---|---|
| $N^{2+}$ and $KI^{+}$ | (Rol, et al., 1960) |
| $H_2^+$, $D_2^+$, $H_3^+$ and $D_3^+$ | (Grønlund & Moore, 1960) |
| $Te_2^+$, $Se_2^+$ and $Cl_2^+$ | (Anderson & Bay, 1974; Johar & Thompson, 1979) |
| $P_2^+$, $As_2^+$, $Sb_2^+$, $Bi_2^+$, $Sb_3^+$ and $Bi_3^+$ | (Johar & Thompson, 1979; Thompson & Johar, 1979) |
| $Ne_2^+$ and $Xe_2^+$ | (Wittmaack, 1979) |
| $O_2^+$ and $CF_3^+$ | (Reuter, 1987) |
| $SF_5^-$ | (Appelhans & Delmore, 1989; Szymczak & Wittmaack, 1994) |
| $SF_5^+$ | (Fuoco et al., 2001; Gillen & Roberson, 1998; Kötter & Benninghoven, 1998; Szymczak & Wittmaack, 1994) |
| $ReO_4^-$ | (Groenewold et al., 1998) |
| $Au_n^+$ | (Benguerba et al., 1991; Demirev et al., 1994) |
| $(CsI)_nCs^+$ | (Diehnelt et al., 2001; Schweikert et al., 1996; Van Stipdonk et al., 1999) |
| $(NaF)_nNa^+$ | (Diehnelt, et al., 2001) |
| $C_{60}^+$ | (Diehnelt, et al., 2001; Schweikert, et al., 1996; Van Stipdonk, et al., 1999) |
| Massive glycerol clusters | (Mahoney, et al., 1991; Wang, et al., 1996) |
| Massive gold clusters | (Tempez, et al., 2004) |

primary ions and the higher sputter yields limit the build-up of molecular damage: molecules maybe sputtered with minimal chemical damage (Gillen & Roberson, 1998; Weibel et al., 2003; Wucher et al., 2004). This has permitted molecular depth profiles to be recorded (Wucher et al., 2004; Wagner, 2005).

Several massive polyatomic primary ion systems have been developed, exhibiting extreme examples of the benefits of polyatomic primary ions. Massive glycerol cluster ions, masses extending to $10^6$–$10^7$, have been used to generate intact molecular ions of peptides (Mahoney et al., 1991, 1992; McMahon, Dookeran, & Todd, 1995; Wang, Cornio, & Markey, 1996). However, this ion source is now seldom used because it cannot be focused to small spots, cannot be pulsed with high time resolution, and can severely pollute the instrument. Nevertheless, it was presumably the development of ESI, MALDI, and liquid metal ion guns that was responsible for the present disinterest in massive glycerol cluster ionization: if it provided information unavailable by other means, these difficulties would have been addressed. For instance, Aksyonov and Williams (2001) have demonstrated that good quality mass spectra can be obtained using this ion source with an *orthogonal* ToF mass analyzer.

Tempez et al. (2004) have also used an orthogonal ToF mass analyzer to obtain high mass resolution SIMS spectra using massive cluster ions, clusters with masses >80,000 Da. Using the massive $Au_{400}^{4+}$ cluster primary ion, they demonstrated ion yield enhancements of 1,000, and signal-to-noise enhancements of 20 for the molecular ions of various peptides when compared to the atomic primary ion $Au^+$. Moreover, this massive cluster ion was shown to produce minimal surface damage because of the low penetration depth and high sputtering. This ion source has not

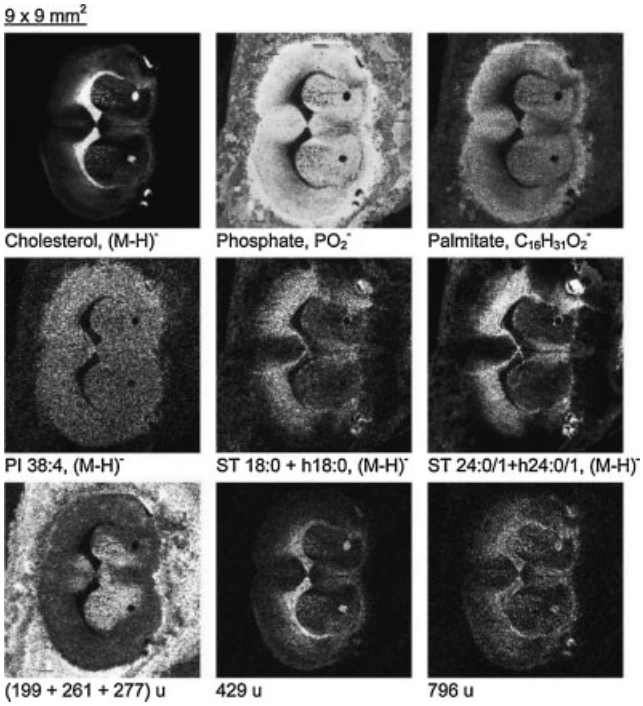


**FIGURE 14.** Gold cluster, $Au_3^+$, TOF-SIMS images from a freeze-dried mouse brain section. Analysis area was $9 \times 9$ mm$^2$. The images show the spatial distributions of cholesterol, phosphate, palmitate, phosphatidylinositol (PI), two sulfatides (ST), and unidentified peaks. These images clearly show that the intensity variations of several biomolecules correlate with anatomical features of the brain. Reprinted with permission from Sjövall, Lausmaa, and Johansson (2004) Copyright 2004 American Chemical Society.

been used for imaging experiments because of the large spot size, approximately 7 mm$^2$. It is this ion source that was used to prepare the gold implanted samples described earlier, which could be used for imaging LDI.

Finally, Schenkel et al. (1999) have demonstrated that significant improvements in secondary ion yields can be obtained using highly charged atomic ions like $Au^{69+}$ the $Xe^{44+}$. However, such primary ions are beyond the reach of most analytical laboratories.

### *4. High Resolution MALDI Microprobe: Smaller Laser Spots*

Spengler et al. have designed and constructed an objective lens for high spatial resolution MALDI imaging (Spengler & Hubert, 2002). As shown in Figure 8b, the objective lens is hollow—the MALDI-generated ions are transported through the objective into the mass spectrometer. This allows the objective to be located directly above the sample and thus permits smaller spot sizes and efficient ion extraction. Figure 15 shows a high-resolution microprobe experiment of a picospot of $\beta$-cyclodextrin doped matrix crystals that clearly shows experimental resolution under 10 μm. Each $1 \times 1$ μm pixel within the pico-spot was estimated to contain 800 zmol of $\beta$-cyclodextrin, yet sufficient signal of the molecular ion was obtained.

These sensitivities appear quite impressive, yet the absence of similar high-resolution studies on the distribution of biomolecules in tissue and cells is notable. It has been explained previously how the small spot size of a highly focused laser and the sample preparation consistent with a high resolution MALDI investigation significantly reduces sensitivity. In addition, the high fluences bore through the sample (Bouschen et al., 2003). This will limit the number of laser shots per pixel to 2–3. MALDI imaging experiments normally used many laser shots at each pixel to improve signal intensity and sensitivity. The loss of sensitivity associated with micron-sized laser spots will probably cause the majority of MALDI imaging experiments to use spot sizes of 10 μm or more.

### *5. High Resolution MALDI Microprobe: Sample Exhaustion*

MALDI imaging experiments have been performed with spatial resolutions that are less than the size of the laser spot size by consuming all of the sample underneath the laser spot and then moving the laser spot a fraction of the laser spot diameter (Jurchen, Rubakhin, & Sweedler, 2005). Consequently, the effective laser spot size is determined by the distance the laser spot has moved. Using this technique, images with a pixel size four times smaller than the laser spot size have been recorded. Further improvements proved unsuccessful because, as pointed

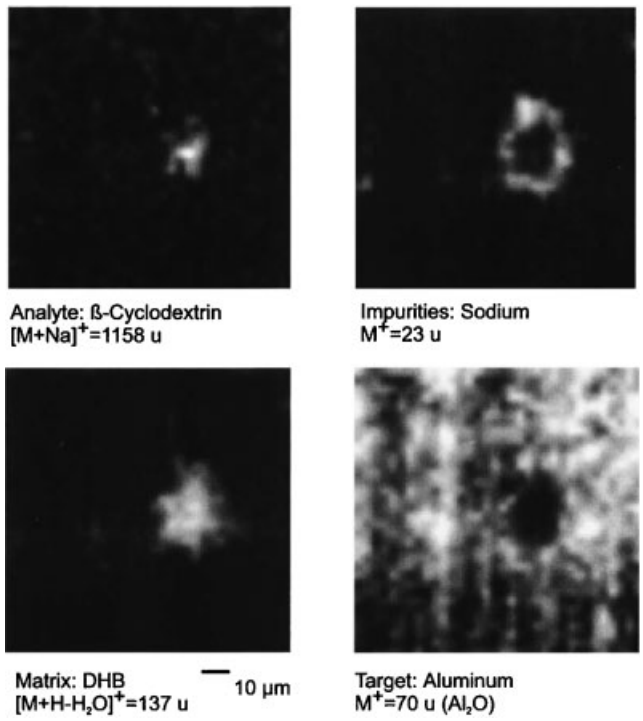


**FIGURE 15.** High-resolution MALDI image obtained using a custom-designed MALDI-TOF that can focus the laser spot to less than 1 μm. The image shows a picospot preparation of $\beta$-cyclodextrin in 2,5-dihydroxybenzoic acid matrix on a flat aluminum target. Pixel size $= 1 \times 1$ μm. Reprinted from Spengler and Hubert (2002), copyright 2002, with permission from Elsevier.

out by the authors, the Gaussian laser beam profile used in the experiments would cause the sample to be illuminated with a low laser fluence prior to analysis with the central, higher fluence region of the laser spot (which exceeds the MALDI fluence threshold). At lower fluences, MALDI does not occur but matrix is removed (Zhigilei et al., 2003a). Consequently with smaller steps, more of the matrix was lost because of these sub-threshold phenomena. The use of a laser spot with a top-hat distribution, formed with an optical fiber or a homogenizer array (Sherrod, McLean, & Russell, 2004), would allow this approach to be used to produce images with even higher spatial resolution.

### 6. Reproducibility: 3D Imaging Mass Spectrometry

The sample preparation necessary for sensitive MALDI imaging of tissue-sections, and particularly its reproducibility, has developed to the extent that the 3D protein distributions in specific anatomical features have been recorded. Figure 16 illustrates how optical image registration and alignment of MALDI MS images with the visual analogs can be used to record 3D protein distributions (Crecelius et al., 2005). In this case, the image displays the distribution of myelin basic protein isoform 8 in the corpus callosum of a mouse brain. This 3D distribution was obtained using 10 sections, equally spaced through the brain. With the continual technological improvements outlined earlier, specifically in acquisition speeds, 3D MALDI imaging will become more practical.

### 7. Advanced Laser Optics

The output of typical lasers is either a gaussian spot or an inhomogeneous area because of a discharge lamp. However, because the laser light approaches the sample from an angle in almost all instruments, the laser spot suffers perspective distortion: a circular spot is converted into an oval spot. It was recently demonstrated how a light homogenizer and a digital micro-mirror array can create arbitrary shapes of uniform laser intensity, thus allowing the analyst to create a square flat-top profile (on sample) for rastering or to examine specific groups of cells (Sherrod, McLean, & Russell, 2004).

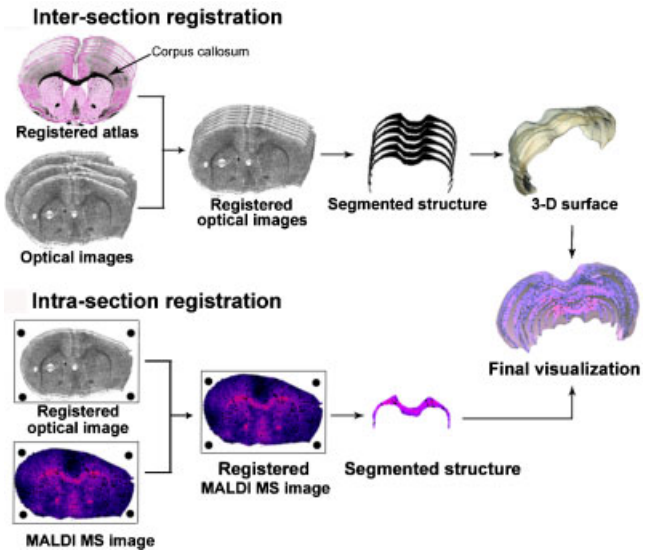


**FIGURE 16.** Schematic of image registration used to record the 3D distribution of proteins within a mouse brain using MALDI. Reprinted from Crecelius et al. (2005), Copyright 2005, with permission from Elsevier. [Color figure can be viewed in the online issue, which is available at www.interscience.wiley.com.]

## B. Mass Analysis and Detection

### 1. Tandem Mass Spectrometry

As the ions analyzed in an SIMS experiment become larger, the need for identification will grow. The Oak Ridge National Laboratory group have lead the field in performing SIMS tandem mass spectrometry experiments, for chemical identification and specification. Initial attempts focused on performing collision-induced dissociation (CID) in a triple quadrupole (Todd et al., 1992; McMahon et al., 1996). However, the scanning nature of quadrupole technologies are not suited to the low intensity of molecular ions in static SIMS, accordingly, the experiment was updated with an ion trap instrument to maximize fragment ion sensitivity. Initial experiments indicated a $\approx$10-fold improvement in sensitivity (Todd & Schaaff, 2002).

The vast majority of SIMS instruments concerned with molecular analysis utilize the high repetition rate and high sensitivity of the ToF analyzer. Recently, it has been demonstrated how the sensitivity enhancements provided by polyatomic primary ions enabled post-source decay, an established MALDI–ToF technique, to be used to obtain diagnostic fragments (Touboul, Brunelle, & Laprévote, 2006). It likely that as the mass range of SIMS expands, it will use more of the tandem mass spectrometry technologies associated with modern MALDI instrumentation. Such capabilities have been exploited to record the spatial distribution of low mass molecules, for example, pharmaceuticals and their metabolites, which can be complicated by interference peaks because of matrix clusters. As the fragments of a pharmaceutical compound are normally different from those of the matrix clusters, chemically specific images have been obtained by using the intensities of the diagnostic fragment ions (Reyzer et al., 2003; Rohner, Staab, & Stoeckli, 2004). For these MS/MS imaging experiments, matrices that lead to a higher degree of fragmentation are normally used, such as sinapinic acid (Reyzer et al., 2003; Rohner, Staab, & Stoeckli, 2004). The high MS/MS performance of triple quadrupole and qQ-ToF instruments could see them emerge as valuable equipment for low-mass imaging mass spectrometry analysis. Note a fast triple quadrupole MALDI instrument was recently reported that can perform MS/MS analysis on up to 10 samples (pixels) per second (Corr et al., 2006).

### 2. Ion Optical Microscope

In the 1990s, sub-micron resolution SIMS images were recorded using a stigmatic imaging mass spectrometer and a position-sensitive detector (Schueler, Sander, & Reed, 1990; Schueler, 1992). This instrument combined high spatial resolution

capabilities with high mass resolution and high transport efficiencies. However, the rapid rise of the liquid metal ion gun forced the development of this technology to be forsaken. Recently, it was demonstrated that high resolution high mass images can be obtained by coupling this technology to a MALDI ion source (Luxembourg et al., 2004) and that the technology is compatible with tissue sections, in which it clearly resolved cellular features (McDonnell et al., 2005). Figure 17A shows an ion-optical microscope image of the matrix ions produced from a sample consisting of doped matrix crystals overlain with a 25 μm pitch TEM grid. The image shows an area of approximately $200 \times 200$ μm. The line scan, Figure 17B, shows how the intensity varies across the line indicated in the image. The experimental spatial resolution of this image, which incorporates the variation in the sample and the capabilities of the instrument (ion optics and detector), was 4 μm (pixel size = 600 nm). It was indicated that the optical detector used in these experiments was the likely cause of the lower resolution (the sub micron images referred to above used a different detector not suited to MALDI).

One of the big advantages of microscope mode imaging is that it allows the analyst to use ionization sources that cannot be focused to a small spot. Single-shot images with an experimental spatial resolution of 4 μm, identical to that for UV–MALDI, have been recorded using IR–MALDI even though the diffraction-limited spot size was 28 μm (Luxembourg et al., 2005).

Unfortunately, the resistive anode encoder (RAE) used as the position-sensitive detector for the early SIMS experiments, which provided sub-micron resolution images, is not compatible with the high ion loads of a MALDI or polyatomic primary ion SIMS experiment. The RAE has a long dead-time, hundreds of nanoseconds. After detection of the first ion, any ion striking the detector within this dead-time is ignored. This technology is suitable for techniques that generate a low ion current (low ion load), such as traditional SIMS, but would lead to unacceptable biases for techniques that produce a high ion load. At present, the MALDI ion-optical microscope is limited to microscope mode imaging of single masses (or mass ranges). To realize the full advantage of MALDI microscope mode imaging, an (x,y,t) detector with multi-hit capabilities and short dead-times is required to ensure that the spectra are not compromised by detection biases.

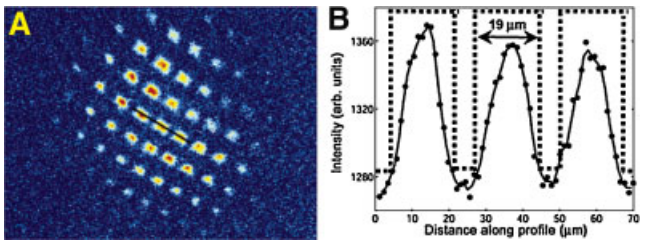


**FIGURE 17.** (**A**) Ion-optical microscope image of the matrix 2,5 dihydroxybenzoic acid obtained from a sample consisting of substance P- and insulin-doped matrix crystals and covered with a 25 μm pitch copper grid (bar 6 μm, space 19 μm). This image clearly shows the grid structure of the sample within the laser spot. (**B**) Shows a line scan taken along the line indicated in (a), clearly revealing the spatial variation of intensity. From a series of such profiles at different locations, the average lateral resolution was determined to be 4 μm (pixel size = 600 nm). Reprinted with permission from Luxembourg et al. (2004), Copyright 2004 American Chemical Society. [Color figure can be viewed in the online issue, which is available at www.interscience.wiley.com.]

### C. Molecular Scanner

MALDI is routinely used to generate intact molecular ions of compounds upto *m/z* 100,000. However, for established technologies such as a microchannel plate (MCP) or a conversion dynode combined with a secondary electron multiplier, the detection sensitivity falls at higher mass, being much more severe for the MCP (Gilmore & Seah, 2000a). Accordingly, efforts have been made to reduce the size of the ions detected.

In the molecular scanner approach, the proteins from a tissue section are electro-blotted through a membrane containing immobilized trypsin (Rohner, Staab, & Stoeckli, 2004). The final capture membrane contains the proteolysis fragments of all of the proteins electro-blotted from the tissue section while retaining spatial information; in this case, the spatial resolution is limited by the blotting step. Figure 18 shows the schematic of the experiment and some results obtained from a mouse brain tissue section. An additional advantage of the molecular scanner approach is the uniform properties of the capture membrane, significant cleaning of the sample and multiplexing the protein signal (each protein produces multiple peptides).

More recently, it has been shown how digestion can be achieved ''in-tissue'' by depositing an array of discrete droplets of a trypsin solution directly onto tissue (Shimma et al., 2006). For efficient digestion, it is necessary to keep the trypsin solution in contact with the tissue for a significant time and at 37°C. Caprioli and workers have achieved this by depositing the array of droplets throughout the digestion time. It is clear that the spatial resolution of in-tissue digestion strategies will be limited by the size of the droplets of digestion solution, for efficient digestion, these dimensions will be greater than 100 μm but still compatible with the majority of microprobe MALDI imaging experiments.

The success of molecular scanner or ''in-tissue'' digestion strategies ultimately depends on the ability to assign the peptides to specific proteins. This has been optimized by using accurate mass FTMS to ensure as many peptides as possible are assigned to proteins.

This panoply of developments clearly shows that significant improvements continue to be made in all aspects of imaging mass spectrometry. Moreover, many of these improvements can be combined. For example, it was recently reported how the sensitivity improvements provided by chemical modification of the surface and polyatomic primary ions are additive (McDonnell et al., 2006). Alternatively, an analyst might use sample exhaustion, a square flattop laser profile, and a ToF–ToF mass analyzer to record the distribution of a pharmaceutical metabolite with high spatial resolution and use MS/MS for identification.

## VIII. SAMPLE ACQUISITION AND PREPARATION

The representivity of an imaging mass spectrometry experiment, in terms of both chemical representivity and spatial integrity, can

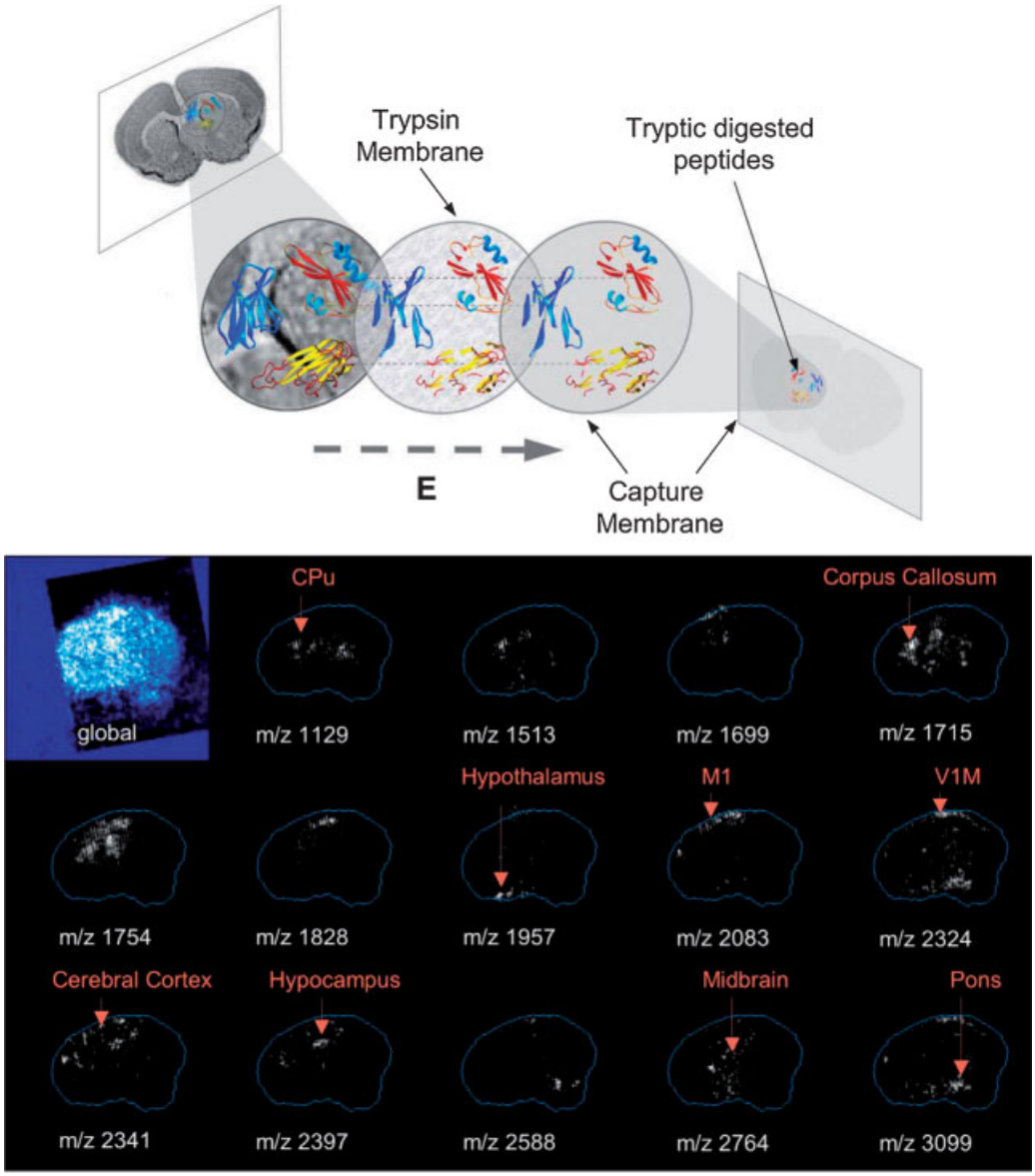


**FIGURE 18.** **Top**: Schematic of the molecular scanner. The tissue section is blotted through an immobilized-trypsin membrane on to a capture membrane, resulting in a mirror image of the original tissue section containing tryptic peptides. This membrane is then analyzed using MALDI imaging. **Bottom**: Chemical images of the capture membrane obtained after applying the molecular scanner to a mouse brain section (CPu: caudate putamen (striatum); M1: primary motor cortex; V1M: primary visual cortex, monocular region). Reprinted from Rohner, Staab, and Stoeckli (2004), copyright 2004, with permission from Elsevier.

only be as good as the worst step in the entire process of sample acquisition, preparation, imaging mass spectrometry, and interpretation. In all sample-handling steps throughout acquisition and preparation, the spatial and chemical integrity must be maintained, within a length scale determined by the spatial resolution of the mass spectrometry technique used.

Sample acquisition and preparation is a very large field. A quick literature search shows that SIMS has been applied to fields as diverse as cosmology, microelectronics, catalysis, atmospheric chemistry, art conservation, combinatorial chemistry, pharmaceutical design, medicine, and fundamental biology. Each of these fields will have their own sample-dependent requirements. This sample preparation will concentrate on biological applications, and detail factors common to all successful experiments using both SIMS and MALDI.

## A. Common Sample Preparation Considerations

Different ionization techniques can be sensitive to different contaminants. In SIMS, polydimethylsiloxanes (PDMS) can be particularly problematic: They are surface-mobile in high vacuum, eventually spreading across all surfaces, have high ionization efficiencies and are difficult to remove. Without sufficient care, they can easily dominate the spectrum of this surface-sensitive technique. The problem with PDMS arises from their prevalence. It is a mould release agent in the manufacture of a wide range of products, including all common plastic containers and bags, lubricants, and even some hair gels. SIMS laboratories are fastidious in their avoidance and use metal containers or those designed for the semi-conductor industry (http://www.entegris. com). Nevertheless, PDMS is difficult to avoid, particularly for samples originating from external sources. Fortunately, it is highly soluble in hexane, and a short rinse is enough to reduce PDMS levels significantly.

Imaging of tissue sections using MALDI or ME-SIMS is significantly improved by washing the tissue prior to matrix deposition (Schwartz, Reyzer, & Caprioli, 2003). A typical wash includes rinsing the tissue in ice-cold 70% ethanol solution for several minutes. This removes excess salts, which can disrupt the matrix crystallization process, complex with the analytes and matrix molecules, and compete for the available charge.

## B. Tissue Sections

It has been established that the proteome of an animal brain changes almost immediately after death. To denature the active proteases and the subsequent disturbance of the proteome, the animal brains were microwaved prior to further processing (Svensson et al., 2003; Che et al., 2005). Several studies have investigated the optimum sample preparation procedures for tissue samples. Typically, the interior of tissue samples is exposed using cryosectioning techniques. Embedding in optimal cutting temperature (OCT) polymer or Tissue-Tek® should be avoided as it can smear across the sample, thus compromising the chemical integrity. Embedding in gelatin (Altelaar et al., 2005) and agarose (Kruse & Sweedler, 2003) has been used to facilitate handling of small or fragile samples but most often cryosectioning is performed directly with the frozen tissue samples (Kruse & Sweedler, 2003; Schwartz, Reyzer, & Caprioli, 2003). The thickness of the tissue sections used is normally 10–20 μm: ultra thin sections can be very fragile and difficult to manipulate, whereas thicker sections need longer to dry and, because they are insulating samples, can adversely affect the performance of the mass analyzer [the gold coating development described earlier reduces the severity of this effect (Scherl et al., 2005)]. Schwartz, Reyzer, and Caprioli (2003) report that it is preferable to deposit the tissue section on to a cold plate and then to quickly warm the plate and tissue section together (thaw mounting). The alternative, placing a room temperature plate onto the cold tissue section, was found to be associated with poorer mass spectra. The sample plate of choice is a transparent conductive slide such as indium-tin-oxide-coated glass slides because they allow visible spectroscopy and mass spectrometry to be performed on the same sample (Chaurand et al., 2004a; Altelaar et al., 2005). The next step of a tissue-section analysis is dependent on the imaging mass spectrometry technique used.

### 1. Tissue Sections—SIMS

The advantage of an SIMS analysis is that no further sample preparation steps are necessary: the sample plate can be mounted and the analysis performed. Impressive biological images of atomic ions and low mass fragments can be obtained directly from tissue. The sensitivity improvements provided by polyatomic primary ions, ME-SIMS, Meta-SIMS, and their combinations are beginning to show sufficient intensity for imaging of intact biomolecules (Nygren et al., 2004; Xu et al., 2004; Touboul et al., 2004a; Brunelle, Touboul, & Laprévote, 2005; McDonnell et al., 2005, 2006; Altelaar et al., 2006). The thin metal coatings can be quickly deposited, with full control of the thickness using commercial sputter coaters while most ME-SIMS experiments have used electrospray deposition (with little washing) to maintain spatial integrity consistent with this high spatial resolution technique (Altelaar et al., 2005; McDonnell et al., 2005).

### 2. Tissue Sections—MALDI

MALDI is normally used for the analysis of peptide and protein distributions at lower spatial resolution, consequently, there is more scope for optimizing the chemical information (sensitivity and number of biomolecules detected). This includes washing, choice of matrix solution, size of matrix crystals, and the method of matrix application. It has been reported that the temperature and humidity of the environment during matrix application affect the MALDI analysis of tissue sections, presumably by influencing protein extraction from the tissue and crystallization. For lower spatial resolution studies, >25 μm, Schwartz, Reyzer, and Caprioli (2003) found that the best results were obtained using sinapinic acid, depositing it directly onto the tissue, and that the optimum solvent solution for matrix application is tissue dependent. More recently, the use of ionic matrices for tissue sections provided considerable improvements in signal intensity (Lemaire et al., 2006) while Chaurand et al. (2004a) have reported that the histology stains Cresyl Violet and Methylene Blue are both compatible with subsequent MALDI analysis. Figure 19 shows an example of a stained tissue section and an array of images showing protein distributions within the same tissue section.

Several methods have been employed to deposit the matrix on to a tissue section, these include manual droplet deposition, the use of a TLC coater, an acoustic pico-spotter and by using small dry crystals to seed the matrix crystals prior to deposition of the matrix solution (Schwartz, Reyzer, & Caprioli, 2003). These methodologies are suited to lower resolution MALDI studies because of the large size of the droplets of matrix solution on the surface. In a separate investigation, Kruse and Sweedler (2003) concluded that when using electrospray deposition (to minimize analyte relocation for higher resolution studies), sinapinic acid gave the best results.

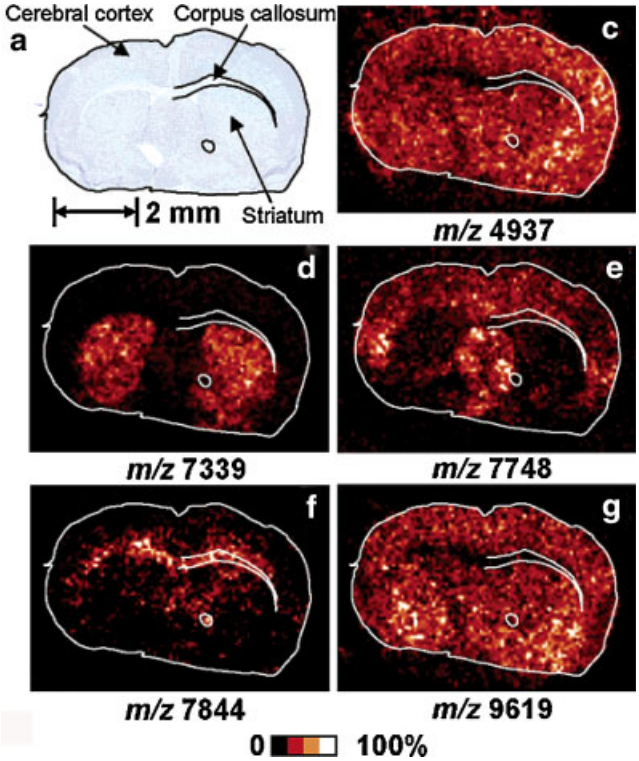


**FIGURE 19.** Combining imaging mass spectrometry with histology: optical image and MALDI protein images obtained after staining with Cresyl Violet. The photograph (**a**) of the Cresyl Violet-stained mouse brain section clearly shows anatomic brain substructures. Subsequent MALDI imaging reveals the distribution of specific biomolecules. Reprinted with permission from Chaurand et al. (2004a), Copyright 2004 American Chemical Society. [Color figure can be viewed in the online issue, which is available at www.interscience.wiley.com.]

### *3. Tissue Sections—Blotting*

Blotting techniques onto organic membranes (Todd et al., 2001) or gold surfaces (Sjövall et al., 2003) have proven attractive because it cleans the sample and provides a more uniform surface (with respect to the original tissue section). Sjövall et al. (2003) demonstrated subcellular distributions could be obtained; nevertheless owing to difficulties with smearing of the sample during the blotting procedure, blotting is seldom used.

## C. Cellular Distributions

Chemical fixation, as used in morphological analysis, has been found to be unsuitable for investigating the cellular distributions of ions and molecules. Cross-linking of the molecular components prevents their liberation and diffusible ions (not bound to macromolecules) are redistributed (Grovenor et al., 2006). For single cell analysis, a snapshot of the biomolecular machinery is typically obtained by rapidly freezing the cells; to prevent ice crystals disturbing the cellular integrity flash freezing using liquid propane is commonly employed to produce vitreous ice throughout the sample. Freeze drying (lyophilization), resin embedding, and freeze-fracture techniques have all been used to study the distribution of *ions* in cells (Cannon et al., 2000; Cliff et al., 2003). Grovenor et al. (2006) recently published a critical evaluation of these preparations. Imaging mass spectrometry of molecules within cells has typically used lyophilization (Altelaar et al., 2005; Monroe et al., 2005). Though these molecular studies did not report the distribution of the highly mobile cations, any diffusion of the molecular components will be significantly less.

This discussion has purposely concentrated on MALDI and SIMS analysis of biological samples. Whereas this covers the majority of MALDI imaging applications performed to date, SIMS imaging mass spectrometry has been applied to a much wider variety of samples (Vickerman & Briggs, 2001). Clearly, the sample preparation is dependent on the sample. In its simplest form, a SIMS measurement involves just placing a clean sample into the mass spectrometer. However, for reliable imaging results, the sample must be prepared so as to expose a clean, flat surface to the primary ion beam (to avoid topographical and contamination artifacts). This has been achieved using both microtoming and polishing. Using graded abrasive papers such as Micro-Mesh™, it is possible to polish a wide range of samples to a flatness compatible with SIMS (Keune & Boon, 2004b). For solid samples, polishing can provide high-quality samples. With softer samples, in which polishing can lead to smearing, microtoming is the method of choice. It can provide flat surfaces with minimal smearing (as with the tissue sections), the thin sections are easily mounted onto sample plates, and thin sections of insulating samples can be analyzed with minimal (or without) re-optimization of the ToF analyzer. Finally, to expose subsurface layers to the primary ion beam (e.g., to remove surface contaminants), the surface layers can be removed using an ion beam (as in a dual beam depth profiling experiment). Ion beam milling with atomic ions limits the imaging analysis to atoms and small molecules: all macromolecules are damaged. The low damage cross sections of new polyatomic primary ions such as $C_{60}^{+}$ and $Au_{400}^{4+}$ have enabled this technique to be used for the preparation of surfaces for molecular analysis (Tempez et al., 2004; Wucher et al., 2004).

To summarize, the optimum sample preparation procedure is highly dependent on the sample, the technique being used and the information required. Table 4 provides a summary of imaging mass spectrometry techniques, and their sample preparations. These protocols should be used as a guide rather than as a definitive set of instructions, and then optimized for the experiment in question should further optimization be required.

# IX. DATA PROCESSING AND VISUALIZATION

Imaging mass spectrometry produces a very large amount of data: a complete mass spectrum for each of a very large number of pixels. Many tools have been developed to visualize and analyze this vast dataset intelligently and efficiently. This includes many basic but widely used features, such as region-of-interest analysis, choice of intensity scales for image display (color palette, linear/logarithmic), image overlay, binning of spectral

**TABLE 4.** Summary of common sample preparation procedures used in imaging mass spectrometry

| Sample | Technique | Preparation |
|---|---|---|
| Tissue section | SIMS | Cryo-microtome |
| | ME-SIMS | Cryo-microtome, short wash, electrospray matrix application |
| | | Cryo-microtome, short wash, gold/silver sputter coating |
| | Meta-SIMS | Cryo-microtome, histological staining (optional), wash, matrix |
| | | application using pneumatic spray or automated droplet |
| | MALDI | deposition, gold coating (optional). |
| Cell | SIMS | Plunge freezing in liquid propane, followed by lyophilization or |
| | | freeze-fracture. Gold coating optional. |

and image data for improved signal-to-noise, intensity profiles (variation of intensity with time or space), and chemical libraries for analyte identification (Vickerman, Briggs, & Henderson, 2002). Figure 20 shows an example including region-of-interest analyses and intensity profiles of a SIMS imaging mass spectrometry experiment of the anterior commissure of a mouse brain (adapted from (Sjövall, Lausmaa, & Johansson, 2004)). It is readily apparent that the region-of-interest analysis efficiently communicates the different lipid compositions and that the intensity profile quantifies the variation in signal with distance.

In addition to these facilities, imaging mass spectrometrists have continued to develop a broad array of tools. These have improved the quality of information extracted from the large data sets, reduced the dimensionality to more practical levels and allowed different imaging data sets to be aligned and compared.

### A. G-SIMS

The high internal energies of the ions produced by SIMS can frequently lead to extensive rearrangement prior to mass analysis. Gilmore and Seah have developed a routine in which the fragmentation behavior of the analytes is extrapolated to lower internal energies (Gilmore & Seah, 2000b). The resulting ''gentle-SIMS'' or G-SIMS spectra contain those ions that ''would be emitted from a surface plasma of very low temperature and thus have little post-emission rearrangement or fragmentation. Those peaks are, thus, directly characteristic of the material without rearrangement and provide a direct interpretation and identification.''

### B. Digital Image Processing

De-noising, edge detection, particle counting, and other similar calculations have all been implemented to quantify the information in images using commercially available packages such as Matlab$^{TM}$ (Tyler, 2001; Wickes, Kim, & Castner, 2003; Brunelle, Touboul, & Laprévote, 2005). In SIMS, spectroscopy multivariate analysis (MVA) is extensively used to distinguish between groups (Wagner, Tyler, & Castner, 2002; Henry, Dupont-Gillain, & Bertrand, 2003; Wagner et al., 2004); from an imaging perspective, these correlations relate to spatial variation (Tyler, 2001, 2006; Biesinger et al., 2002; McDonnell et al., 2003; Wickes, Kim, & Castner, 2003; Sjövall, Lausmaa, & Johansson, 2004). Typically, MVA is used to increase the contrast of spatial variation: it has been used to distinguish different regions in imaging of tissue (Sjövall, Lausmaa, & Johansson, 2004; McCombie et al., 2005), single cells (Ostrowski et al., 2004), and lipid monolayers (Biesinger et al., 2002). MVA is adept at finding correlations, this ability is now being exploited for the automated alignment of different image data sets (Broersen & van Liere, 2006).

MVA has proven more useful in SIMS than in MALDI imaging, whereas MALDI spectra contain mostly molecular ions (and thus chemically specific) SIMS spectra have been dominated by numerous lower mass fragments. MVA is adept at determining correlations in highly complex data, and has been widely used to identify correlations between these fragments. The results provided by MVA are influenced by preprocessing, for example, logarithmic scaling of the intensities ensures that the lower intensity but structurally informative high mass fragments and molecular ions contribute to the MVA differentiation (Wagner et al., 2004). The high-mass sensitivity improvements outlined because of polyatomic primary ions and surface modification will aid such chemical differentiation.

### C. Differential Image Distortion Correction

Mass spectrometers employing stigmatic ion optics can frequently produce distorted images, such as pincushion. It has been

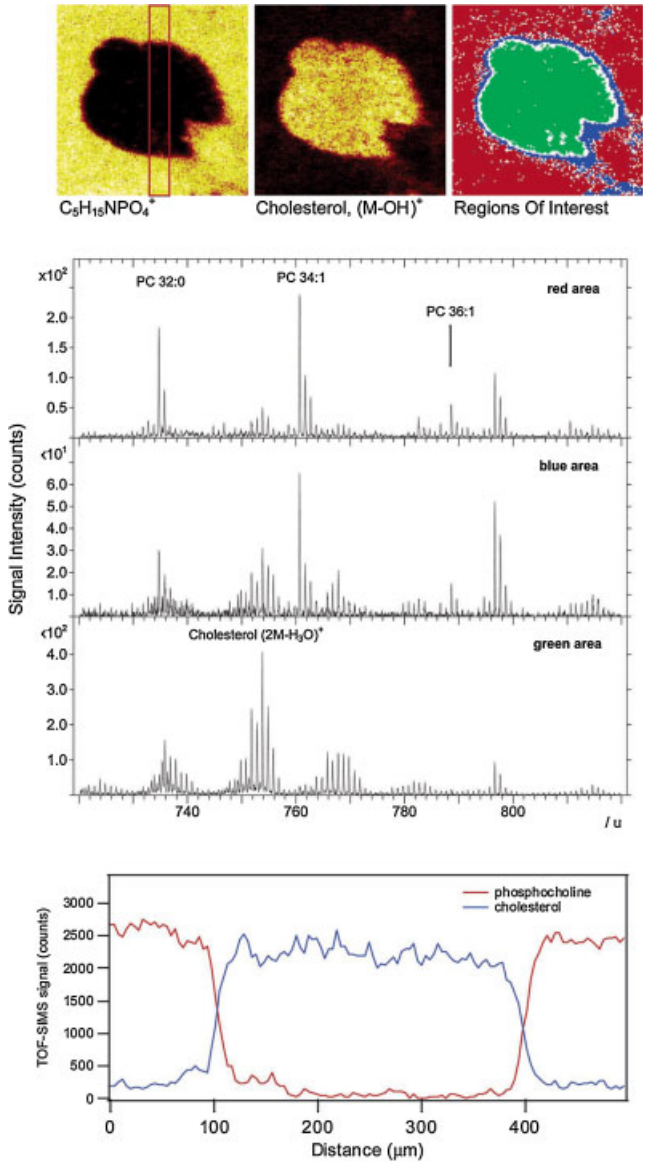


**FIGURE 20.** The **upper panel** shows the phosphocholine and cholesterol images and regions-of-interest selected using principal component analysis. The **middle panel** shows the positive TOF-SIMS spectra from each region-of-interest, and the **lower panel** shows signal intensity profiles for phosphocholine and cholesterol along the vertical direction indicated in the phosphocholine image. Reprinted with permission from Sjövall, Lausmaa, and Johansson (2004), Copyright 2004 American Chemical Society. [Color figure can be viewed in the online issue, which is available at www.interscience.wiley.com.]

demonstrated that these mass-dependent distortion fields can be experimentally determined and corrected (Pollak, Stubbings, & Hutter, 2001). Three images of the same sample, each offset by a known distance are recorded. The different positions of identifiable features are then used to calculate the distortion field for each mass.

### D. Large Area, High Resolution Imaging

In some studies, it is desirable to know the distribution of a biomolecule or pharmaceutical on both the larger scale and the smaller scale. Larger scale, or lower resolution images, indicate the tissue or organ where the molecule resides, and high-resolution images provide crucial information about its cellular localization. Several publications have shown large-scale distributions, and then recorded higher resolution images of a small region of the sample (Touboul et al., 2004a, 2005; Brunelle, Touboul, & Laprévote, 2005). This approach requires the analyst to quickly decide which region will be subject to a high resolution analysis or to repeat the experiment. Alternatively, large-area, high resolution images have been recorded by aligning many high-resolution images and then combining the data sets (Altelaar et al., 2005, 2006; McDonnell et al., 2005, 2006). One of these also includes the alignment and combining of microscope mode imaging data sets, a much more data-intensive technique for which parallel computing capabilities have been developed.

It is quite evident that there are many ongoing developments in imaging mass spectrometry in terms of ion generation, mass separation, and data processing. This improved analytical performance is being exploited in many fields. In the next section, like the preceding sections of this review, we will concentrate on biological applications, the applications currently driving imaging mass spectrometry.

## X. APPLICATIONS

SIMS has a long history in imaging of atomic and low mass ions. It has been used extensively for analyzing semi-conductors and polymeric systems, and has been applied to fields as diverse as geology, catalysis, and cultural conservation. The biological applications included here represent the application that motivates both the SIMS and MALDI communities, and for which most developments are targeted. For this reason, and to provide a rational comparison with MALDI imaging, where possible examples of SIMS imaging experiments have been limited to biological applications. The reader is directed to the most recent SIMS reviews for an overview of other SIMS applications (Adriaens, Van Vaeck, & Adams, 1999; Vickerman & Briggs, 2001).

### A. Disease

As explained in the Introduction, many ailments and immune responses are associated with altered spatial distributions and/or modified biomolecules. Figure 1 clearly showed how imaging mass spectrometry rapidly identified which proteins are associated with a tumor. Moreover, it has recently been shown how the proteomics patterns obtained directly from fresh frozen lung-tumor tissue could be used to classify histological groups and to distinguish between patients with poor or good prognoses (Yanagisawa et al., 2003).

One of the motives for recording the cholesterol and lipid images shown in Figure 14 is the increasing knowledge about the

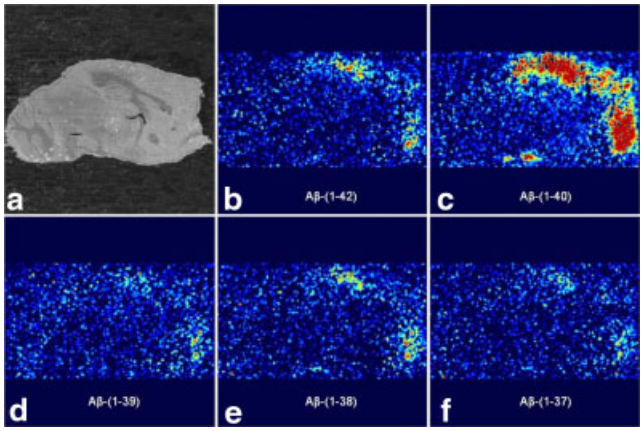


**FIGURE 21.** MALDI imaging mass spectrometry of an Alzheimer's disease model brain section. (**a**) Optical image of the sagittal AD brain section; Chemical images of the amyloid beta (Aβ) peptides, (**b**) Aβ-(1–42), *m/z* 4,515.1; (**c**) Aβ-(1–40), *m/z* 4,330.9; (**d**) Aβ-(1–39), *m/z* 4,231.7; (**e**) Aβ-(1–38), *m/z* 4,132.6; (**f**) Aβ-(1–37), *m/z* 4,075.5. Reprinted from Rohner, Staab, and Stoeckli (2004), copyright 2004, with permission from Elsevier. [Color figure can be viewed in the online issue, which is available at www.interscience.wiley.com.]

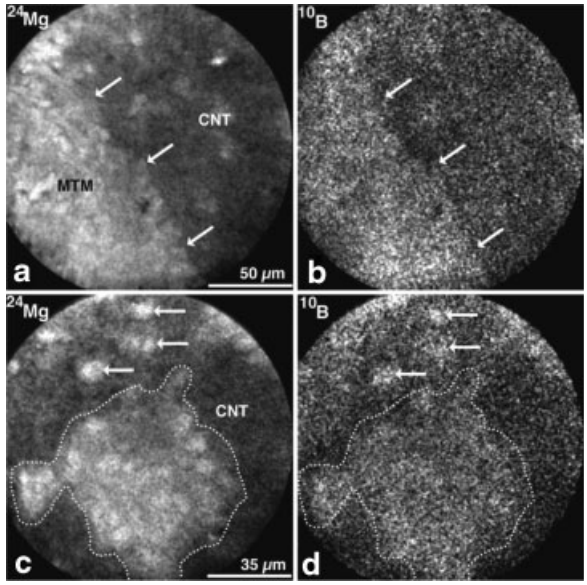


**FIGURE 22.** $^{24}$Mg and $^{10}$B distribution in the main tumor mass (MTM) and clusters of tumor cells infiltrating the normal brain of male Fischer 344 rats bearing F98 glioma. The ion images were acquired from freeze-dried 4 μm thick cryosections from two different rats. Ion images (**a**) and (**b**) show the distributions of $^{24}$Mg and $^{10}$B, respectively, after administration of *p*-boronophenylalanine with no disruption of the blood brain barrier. Ion images (**c**) and (**d**) show the $^{24}$Mg and $^{10}$B distributions in another tissue section after administration of *p*-boronophenylalanine but with disruption of the blood brain barrier. The arrows in a and b indicate an interface between a portion of the main tumor mass and normal brain tissue. The arrows in c and d, point to individual tumor cell nuclei showing significantly higher levels of $^{24}$Mg and $^{10}$B than normal brain tissue. Reprinted with permission from Smith et al. (2001), Copyright 2001 American Association for Cancer Research.

role of these compounds in various clinical disorders, such as Alzheimer's disease (Puglielli, Tanzi, & Kovacs, 2003; Cutler et al., 2004). Elevated cholesterol levels have been found to increase the levels of β-amyloid precursor protein, the abnormal accumulation of peptides derived from this protein is characteristic of all forms of Alzheimer's disease [reproduced from (Rohner, Staab, & Stoeckli, 2004)]. Figure 21 shows MALDI microprobe images of the spatial distribution of several of these peptides in brain sections taken from model rodents. These images show that amyloid beta (Aβ) peptide (1–40) is the most abundant peptide and that the peptides are principally located in two very intense areas located in the parietal and the occipital cortical lobe and a third, smaller region, close to the low part of Sylvian fissure, that is, in the hippocampus region.

Parkinson's disease, muscle damage (Touboul et al., 2004b), vitamin D deficiency (Chandra, Smith, & Morrison, 2000), different carcinomas and demyelination, which occurs in stroke victims, (Todd et al., 2001) have all been investigated using imaging mass spectrometry, and many other pathological applications continue. In addition, the requirement for targeted treatment of these ailments has lead to the use of imaging mass spectrometry in the development of the treatments. Boron neutron capture therapy is arguably the most spectacular example. Figure 22 shows high resolution dynamic SIMS images of the $^{24}$Mg and $^{10}$B distributions in the main tumor mass (MTM) and clusters of tumor cells infiltrating the contiguous normal brain tissue (CNT) of two different male rats [reproduced form (Smith et al., 2001)]. The image clearly shows the localization of boron in the tumors. Neutron capture by these boron atoms leads to the release of short-range radiation and the death of the cells containing the boron. Selective accumulation of boron in tumor cells followed by neutron capture can thus lead to selective destruction of cancer cells, and has been undergoing clinical trials in the United States, Europe, and Japan (Hatanaka & Nakagawa, 1994; Gabel et al., 1997; Nakagawa & Hatanaka, 1997; Chanana et al., 1999). Figure 23 shows the distribution of boron neutron capture therapy agents in single cells (Chandra et al., 2002).

MALDI and SIMS imaging mass spectrometry have been used to record the spatial distributions of pharmaceuticals and their metabolites in tissue. (Clerc, Fourre, & Fragu, 1997; Belu et al., 2000; Reyzer et al., 2003; Bunch, Clench, & Richards, 2004; Rohner, Staab, & Stoeckli, 2004) The tandem mass spectrometry developments of MALDI imaging mass spectrometry were instigated to distinguish pharmaceuticals from similar-mass matrix adducts (see Section VII). Figure 24 shows an impressive example of how MALDI imaging tandem mass spectrometry can be used to map pharmaceuticals and their metabolites within whole body sections. In addition to this ''final use'' aspect of pharmaceutical development, namely the mode of action of the drug, imaging mass spectrometry has been applied to drug delivery systems (Belu et al., 2000).

## B. Biology

Imaging mass spectrometry has been used to investigate several aspects of fundamental biological importance. For example, the high resolution ToF–SIMS analysis of the mating *Tetrahymena*

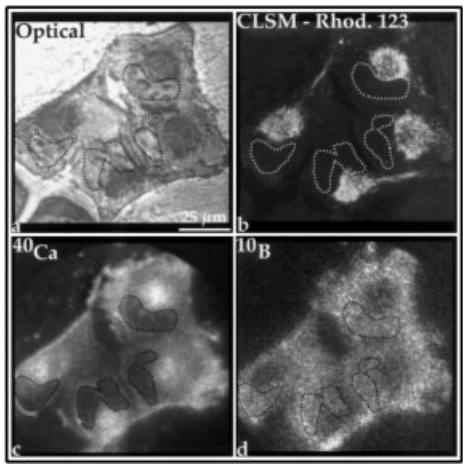


**FIGURE 23.** Confocal laser scanning microscopy (CLSM) and SIMS imaging of T98G human glioblastoma cells treated with 110 μg/mL boron equivalent of *p*-boronophenylalanine for 6 hr. For the last 30 min of this treatment, the cells were also exposed to rhodamine 123 for labeling mitochondria. A reflected light optical image (**a**) shows four fractured freeze-dried cells with discernible nuclei (dotted lines) and the perinuclear organelle-rich cytoplasmic regions. CLSM imaging of rhodamine 123 fluorescence in the same cells (**b**) reveals high density of mitochondria in the perinuclear organelle-rich regions. SIMS analysis of the same cells reveals subcellular isotopic distributions of $^{40}$Ca (**c**) and $^{10}$B (**d**). Reprinted with permission from Chandra et al. (2002), Copyright 2002 American Association for Cancer Research.

shown in Figure 10, which revealed lower concentrations of the lamellar lipid phosphatidylcholine in the areas of highly curved fused membrane. Figure 25 shows a high spatial resolution SIMS imaging study of single cells in which the $^{13}C$-labeled fatty acid oleic acid was used to follow transport of fatty acids into the cell interior where they are stored in lipid droplets (adipocytes). The concentration of labeled lipid in the intracellular lipid droplets was found to be much higher than that outside cell, whereas that in the cytoplasm was lower than that outside the cell. This was interpreted as indicating that that the free fatty acids may be pumped into the adipocytes against their electro-chemical potential (Kleinfeld, Kampf, & Lechene, 2004).

High resolution SIMS measurements using stable isotope labeling have been applied to tissue sections, cells, and model lipid systems (Kraft et al., 2006; Lechene et al., 2006). The high resolution of dynamic SIMS imaging is clearly demonstrated in Figure 26, which shows karyotypes of all 46 human chromosomes constructed out of high resolution $Mg^{2+}$ and $Ca^{2+}$ SIMS images. Next to each of the $Mg^{2+}$ images, the corresponding positive G-bands ideogram is reproduced. Several sites correlating SIMS bands with heterochromatic regions on both chromosomes ''p'' and ''q'' arms are highlighted with horizontal lines. An earlier study by the same group has revealed the crucial role of cations in determining the higher order structure of chromosomes (Strick et al., 2001).

On a larger scale, SIMS imaging of phospholipids has been used to follow the development of brain structures and to study ailments that disrupt these structures (Todd et al., 2001). The majority of MALDI imaging experiments concern brain tissue sections. MALDI imaging has also been used to study tissue sections taken from epididymis (Chaurand et al., 2003), epidermis (Bunch, Clench, & Richards, 2004), joint cartilage (Rohner, Staab, & Stoeckli, 2004), prostate (Stoeckli et al., 2001), inverterbrate ganglia (Kruse & Sweedler, 2003), and even whole body sections. These studies have revealed protein expression and their distribution, processing of the protein at specific locations and the effects of numerous pathologies.

### C. Arrays and Separations

The fast imaging capabilities of modern imaging instruments have been used to rapidly analyze combinatorial libraries and other arrays. Using modern polyatomic primary ions, molecular ions of small peptides have been localized on their respective beads (Xu et al., 2004). Moreover, the fragments typically observed with SIMS analysis permitted these peptides to sequenced, thus demonstrating the crucial issue of context for whether fragmentation is advantageous or a problem: in this example, the sequence information is useful, whereas in complex systems it limits specificity and complicates assignment. Arlinghaus and workers have exploited the highly sensitive detection of small fragment ions (of much larger molecules) to enable fast, and sensitive read-outs of DNA binding arrays: peptide nucleic (PNA) microarrays are arrays of synthetic DNA mimics that have an amide backbone instead of phosphate groups. Consequently, DNA binding can be identified by the presence of phosphate fragments in the SIMS spectra; the high ion yields associated with phosphate ions and the large number of phosphate groups in each DNA strand (intrinsic amplification of the signal) ensures high detection efficiency (Brandt et al., 2003).

## XI. COMBINING WITH OTHER IMAGING TECHNIQUES

''Analytical images are almost always obtained with the purpose of determining correspondence between at least two chemical or physical features. However, it frequently happens that only one feature is apparent with a particular type of image, and another analytical method must be used to display the complementary feature.''(Schaaff, McMahon, & Todd, 2002) The need for complementing imaging mass spectrometry experiments with additional techniques is widely appreciated.

### A. UV/VIS Imaging

UV/VIS imaging is by far the most common technique used to understand chemical images. Visual inspection, whether with high magnification microscopes or just the optical system present in the mass spectrometer, is ubiquitous. Several groups now use indium-tin-oxide-coated slides to facilitate light microscopy and imaging mass spectrometry of the same sample (Chaurand, Schwartz, & Caprioli, 2004c; Altelaar et al., 2005) and histological staining protocols compatible with MALDI have been developed (Chaurand et al., 2004a). The 3D image shown in Figure 16 demonstrated the utility of aligning imaging mass spectrometry results with visual images (Crecelius et al., 2005). Todd and workers have shown how

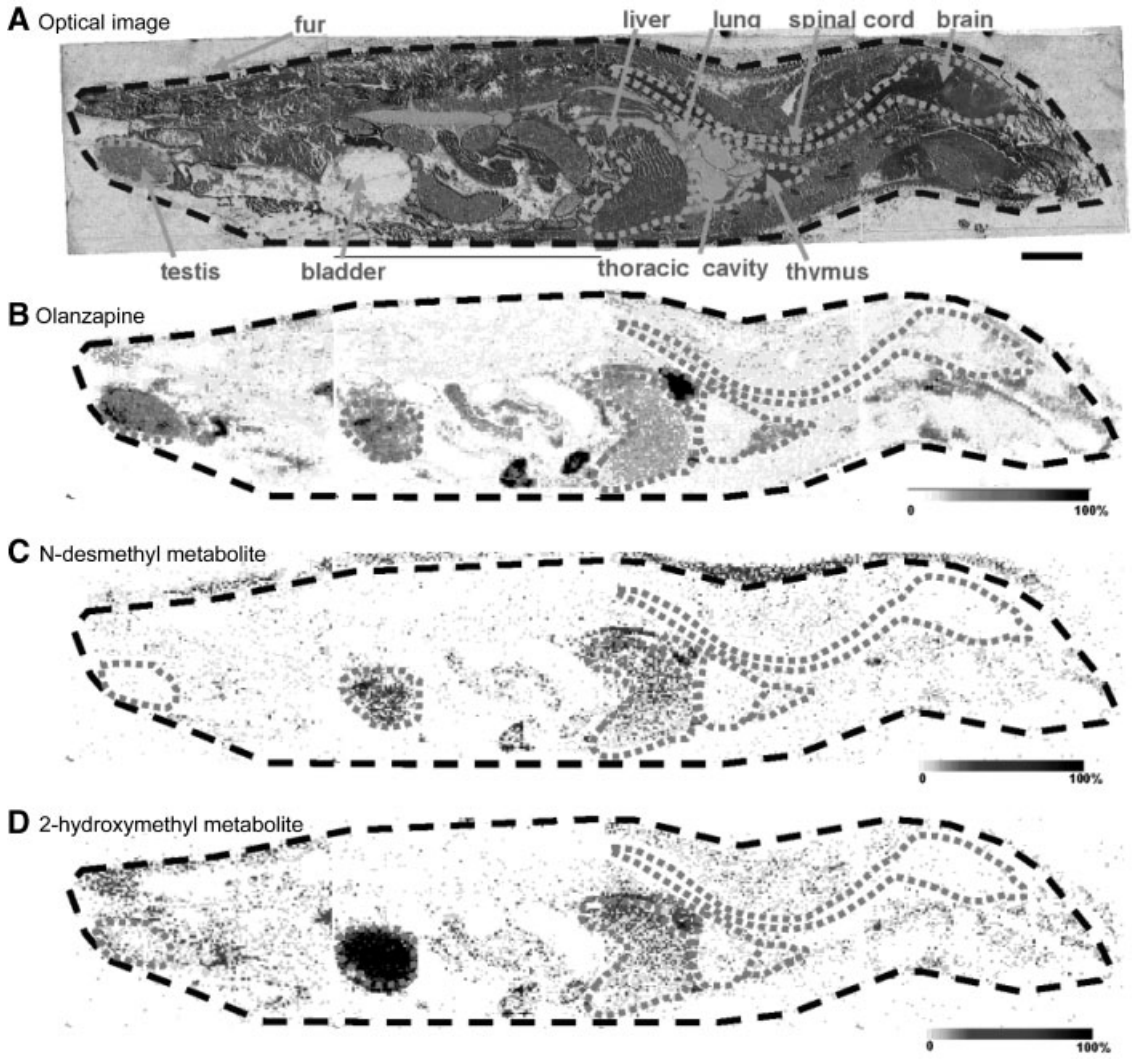


**FIGURE 24.** MALDI imaging tandem mass spectrometry is used to map the distribution of a pharmaceutical and its metabolites, ensuring they are distinguished, in a whole rat sagittal tissue section. The animal was sacrificed 6 hr after dosing with olanzapine. (**A**) Shows an optical image of the rat tissue section with the organs outlined by grey dotted lines. (**B**) Shows the distribution of the olanzapine using MS/MS for enhanced specificity, (**C**) Shows the distribution of the *N*-desmethyl metabolite using MS/MS, and (**D**) The distribution of the 2-hydroxymethyl metabolite using MS/MS. Scale bar=1 cm. Adapted with permission from Khatib-Shahidi et al. (2006), Copyright 2006 American Chemical Society.

this alignment (correlation) can be semi-automated (Schaaff, McMahon, & Todd, 2002). Finally, the high spatial resolution MALDI imaging instrument developed by Spengler and workers allows confocal microscopy of the sample using the same optical elements as those used for the MALDI imaging experiments (Spengler & Hubert, 2002).

### B. Electron Microscopy

The high-resolution images afforded by electron microscopy are frequently used to provide a microscopic view of the sample. For high spatial resolution measurements, electron microscopy images are frequently used to understand the chemical images (Keune & Boon, 2004b; Takaya et al., 2002). It has also been used to investigate sample preparation procedures for MALDI, ME-SIMS, and SIMS experiments (Sjövall et al., 2003; Hanton et al., 2004; Altelaar et al., 2005) and to characterize surface changes that occur after laser or primary ion irradiation (Fournier et al., 1997; Yamada et al., 2001; Fournier, Tabet, & Bolbach, 2002). Scanning electron microscopy studies in combination with energy dispersive X-ray analysis (SEM-EDX) is an alternative method for determining the spatial distribution of the elements.

### C. Atomic Force Microscopy

Atomic force microscopy has been used to investigate changes to the surface after irradiation (Yamada et al., 2001), to correct for

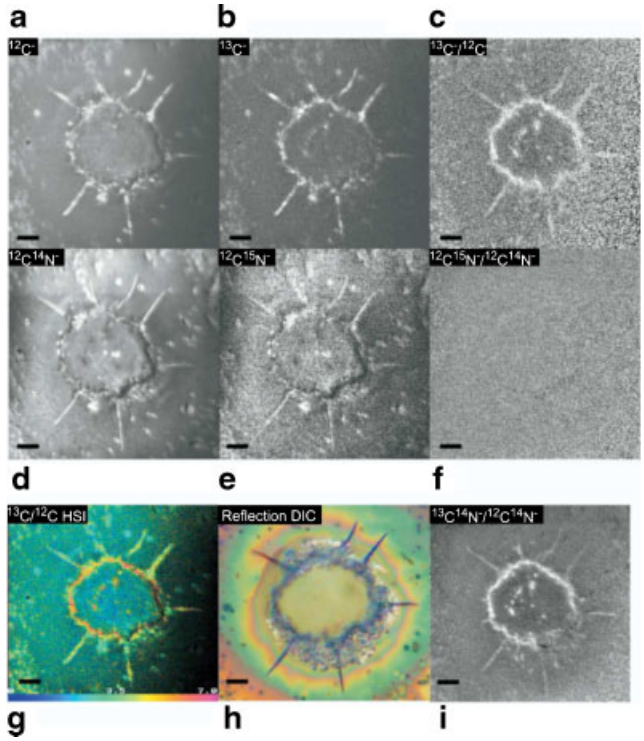


**FIGURE 25.** Unwashed 3T3F442A cells treated with $^{13}$C-oleate:bovine serum albumin. Images of cells dried with argon after incubation with $^{13}$C-oleate. (**a**–**e**) are images of $^{12}C^-$ (a), $^{13}C^-$ (b), their ratio $^{13}C/^{12}C$ (c), $^{12}C^{14}N^-$ (d), $^{12}C^{15}N^-$ (e), and their ratio $^{12}C^{15}N/^{12}C^{14}N$ (**f**). (**g**) Shows a hue saturation intensity image of the $^{13}C/^{12}C$ ratio image and (**h**) is an optical image of the same cells taken before the imaging mass spectrometry experiment. The image (**i**), $^{13}C^{14}N/^{12}C^{14}N$, reveals the excess $^{13}C$ in the lipid. The scale bar in all panels is 5 μm in length. Reprinted from Kleinfeld, Kampf, and Lechene (2004), copyright 2004, with permission from Elsevier. [Color figure can be viewed in the online issue, which is available at www.interscience.wiley.com.]

different sputter rates in 3D SIMS images (Wagter et al., 1997), and to correlate the phase behavior of lipid films with the chemical images produced using SIMS (Sostarecz et al., 2004). These examples demonstrate both qualities of AFM, quantitative topographical information, and the ability to distinguish physical attributes that can then be correlated with molecular maps.

MALDI images have been co-registered with optical (Crecelius et al., 2005) and magnetic resonance (Sinha et al., 2006) images in order combine these two techniques. The multivariate technique cross-correlation analysis has been used to combine data sets from different imaging modalities, as diverse as Fourier transform infrared imaging and SIMS. These techniques differed in spatial resolution by more than order of magnitude and analyze different molecular aspects, nevertheless cross correlation analysis allowed the spatial distribution defined by SIMS to be used to acquire region-specific IR spectral information. In this regard, cross correlation analysis techniques will allow a wide variety of imaging techniques to be applied to biological systems [see (Navratil, Mabbott, & Arriaga, 2006) for a brief review of 11 microscopy techniques] and their results compared and combined with those obtained using imaging mass spectrometry. In the near future, MALDI imaging will certainly be combined with the non-invasive imaging techniques positron emission tomography (PET), computed tomography (CT), and near infrared fluorescence (NIRF). With suitable labels, PET (Weissleder, 2006) and NIRF (Chen et al., 2002; Hintersteiner et al., 2005) have been used to record the *in-vivo* spatial distribution of peptides and proteins in living animals, and can provide early diagnosis of diseases. One can certainly envisage a future in which imaging mass spectrometry, and proteomics in general, are used to identify biomarkers of disease that are then targeted by suitable labels for *in-vivo* PET or NIRF imaging in live organisms.

## XII. SUMMARY AND OUTLOOK

The emergence of MALDI imaging mass spectrometry has provided fresh impetus to the entire field of imaging mass spectrometry. It is now commercially available and is widely used to record the spatial distributions of numerous peptide and protein ions, in parallel and without a label, from tissue sections and cells. It has been applied to study the changes in protein expression levels and distributions associated with a range of pathologies, including the age-related diseases of mounting concern in the western hemisphere, Alzheimer's, Parkinson's, and cancer. Furthermore, the same techniques are used to trace the distribution of pharmaceuticals and their metabolites within organs and complete animals, as well as to investigate the resulting changes in the organ's proteome. The potential of MALDI imaging has driven many developments covering all aspects of the experiment. Advances in data acquisition now allow fast MALDI imaging with high spatial resolution. In microprobe mode, sub micron laser spots can be combined with 1 kHz sustained data acquisitions to provide practical high-resolution capabilities. Alternatively, the MALDI ion-optical microscope can deliver similar high spatial resolution abilities for both UV and IR MALDI because the spatial information is retained from within the laser spot. This approach also circumvents the loss of sensitivity associated with highly focused lasers and is intrinsically faster than a microprobe approach.

Developments in sample preparation have also continued unabated. Gold coating and ionic matrices have significantly improved the sensitivity of MALDI analysis of tissue section samples. Multiple investigations have now established effective sample preparation procedures for a variety of tissues and spatial resolutions, and have even determined which histology stains are compatible with MALDI analysis. In these regards, MALDI imaging mass spectrometry is fast approaching critical mass. An indication of the rapidly growing interest in imaging mass spectrometry is the establishment of imaging mass spectrometry sessions in the majority of mass spectrometry conferences. The 2006 American Society of Mass Spectrometry Conference allocated two oral and two poster sessions to imaging mass spectrometry.

The new interest in imaging mass spectrometry has largely been driven by MALDI analysis of tissue sections. Yet this

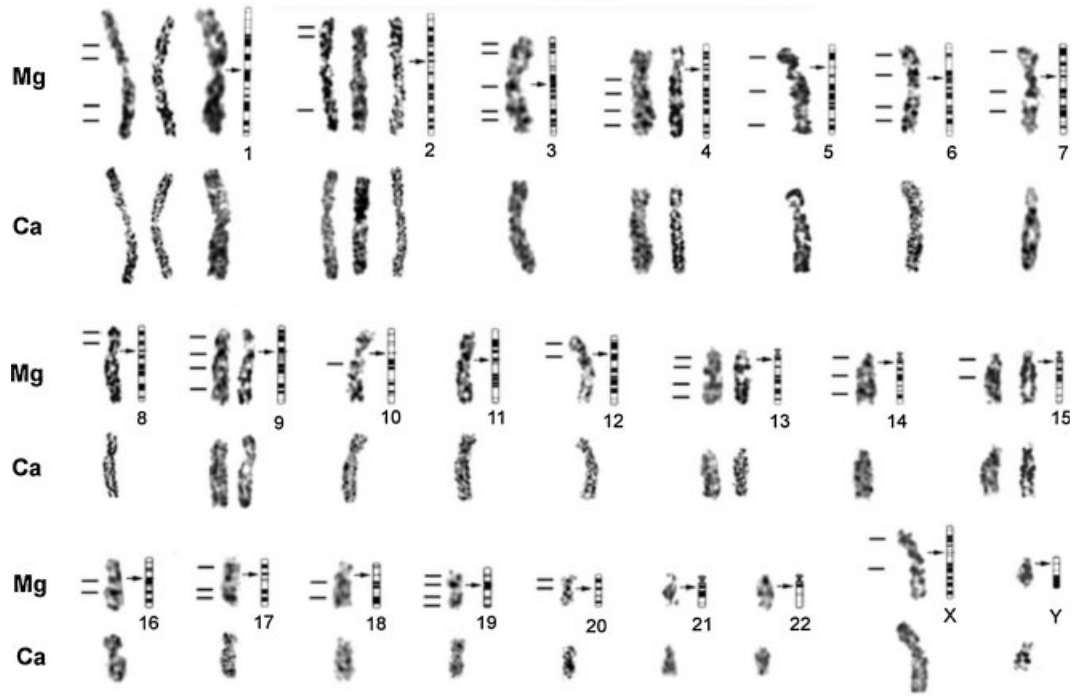


**FIGURE 26.** Karyotype for all 46 human chromosomes constructed out of $Mg^{2+}$ and $Ca^{2+}$ SIMS images. Next to each of the $Mg^{2+}$ images, the corresponding positive G-bands ideogram is reproduced. Several sites correlating SIMS bands with heterochromatic regions on both chromosomes "p" and "q" arms are highlighted with horizontal lines. Horizontal arrows point to the location of the chromosomal centromere. Reprinted from Strissel et al. (2005), Copyright 2005, with permission from Elsevier.

success has greatly reinvigorated SIMS imaging mass spectrometry. The majority of the recent developments in SIMS have concentrated on improving the sensitivity for high mass molecules, such that the high spatial resolution capabilities of established instrumentation can be exploited for sub cellular imaging of specific biomolecules. Polyatomic primary ion beams, matrix-enhanced SIMS, gold coating, and their combinations have all increased the sensitivity of SIMS for high mass molecules. It is now possible to record the spatial variation of lipids, cholesterol, ceramides, and vitamins within single cells and tissue sections, using their chemically diagnostic molecular ions. Several groups now use the complementary information provided by SIMS and MALDI to obtain proteomics, lipid, and vitamin distributions within the same tissue section. The low ion doses of a static SIMS experiment ensure there is sufficient material remaining for a subsequent MALDI experiment.

Many of the developments outlined in this review can be combined, the results can then be analyzed using multivariate techniques or combined with information from other imaging techniques using cross correlation analysis. These results can then be compared with the results of global proteomics/lipidomics strategies applied to spatially resolved samples, either through voxelization, laser-capture microdissection, or any other sample preparation protocol. It is this potential, which is slowly being fulfilled, to obtain extensive spatially resolved biomolecular information, an absolute necessity for a thorough picture of the molecular processes underpinning biological and pathological processes or to track the distribution of pharmaceuticals that is attracting ever more interest.

## ACKNOWLEDGMENTS

This work is part of research program nr. 49 "Mass spectrometric imaging and structural analysis of biomacromolecules" of the "Stichting voor Fundamenteel Onderzoek der Materie (FOM)", which is financially supported by the "Nederlandse organisatie voor Wetenschappelijk Onderzoek (NWO)."

## REFERENCES

Adriaens A, Van Vaeck L, Adams F. 1999. Static secondary ion mass spectrometry (S-SIMS) Part 2: Material science applications. Mass Spectom Rev 18:48–81.

Adriaensen L, Vangaever F, Gijbels R. 2004a. Metal-assisted secondary ion mass spectrometry: Influence of Ag and Au deposition on molecular ion yields. Anal Chem 76:6777–6785.

Adriaensen L, Vangaever F, Gijbels R. 2004b. Organic SIMS: The influence of time on the ion yield enhancement by silver and gold deposition. Appl Surf Sci 231-232:256–260.

Adriaensen L, Vangaever F, Lenaerts J, Gijbels R. 2006. S-SIMS and MetA-SIMS study of organic additives in thin polymer coatings. Appl Surf Sci 252:6628–6631.

Aebersold R, Mann M. 2003. Mass spectrometry-based proteomics. Nature Insights 422:198–207.

Aksyonov SA, Williams P. 2001. Impact desolvation of electrosprayed microdroplets—A new ionization method for mass spectrometry of large biomolecules. Rapid Commun Mass Spectrom 15:2001–2006.

Altelaar AFM, Minnen Jv, Jiménez CR, Heeren RMA, Piersma SR. 2005. Direct molecular imaging of lymnaea stagnalis nervous tissue at subcellular spatial resolution by mass spectrometry. Anal Chem 77:735–741.

Altelaar AFM, Klinkert I, Jalink K, de Lange RPJ, Adan RAH, Heeren RMA, Piersma SR. 2006. Gold-enhanced biomolecular surface imaging of cells and tissue by SIMS and MALDI mass spectrometry. Anal Chem 78:734–742.

Alves S, Kalberer M, Zenobi R. 2003. Direct detection of particles formed by laser ablation of matrices during matrix-assisted laser desorption/ionization. Rapid Comm Mass Spectrom 17:2034–2038.

Amado FML, Domingues P, Santana-Marques MG, Ferrer-Correia AJ, Tomer aKB. 1997. Discrimination effects and sensitivity variations in matrix-assisted laser desorption/ionization. Rapid Commun Mass Spectrom 11:1347–1352.

Anderson HH, Bay HL. 1974. Nonlinear effects in heavy-ion sputtering. J Appl Phys 45:953–954.

Appelhans AD, Delmore JE. 1989. Comparison of polyatomic and atomic primary beams for secondary ion mass spectrometry of organics. Anal Chem 61:1087–1093.

Arlinghaus HF, Fartmann M, Kriegeskotte C, Dambach S, Wittig A, Sauerwein W, Lipinsky D. 2004. Subcellular imaging of cell cultures and tissue for boron localization with laser-SNMS. Surf Interface Anal 36:698–701.

Arlinghaus HF, Kriegeskotte C, Fartmann M, Wittig A, Saurwein W, Lipinsky D. 2006. Mass spectrometric characterization of elements and molecules in cell cultures and tissues. Appl Surf Sci 252:6941–6948.

Bastiaens PIH, Pepperkok R. 2000. Observing proteins in their natural habitat: The living cell. TIBS 25:631–637.

Beavis RC, Chait BT. 1991. Velocity distributions of intact high mass polypeptide molecule ions produced by matrix assisted laser desorption. Chem Phys Lett 181:479–484.

Beck KM, Hess WP. http://www.emsl.pnl.gov/instruments/instrument_pages/1029.html.

Belov ME, Myatt CP, Derrick PJ. 1998. Chemical ionization of neutral peptides produced by matrix-assisted laser desorption. Chem Phys Lett 284:412–418.

Belu AM, Davies MC, Newton JM, Patel N. 2000. TOF-SIMS characterization and imaging of controlled-release drug delivery systems. Anal Chem 72:5625–5638.

Benguerba M, Brunelle A, Della-Negra S, Depauw J, Joret H, Le Beyec Y, Blain MG, Schweikert EA, Assayag GB, Sudraud P. 1991. Impact of slow gold clusters on various solids: Nonlinear effects in secondary ion emission. Nucl Instr Meth Phys Res B 62:8–22.

Benninghoven A. 1970. Die analyse monomolekularer Festkörperoberflächenschichten mit Hilfe der Sekundärionenemission. Z Physik 230: 403–417.

Benninghoven A. 1987. Secondary ion mass spectrometry. New York: J. Wiley.

Bergquist J, Palmblad M, Wetterhall M, Håkansson P, Markides K. 2002. Peptide mapping of proteins in human body fluids using electrospray ionization Fourier transform ion cyclotron resonance mass spectrometry. Mass Spectrom Rev 21:2–15.

Biesinger MC, Paepegaey P-Y, McIntyre NS, Harbottle RR, Peterson NO. 2002. Principal component analysis of TOF-SIMS images of organic monolayers. Anal Chem 74:5711–5716.

Binz P-A, Müller M, Walther D, Bienvenut WV, Gras R, Hoogland C, Bouchet G, Gasteiger E, Fabbretti R, Gay S, Palagi P, Wilkins MR, Rouge V, Tonella L, Paesano S, Rossellat G, Karmime A, Bairoch A, Sanchez J-C, Appel RD, Hochstrasser DF. 1999. A molecular scanner to automate proteomic research and to display proteome images. Anal Chem 71:4981–4988.

Blain MG, Della-Negra S, Joret H, Le Beyec Y, Schweikert EA. 1989a. Desorption yields using KeV polyatomic projectiles. J Phys-Paris 50:147–153.

Blain MG, Della-Negra S, Joret H, Le Beyec Y, Schweikert EA. 1989b. Secondary-ion yields from surfaces bombarded with keV molecular and cluster ions. Phys Rev Lett 63:1625–1628.

Blain MG, Della-Negra S, Joret H, Le Beyec Y, Schweikert EA. 1990. A new experimental-method for determining ion yields from surfaces bombarded by complex heterogeneous ions. J Vac Sci Technol 8:2265–2268.

Bouschen W, Kirsch D, Maass K, Spengler B. 2003. 16th International Mass Spectrometry Conference, Edinburgh, UK, August 31–September 5 2003.

Brandt O, Feldner J, Stephan A, Schröder M, Schnölzer M, Arlinghaus HF, Hoheisel JD, Jacob A. 2003. PNA microarrays for hybridisation of samples. Nucleic Acids Res 31:e119.

Breuker K, Knochenmuss R, Zhang J, Stortelder A, Zenobi R. 2003. Thermodynamic control of final ion distributions in MALDI: In-plume proton transfer reactions. Int J Mass Spectrom 226:211–222.

Briggs D, Seah MP. 1992. Practical surface analysis. Chichester: J. Wiley.

Broersen A, van Liere R. 2006. IEEE-VGTC Symposium on Visualization.

Brown RS, Lennon JJ. 1995. Mass resolution improvement by incorporation of pulsed ion extraction in a matrix-assisted laser desorption/ionization linear time-of-flight mass spectrometer. Anal Chem 67:1998–2003.

Brunelle A, Touboul D, Laprévote O. 2005. Biological tissue imaging with time-of-flight secondary ion mass spectrometry and cluster ion sources. J Mass Spectrom 40:985–999.

Bunch J, Clench MR, Richards DS. 2004. Determination of pharmaceutical compounds in skin by imaging matrix-assisted laser desorption/ionisation mass spectrometry. Rapid Commun Mass Spectrom 18: 3051–3060.

Cannon DM Jr, Pacholski ML, Winograd N, Ewing AG. 2000. Molecule specific imaging of freeze-fractured, frozen-hydrated model membrane systems using mass spectrometry. J Am Chem Soc 122:603–610.

Castaing R, Slodzian G. 1962. Microanalyse par émission ionique secondaire. Journal de Microscopie 1:395–410.

Cech NB, Enke CG. 2001. Practical implications of some recent studies in electrospray ionization fundamentals. Mass Spectom Rev 20:362–387.

Chabala JM, Soni KK, Li J, Gavrilov KL, Levi-Setti R. 1995. High-resolution chemical imaging with scanning ion probe SIMS. Int J Mass Spectrom 143:191–212.

Chanana AD, Capala J, Chadha M, Coderre JA, Diaz AZ, Elowitz EH, Iwai J, Joel DD, Liu HB, Ma R, Pendzick N, Peress NS, Shady MS, Slatkin DN, Tyson GW, Wielopolski L. 1999. Boron neutron capture therapy for glioblastoma multiforme: Interim results from the phase I/II dose-escalation studies. Neurosurgery (Baltimore) 44:1182–1193.

Chandra S. 2001. The discovery of a cell division regulated calcium entry phenomenon in mammalian cells with the isotopic imaging technique of ion microscopy. Mol Biol Cell 12 (Suppl):141S.

Chandra S, Smith DR, Morrison GH. 2000. Subcellular imaging by dynamic SIMS ion microscopy. Anal Chem 72:104A–114A.

Chandra S, Kabalka GW, Lorey DR II, Smith DR, Coderre JA. 2002. Imaging of fluorine and boron from fluorinated boronophenylalanine in the same cell at organelle resolution by correlative ion microscopy and confocal laser scanning microscopy. Clin Cancer Res 8:2675–2683.

Chatterjee R, Postawa Z, Winograd N, Garrison BJ. 1999. Molecular dynamics simulation study of molecular ejection mechanisms: keV particle bombardment of $C_6H_6$/Ag{111}. J Phys Chem B 103:151–163.

Chaurand P, Fouchécourt S, Da Gue BB, Xu BJ, Reyzer ML, Orgebin-Crist M-C, Caprioli RM. 2003. Profiling and imaging proteins in the mouse epididymis by imaging mass spectrometry. Proteomics 3:2221–2239.

Chaurand P, Schwartz SA, Billheimer D, Xu BJ, Crecelius A, Caprioli RM. 2004a. Integrating histology and imaging mass spectrometry. Anal Chem 76:1145–1155.

Chaurand P, Schwartz SA, Caprioli RM. 2004b. Assessing protein patterns in disease using imaging mass. J Proteome Res 3:245–252.

Chaurand P, Schwartz SA, Caprioli RM. 2004c. Profiling and imaging proteins in tissue sections by MS. Anal Chem 76:86A–93A.

Che F-Y, Lim J, Pan H, Biswas R, Fricker LD. 2005. Quantitative neuropeptidomics of microwave-irradiated mouse brain and pituitary. Mol Cell Proteom 4:1391–1405.

Chen J, Tung C-H, Mahmood U, Ntziachristos V, Gyurko R, Fishman MC, Huang PL, Weissleder R. 2002. In vivo imaging of proteolytic activity in atherosclerosis. Circulation 105:2766–2771.

Cheng J, Wucher A, Winograd N. 2006. Molecular depth profiling with cluster ion beams. J Phys Chem B 110:8329–8336.

Clerc J, Fourre C, Fragu P. 1997. SIMS microscopy: Methodology, problems and perspectives in mapping drugs and nuclear medicine compounds. Cell Bio Int 21:619–633.

Cliff B, Lockyer N, Jungnickel H, Stephens G, Vickerman JC. 2003. Probing cell chemistry with time-of-flight secondary ion mass spectrometry: Development and exploitation of instrumentation for studies of frozen-hydrated biological material. Rapid Commun Mass Spectrom 17: 2163–2167.

Cohen SL, Chait BT. 1996. Influence of matrix solution conditions on the MALDI-MS analysis of peptides and proteins. Anal Chem 68:31–37.

Colliver TL, Brummel CL, Pacholski ML, Swanek FD, Ewing AG, Winograd N. 1997. Atomic and molecular imaging at the single-cell level with TOF-SIMS. Anal Chem 69:2225–2231.

Corr JJ, Kovarik P, Schneider BB, Hendrikse J, Loboda A, Covey TR. 2006. Design considerations for high speed quantitative mass spectrometry with MALDI ionization. J Am Soc Mass Spectrom 17:1129–1141.

Cotter RJ. 1999. The new time-of-flight mass spectrometry. Anal Chem 445A–451A.

Crecelius AC, Cornett DS, Caprioli RM, Williams B, Dawant BM, Bodenheimer B. 2005. Three-dimensional visualization of protein expression in mouse brain structures using imaging mass spectrometry. J Am Soc Mass Spectrom 16:1093–1099.

Cutler RG, Kelly J, Storie K, Pedersen WA, Tammara A, Hatanpaa K, Troncoso JC, Mattson MP. 2004. Involvement of oxidative stress-induced abnormalities in ceramide and cholesterol metabolism in brain aging and Alzheimer's disease. PNAS 101: 2070–2075.

Dambach S, Fartmann M, Kriegeskotte C, Brüning C, Hellweg S, Wiesmann HP, Lipinsky D, Arlinghaus HF. 2004. ToF-SIMS and laser-SNMS analysis of apatite formation in extracellular protein matrix of osteoblasts in vitro. Surf Interface Anal 36:711–715.

Delcorte A. 2001. Fundamental aspects of organic SIMS. In: Vickerman JC, Briggs D, editors. ToF-SIMS: Surface analysis by mass spectrometry. Chichester: IM Publications. pp 161–194.

Delcorte A, Bertrand P. 2005. Metal salts for molecular ion yield enhancement in organic secondary ion mass spectrometry: A critical assessment. Anal Chem 77:2107–2115.

Delcorte A, Garrison BJ. 2000. High yield events of molecular emission induced by kiloelectron particle bombardment. J Phys Chem B 104: 6785–6800.

Delcorte A, Garrison BJ. 2003. Particle-induced desorption of kilodalton molecules embedded in a matrix: A molecular dynamics study. J Phys Chem B 107:2297–2310.

Delcorte A, Garrison BJ. 2004. Kiloelectronvolt argon-induced molecular desorption from a bulk polystyrene solid. J Phys Chem B 108:1562–15661.

Delcorte A, Segda BG, Garrison BJ, Bertrand P. 2000. Inferring ejection distances and a surface energy profile in keV particle bombardment experiments. Nucl Instr Meth Phys Res B 171:277–290.

Delcorte A, Bour J, Aubriet F, Muller J-F, Bertrand P. 2003. Sample metallization for performance improvement in desorption/ionization of kilodalton molecules: Quantitative evaluation, imaging secondary ion MS, and laser ablation. Anal Chem 75:6875–6885.

Demirev PA, Eriksson J, Zubarev RA, Papaléo R, Brinkmalm G, Håkansson P, Sundqvist BUR. 1994. Ion desorption from organic and inorganic targets induced by 100 keV gold cluster ions. Nucl Instr Meth Phys Res B 88:138–142.

Diehnelt CW, van Stipdonk MJ, Schweikert EA. 2001. Effectiveness of atomic and polyatomic primary ions for organic secondary ion mass spectrometry. Int J Mass Spectrom 207:111–122.

Dreger M. 2003. Subcellular proteomics. Mass Spectom Rev 22:27–56.

Dreisewerd K. 2003. The desorption process in MALDI. Chem Rev 103:395–425.

Durrant SF. 1999. Laser ablation inductively coupled plasma mass spectrometry: Achievements, problems, prospects. J Anal At Spect 14:1385–1403.

Durrant SF, Ward NI. 2005. Recent biological and environmental applications of laser ablation inductively coupled plasma mass spectrometry (LA-ICP-MS). J Anal At Spect 20:821–829.

Edirisinghe PD, Lateef SS, Crot CA, Hanley L, Pellin MJ, Calaway WF, Moore JF. 2004. Derivatization of surface-bound peptides for mass spectrometric detection via threshold single photon ionization. Anal Chem 76:4267–4270.

Ens W, Piyadasa G, Collado V, Krokhi O, Loboda A, McNabb JR, Qiao H, Spicer V, Standing KG. 2005. 53rd ASMS conference on mass spectrometry, San Antonio.

ESI special issue. 2000. Anal Chim Acta 406:1–118.

Fenn JB, Mann M, Meng CK, Wong SF, Whitehouse CM. 1989. Electrospray ionization for mass-spectrometry of large biomolecules. Science 246:64–71.

Forbes AJ, Patrie SM, Taylor GK, Kim YB, Jiang LH, Kelleher NL. 2004. Targeted analysis and discovery of posttranslational modifications in proteins from methanogenic archaea by top-down MS. Proc Natl Acad Sci U.S.A 101:2678–2683.

Fournier I, Beavis RC, Blais JC, Tabet JC, Bolbach G. 1997. Hysteresis effects observed in MALDI using oriented, protein-doped matrix crystals. Int J Mass Spectrom 169/170:19–29.

Fournier I, Tabet JC, Bolbach G. 2002. Irradiation effects in MALDI and surface modifications Part I: Sinapinic acid monocrystals. Int J Mass Spectrom 219:515–523.

Fuoco ER, Gillen G, Wijesundara MBJ, Wallace WE, Hanley L. 2001. Surface analysis studies of yield enhancements in secondary ion mass spectrometry by polyatomic projectiles. J Phys Chem B 105:3950–3956.

Gabel D, Preusse D, Haritz D, Grochulla F, Haselsberger K, Frankhauser H, Ceberg C, Peters H-D, Klotz U. 1997. Pharmacokinetics of $Na_2B_{12}H_{11}SH$ (BSH) in patients with malignant brain tumors as prerequisite for a Phase I clinical trial of boron neutron capture therapy. Acta Neurochir 139:606–612.

Garrison BJ, Delcorte A, Zhigilei LV, Itina TE, Krantzman KD, Yingling YG, McQuaw CM, Smiley EJ, Winograd N. 2002. Big molecule ejection—SIMS vs. MALDI. Appl Surf Sci 203:1–4.

Georgiou S, Hillenkamp F. guest editors. 2003. Laser ablation of molecular substrates. Chem Rev 103:317–644.

Gillen G, Roberson S. 1998. Preliminary evaluation of an $SF_5^+$ polyatomic primary ion beam for analysis of organic thin films by secondary ion mass spectrometry. Rapid Commun Mass Spectrom 12:1303–1312.

Gilmore IS, Seah MP. 2000a. Ion detection efficiency in SIMS: Dependencies on energy, mass and composition for microchannel plates used in mass spectrometry. Int J Mass Spectrom 202:217–229.

Gilmore IS, Seah MP. 2000b. Static SIMS: Toward unfragmented mass spectra—The G-SIMS procedure. Appl Surf Sci 161:465–480.

Gilmore IS, Seah MP. 2002. Electron flood gun damage in the analysis of polymers and organics in time-of-flight SIMS. Appl Surf Sci 187:89–100.

Groenewold GS, Gianotto AK, Olson JE, Appelans AD, Ingram JC, Delmore JE, Shaw AD. 1998. Static SIMS investigation of tetraethylammonium bromide on soil particles using $REO_4^-$ and $Ga^+$ projectiles. Int J Mass Spectrom Ion Proc 174:129–142.

Grønlund F, Moore WJ. 1960. Sputtering of silver by light ions with energies from 2 to 12 kev. J Chem Phys 32:1540–1545.

Grovenor CRM, Smart KE, Kilburn M, Shore B, Dilworth JR, Martin B, Hawes C, Rickaby REM. 2006. Specimen preparation and calibration for nanoSIMS analysis of biological materials. Appl Surf Sci 252: 6917–6924.

Guilhaus M, Mlynski V, Selby D. 1997. Perfect timing time-of-flight mass spectrometry. Rapid Commun Mass Spectrom 11:951–962.

Guilhaus M, Selby D, Mlynski V. 2000. Orthogonal acceleration time-of-flight mass spectrometry. Mass Spectom Rev 19:65–107.

Guilliot S, Chaurand P, Stoeckli M, Caprioli RM. 1999. 47th ASMS Conference, Dallas.

Hanahan D, Weinberg RA. 2000. The hallmarks of cancer. Cell 100:57–70.

Hanton SD, Cornelio Clark PA, Owens KG. 1999. Investigations of matrix-assisted laser desorption/ionization sample preparation by time-of-flight secondary ion mass spectrometry. J Am Soc Mass Spectrom 10:104–111.

Hanton SD, Hyder IZ, Stets JR, Owens KG, Blair WR, Guttman CM, Giuseppetti AA. 2004. Investigations of electrospray sample deposition for polymer MALDI mass spectrometry. J Am Soc Mass Spectrom 15: 168–179.

Hatanaka H, Nakagawa Y. 1994. Clinical results of long-surviving brain tumor patients who underwent boron neutron capture therapy. Int J Radiat Oncol Biol Phys 28:1061–1066.

Heck AJR, van den Heuvel RHH. 2004. Investigation of intact protein complexes by mass spectrometry. Mass Spectom Rev 23:368–389.

Henry M, Dupont-Gillain C, Bertrand P. 2003. Conformation change of albumin adsorbed on polycarbonate membranes as revealed by ToF-SIMS. Langmuir 19:6271–6276.

Hillenkamp F, Unsold E, Kaufmann R, Nitsche R. 1975. Laser microprobe mass analysis of organic materials. Nature 256:119–120.

Hintersteiner M, Enz A, Frey P, Jaton A-L, Kinzy W, Kneuer R, Neumann U, Rudin M, Staufenbiel M, Stoeckli M, Wiederhold K-H, Gremlich H-U. 2005. *In vivo* detection of amyloid-beta deposits by near-infrared imaging using an oxazine-derivative probe. Nature Biotechnol 23:577–583.

Hofstadler SA, Sannes-Lowery KA, Hannis JC. 2005. Analysis of nucleic acids by FTICR MS. Mass Spectom Rev 24:265–285.

Horneffer V, Forsmann A, Strupat K, Hillenkamp F, Kubitscheck U. 2001. Localization of analyte molecules in MALDI preparations by confocal laser scanning microscopy. Anal Chem 73:1016–1022.

Horneffer V, Reichelt R, Strupat K. 2003. Protein incorporation into MALDI-matrix crystals investigated by high resolution field emission scanning electron microscopy. Int J Mass Spectrom 226:117–131.

Hutter H, Nowikow K, Gammer K. 2001. Visualization of 3D-SIMS measurements. Appl Surf Sci 179:161–166.

Johar SS, Thompson DA. 1979. Spike effects in heavy-ion sputtering of Ag, Au and Pt thin-films. Surf Sci 90:319–330.

Jurchen JC, Rubakhin SS, Sweedler JV. 2005. MALDI-MS imaging of features smaller than the size of the laser beam. J Am Soc Mass Spectrom 16:1654–1659.

Karas M, Krüger R. 2003b. Ion formation in MALDI: The cluster ionization mechanism. Chem Rev 103:427–439.

Karas M, Bachmann D, Bahr U, Hillenkamp F. 1987. Matrix-assisted ultraviolet laser desorption of non-volatile compounds. Int J Mass Spectrom Ion Proc 78:53–68.

Karas M, Bahr U, Fournier I, Glückmann M, Pfenninger A. 2003a. The initial-velocity as a marker for different desorption-ionization mechanisms in MALDI. Int J Mass Spectrom 226:239–248.

Kebarle P. 2000. A brief overview of the present status of the mechanisms involved in electrospray mass spectrometry. J Mass Spectrom 35:804–817.

Kelleher NL, Zubarev RA, Bush K, Furie B, Furie BC, McLafferty FW, Walsh CT. 1999. Localization of labile postranslational modifications by electron capture dissociation: The case of gamma-carboxyglutamic acid. Anal Chem 71:4250–4253.

Keune K, Boon JJ. 2004a. Enhancement of the static SIMS secondary ion yields if lipid moieties by ultrathin gold coating of aged oil paint surfaces. Surf Interface Anal 36:1620–1628.

Keune K, Boon JJ. 2004b. Imaging secondary ion mass spectrometry of a paint cross section taken from an early Netherlandish painting by Rogier van der Weyden. Anal Chem 76:1374–1385.

Khatib-Shahidi S, Andersson M, Herman JL, Gillespie TA, Caprioli RM. 2006. Direct molecular analysis of whole-body animal tissue sections by imaging MALDI mass spectrometry. Anal Chem 78:6448–6456.

Kiernan UA, Nedelkov D, Tubbs KA, Niederkofler EE, Nelson RW. 2004. Proteomic characterization of novel serum amyloid P component variants from human plasma and urine. Proteomics 4:1825–1829.

King BV, Zimmermann C, Riederer DE, Rosencrance SW, Garrison BJ, Winograd N. 1998. Angle and energy distributions of neutral atoms sputtered from $Ni_3Al(100)$. Rapid Commun Mass Spectrom 12:1236–1240.

Kleinfeld AM, Kampf JP, Lechene C. 2004. Transport of $^{13}C$-oleate in adipocytes measured using multi imaging mass spectrometry. J Am Soc Mass Spectrom 15:1572–1580.

Knochenmuss R, Zenobi R. 2003. MALDI ionization: The role of in-plume processes. Chem Rev 103:441–452.

Kollmer F, Bourdos N, Kamischke R, Benninghoven A. 2003. Nonresonant Laser-SNMS and TOF-SIMS analysis of sub-mm particles. Appl Surf Sci 203-204:238–243.

Kötter F, Benninghoven A. 1998. Secondary ion emission from polymer surfaces under $Ar^+$, $Xe^+$ and $SF_5^+$ ion bombardment. Appl Surf Sci 133:47–57.

Kraft ML, Weber PK, Longo ML, Hutcheon ID, Boxer SG. 2006. Phase separation of lipid membranes analyzed with high-resolution secondary ion mass spectrometry. Science 313:1948–1951.

Krude H, Grüters A. 2000. Implications of proopiomelanocortin (POMC) mutations in humans: The POMC deficiency syndrome. TEM 11:15–21.

Kruse R, Sweedler JV. 2003. Spatial profiling invertebrate ganglia using MALDI MS. J Am Soc Mass Spectrom 14:752–759.

Kumar A, Agarwal S, Heyman JA, Matson S, Heidtman M, Piccirillo S, Umansky L, Drawid A, Jansen R, Liu Y, Cheung K-H, Miller P, Gerstein M, Roeder GS, Snyder M. 2002. Subcellular localization of the yeast proteome. Genes Dev 16:707–719.

Lechene C, Hillion F, McMahon G, Benson D, Kleinfeld AM, Kampf JP, Distel D, Luyten Y, Bonventre J, Hentschel D, Park KM, Ito S, Schwartz M, Benichou G, Slodzian G. 2006. High-resolution quantitative imaging of mammalian and bacterial cells using stable isotope mass spectrometry. J Biol 5:20.

Lee JW, Kim KJ, Kim HK, Moon DW. 2005. Deconvolution of SIMS depth profiles of As multiple delta layers in silicon. Surf Interface Anal 37: 176–180.

Lemaire R, Tabet JC, Ducoroy P, Hendra JB, Salzet M, Fournier I. 2006. Solid ionic matrixes for direct tissue analysis and MALDI imaging. Anal Chem 78:809–819.

Liebl H. 1967. Ion microprobe mass analyzer. J Appl Phys 38:5277–5283.

Lockyer NP. 2001. Laser post-ionisation for molecular analysis. In: Vickerman JC, Briggs D, editors. ToF-SIMS: Surface analysis by mass spectrometry. Chichester: IM Publications. pp 347–443.

Loo JA. 1997. Studying noncovalent protein complexes by electrospray ionization mass spectrometry. Mass Spectom Rev 16:1–23.

Loo RRO, Hayes R, Yang YN, Hung F, Ramachandran P, Kim N, Gunsalus R, Loo JA. 2005. Top-down, bottom-up, and side-to-side proteomics with virtual 2-D gels. Int J Mass Spectrom 240:317–325.

Luxembourg SL, Heeren RMA. 2006. Fragmentation at and above surfaces in SIMS: Effects of biomolecular yield enhancing surface modifications. Int J Mass Spectrom 253:181–192.

Luxembourg SL, McDonnell LA, Duursma M, Guo X, Heeren RMA. 2003. Effect of local matrix crystal variations in matrix-assisted ionization techniques for mass spectrometry. Anal Chem 75:2333–2341.

Luxembourg SL, Mize TH, McDonnell LA, Heeren RMA. 2004. High-spatial resolution mass spectrometric imaging of peptide and protein distributions on a surface. Anal Chem 76:5339–5344.

Luxembourg SL, McDonnell LA, Mize TH, Heeren RMA. 2005. Infrared mass spectrometric imaging below the diffraction limit. J Proteome Res 4:671–673.

Maharrey S, Bastasz R, Behrens R, Highley A, Hoffer S, Kruppa G, Whaley J. 2004. High mass resolution SIMS. Appl Surf Sci 231-232:972–975.

Mahoney JF, Perel J, Ruatta SA, Martino PA, Husain S, Lee TD. 1991. Massive cluster impact mass spectrometry: A new desorption method for the analysis of large biomolecules. Rapid Commun Mass Spectrom 5:441–445.

Mahoney JF, Perel J, Lee TD, Martino PA, Williams P. 1992. Schock wave model for sputtering biomolecules using massive cluster impacts. J Am Soc Mass Spectrom 3:311–317.

Manabe T. 2003. Analysis of complex protein-polypeptide systems for proteomic studies. J Chromatog B 787:29–41.

McCombie G, Staab D, Stoeckli M, Knochenmuss R. 2005. Spatial and spectral correlations in MALDI mass spectrometry images by clustering and multivariate analysis. Anal Chem 77:6118–6124.

McDonnell LA, Luxembourg SL, Mize TH, Koster S, Eijkel GB, Verpoorte E, de Rooij NF, Heeren RMA. 2003. Using matrix peaks to map topography: Increased mass resolution and enhanced sensitivity in chemical imaging. Anal Chem 75:4373–4381.

McDonnell LA, Piersma SR, Altelaar AFM, Mize TH, Luxembourg SL, Verhaert PDEM, van Minnen J, Heeren RMA. 2005. Subcellular imaging mass spectrometry of brain tissue. J Mass Spectrom 40:160–168.

McDonnell LA, Heeren RMA, de Lange RPJ, Fletcher IW. 2006. Higher sensitivity secondary ion mass spectrometry of biological molecules for high resolution, chemically specific imaging. J Am Soc Mass Spectrom 17:1195–1202.

McLean JA, Russell WK, Russell DH. 2003. A high repetition rate (1 kHz) microcrystal laser for high throughput atmospheric pressure maldi-quadrupole-time-of-flight mass spectrometry. Anal Chem 75:648–654.

McLean JA, Stumpo KA, Russell DH. 2005. Size-selected (2–10 nm) gold nanoparticles for matrix assisted laser desorption ionization of peptides. J Am Chem Soc 127:5304–5305.

McMahon JM, Dookeran NN, Todd PJ. 1995. Organic ion imaging beyond the limit of static secondary ion mass spectrometry. J Am Soc Mass Spectrom 6:1047–1058.

McMahon JM, Short RT, McCandlish CA, Brenna JT, Todd PJ. 1996. Identification and mapping of phosphocholine in animal tissue by static secondary ion mass spectrometry and tandem mass spectrometry. Rapid Commun Mass Spectrom 10:335–340.

Medzihradszky KF, Campbell JM, Baldwin MA, Falick AM, Juhasz P, Vestal ML, Burlingame AL. 2000. The characteristics of peptide collision-induced dissociation using a high-performance MALDI-TOF/TOF tandem mass spectrometer. Anal Chem 72:552–558.

Monroe EB, Jurchen JC, Lee J, Rubakhin SS, Sweedler JV. 2005. Vitamin E Imaging and Localization in the Neuronal Membrane. J Am Chem Soc 127.

Muramoto T, Tamamura Y. 2002. MD Simulation of cluster ejection due to sputtering by polyatomic projectiles. Appl Surf Sci 9221:1–5.

Murayama Y, Komatsu M, Hashimoto H. 2005. SIMSXV.

Nakagawa Y, Hatanaka H. 1997. Boron neutron capture therapy: Clinical brain tumor studies. J Neuro-Oncol 33:105–115.

Navratil M, Mabbott GA, Arriaga EA. 2006. Chemical microscopy applied to biological systems. Anal Chem 78:4005–4020.

Nedelkov D, Tubbs KA, Niederkofler EE, Kiernan UA, Nelson RW. 2004. High-throughput comprehensive analysis of human plasma proteins: A step toward population proteomics. Anal Chem 76:1733–1737.

Nelson RW, Nedelkov D, Tubbs KA, Kiernan UA. 2004. Quantitative mass spectrometric immunoassay of insulin like growth factor 1. J Proteome Res 3:851–855.

Nguyen TC, Ward DW, Townes JA, White AK, Krantzman KD. 2000. A theoretical investigation of the yield-to-damage enhancement with polyatomic projectiles in organic SIMS. J Phys Chem B 107:8221–8228.

Nicola AJ, Muddiman DC, Hercules DM. 1996. Enhancement of ion intensity in time-of-flight secondary-ionization mass spectrometry. J Am Soc Mass Spectrom 7:467–472.

Novikov A, Caroff M, Della-Negra S, Lebeyec Y, Pautrat M, Schultz JA, Tempez A, Wang H-YJ, Jackson SN, Woods AS. 2004. Matrix-implanted laser desorption/ionization mass spectrometry. Anal Chem 76:7288–7293.

Nygren H, Malmberg P, Kriegeskotte C, Arlinghaus HF. 2004. Bioimaging TOF-SIMS: Localization of cholesterol in rat kidney sections. FEBS Lett 566:291–293.

Ostrowski SG, Van Bell CT, Winograd N, Ewing AG. 2004. Mass spectrometric imaging of highly curved membranes during tetrahymena mating. Science 305:71–73.

Paša-Tolić L, Jensen PK, Anderson GA, Lipton MS, Peden KK, Martinović S, Tolić N, Bruce JE, Smith RD. 1999. High throughput proteome-wide precision measurements of protein expression using mass spectrometry. J Am Chem Soc 121:7949–7950.

Phizicky E, Bastiaens PIH, Zhu H, Snyder M, Fields S. 2003. Protein analysis on a proteomic scale. Nature 422:208–215.

Pierson J, Norris JL, Aerni H-R, Svenningsson P, Caprioli RM, Andrén PE. 2004. Molecular profiling of experimental Parkinson's disease: Direct analysis of peptides and proteins on brain tissue sections by MALDI mass spectrometry. J Proteome Res 3:289–295.

Pollak C, Stubbings T, Hutter H. 2001. Differential image distortion correction. Microsc Microanal 7:335–340.

Postawa Z, Czerwinski B, Szewczyk M, Smiley EJ, Winograd N, Garrison BJ. 2003. Enhancement of sputtering yields due to $C_{60}$ versus Ga bombardment of Ag{111} as explored by molecular dynamics simulations. Anal Chem 75:4402–4407.

Postawa Z, Czerwinski B, Szewczyk M, Smiley EJ, Winograd N, Garrison BJ. 2004. Microscopic insights into the sputtering of Ag{111} induced by $C_{60}$ and Ga bombardment. J Phys Chem B 108:7831–7838.

Pritchard LE, Turnbull AV, White A. 2002. Pro-opiomelanocortin processing in the hypothalamus: Impact on melanocortin signalling and obesity. J Endocrinol 172:411–421.

Puglielli L, Tanzi RE, Kovacs DM. 2003. Alzheimer's disease: The cholesterol connection. Nature Neurosci 6:345–351.

Reuter W. 1987. Secondary ion emission from metal targets under $CF_3^+$ and $O_2^+$ bombardment. Anal Chem 59:2081–2087.

Reyzer ML, Hsieh Y, Ng K, Korfmacher WA, Caprioli RM. 2003. Direct analysis of drug candidates in tissue by matrix-assisted laser desorption/ionization mass spectrometry. J Mass Spectrom 38:1081–1092.

Rickman RD, Verkhoturov SV, Schweikert EA. 2004. Cluster secondary ion mass spectrometry: An insight into ''super-efficient'' collision cascades. Appl Surf Sci 231-232:54–58.

Roddy TP, Cannon DM Jr, Ostrowski SG, Ewing AG, Winograd N. 2003. Proton transfer in time-of-flight secondary ion mass spectrometry studies of frozen-hydrated dipalmitoylphosphatidylcholine. Anal Chem 75:4087–4094.

Rohner TC, Staab D, Stoeckli M. 2004. MALDI mass spectrometric imaging biological tissue sections. Mech Ageing Dev 126:177–185.

Rol PK, Fluit JM, Kistemaker J. 1960. Sputtering of Copper by bombardment with ions of 5–25 KeV. Physica 26:1000–1008.

Rubakhin SS, Greenough WT, Sweedler JV. 2003. Spatial profiling with MALDI MS: Distribution of neuropeptides within single neurons. Anal Chem 75:5374–5380.

Schaaff TG, McMahon JM, Todd PJ. 2002. Semiautomated analytical image correlation. Anal Chem 74:4361–4369.

Schenkel T, Hamza AV, Barnes AV, Newman MW, Machicoane G, Niedermayer T, Hattass M, McDonald JW, Schneider DH, Wu KJ, Odom RJ. 1999. Surface analysis by highly charged ion based secondary ion mass spectrometry. Physica Scripta T80:73–75.

Scherl A, Zimmermann-Ivol CG, Di Dio J, Vaezzadeh AR, Binz P-A, Amez-Droz M, Cochard R, Sanchez J-C, Glückmann M, Hochstrasser DF. 2005. Gold coating of non-conductive membranes before matrix-assisted laser desorption/ionization tandem mass spectrometric analysis prevents charging effect. Rapid Commun Mass Spectrom 19:605–610.

Schriver KE, Chaurand P, Caprioli RM. 2003. High resolution imaging mass spectrometry: Characterization of ion yields and spot sizes. 51st ASMS Conference on Mass Spectrometry and Allied Topics, Montreal, Canada. Sci 231-232:485-489.

Schueler BW. 1992. Microscope imaging by time-of-flight secondary ion mass spectrometry. Microsc Microanal Microstruct 3:119–139.

Schueler B, Sander P, Reed DA. 1990. A time-of-flight secondary ion microscope. Vacuum 41:1661–1664.

Schwartz SA, Reyzer ML, Caprioli RM. 2003. Direct tissue analysis using matrix-assisted laser desorption/ionization mass spectrometry: Practical aspects of sample preparation. J Mass Spectrom 38:699–708.

Schweikert EA, van Stipdonk MJ, Harris RD. 1996. A comparison of desorption yields from $C_{60}^{+}$ to atomic and polyatomic projectiles at keV energies. Rapid Commun Mass Spectrom 10:1987–1991.

Sherrod SD, McLean JA, Russell DH. 2004. Advanced optics for imaging mass spectrometry using MALDI-TOFMS. 52nd ASMS conference on mass spectrometry and allied topics, Nashville, Tennessee.

Shimma S, Furuta M, Ichimura K, Yoshida Y, Setou M. 2006. A novel approach to in situ proteome analysis using chemical inkjet printing technology and MALDI-QIT-TOF tandem mass spectrometer. J Mass Spectrom Soc Jpn 54:2006.

Simpson JC, Wellenreuther R, Poustka A, Pepperkok R, Wiemann S. 2000. Systematic subcellular localization of novel proteins identified by large-scale cDNA sequencing. EMBO Reports 1:287–292.

Sinha TK, Luci JJ, Shahidi SK, Dawant BM, Gore JC, Cornett DS. 2006. 54th ASMS Conference on Mass Spectrometry and Allied Topics, Seattle, WA.

Sjövall P, Lausmaa J, Nygren H, Carlsson L, Malmberg P. 2003. Imaging of membrane lipids in single cells by imprint-imaging time-of-flight secondary ion mass spectrometry. Anal Chem 75:3429–3434.

Sjövall P, Lausmaa J, Johansson B. 2004. Mass spectrometric imaging of lipids in brain tissue. Anal Chem 76:4271–4278.

Sjövall P, Johansson B, Lausmaa J. 2006. Localization of lipids in freeze-dried mouse brain sections by imaging TOF-SIMS. Appl Surf Sci 252:6966–6974.

Slodzian G, Daigne B, Girard F, Boust F, Hillion F. 1992. Scanning secondary ion analytical microscopy with parallel detection. Biol Cell 74:43–50.

Smith RD. 2000. Evolution of ESI-mass spectrometry and Fourier transform ion cyclotron resonance for proteomics and other biological applications. Int J Mass Spectrom 200:509–544.

Smith DR, Chandra S, Barth RF, Yang W, Joel DD, Coderre JA. 2001. Quantitative imaging and microlocalization of boron-10 in brain tumors and infiltrating tumor cells by SIMS ion microscopy: Relevance to neutron capture therapy. Cancer Res 61:8179–8187.

Sostarecz AG, McQuaw CM, Ewing AG, Winograd N. 2004. Phosphatidylethanolamine-induced cholesterol domains chemically identified with mass spectrometric imaging. J Am Chem Soc 126:13882–13883.

Spengler B, Hubert M. 2002. Scanning microprobe matrix-assisted laser desorption ionization (SMALDI) mass spectrometry—Instrumentation for sub-micrometer resolved LDI and MALDI surface analysis. J Am Soc Mass Spectrom 13:735–748.

Spengler B, Kirsch D. 2003. On the formation of initial velocities in matrix-assisted laser desorption ionization: Virtual desorption time as an additional parameter describing ion ejection dynamics. Int J Mass Spectrom 226:71–83.

Stoeckli M, Farmer TB, Caprioli RB. 1999. Automated mass spectrometry imaging with a matrix-assisted laser desorption ionization time-of-flight instrument. J Am Soc Mass Spectrom 10:67–71.

Stoeckli M, Chaurand P, Hallahan DE, Caprioli RM. 2001. Imaging mass spectrometry: A new technology for the analysis of of protein expression in mammalian tissues. Nature Medicine 7:493–496.

Strick R, Strissel PL, Gavrilov K, Levi-Setti R. 2001. Cation–chromatin binding as shown by ion microscopy is essential for the structural integrity of chromosomes. J Cell Biol 155:899–910.

Strissel PL, Strick R, Gavrilov KL, Levi-Setti R. 2005. Specific $Mg^{2+}$ binding at human and Indian muntjac chromosomal Giemsa bands. Appl Surf Sci 231-232:485–489.

Svensson M, Sköld K, Svenningsson P, Andren PE. 2003. Peptidomics-based discovery of novel neuropeptides. J Proteome Res 2:213–219.

Sze SK, Ge Y, Oh H, McLafferty FW. 2002. Top-down mass spectrometry of a 29-kDa protein for characterization of any posttranslational modification to within one residue. Proc Natl Acad Sci U.S.A 99:1774–1779.

Szymczak W, Wittmaack K. 1994. Evidence for strongly enhanced yields of negative molecular secondary ions due to bombardment with $SF_n$ cluster ions. Nucl Instr Meth Phys Res B 88:149–153.

Taban IM, Altelaar AFM, Fuchser J, van der Burgt YEM, McDonnell LA, Baykut G, Heeren RMA. 2006. Imaging of peptides in the rat brain using MALDI-FTICR mass spectrometry. J Am Soc Mass Spectrom 18:145–151.

Takaya K, Okabe M, Sawataishi M, Takashima H, Yoshida T. 2002. Fine structures and ion images on fresh frozen ultrathin sections by transmission electron and scanning ion microscopy. Appl Surf Sci 203–204:684–688.

Tempez A, Schultz JA, Della-Negra S, Depauw J, Jacquet D, Novikov A, Lebeyec Y, Pautrat M, Caroff M, Ugarov M, Bensaoula H, Gonin M, Fuhrer K, Woods A. 2004. Orthogonal time-of-flight secondary ion mass spectrometric analysis of peptides using large gold clusters as primary ions. Rapid Commun Mass Spectrom 18:371–376.

Tempez A, Ugarov M, Egan T, Schultz JA, Novikov A, Della-Negra S, Lebeyec Y, Pautrat M, Caroff M, Smentkowski VS, Wang H-YJ, Jackson SN, Woods AS. 2005. Matrix implanted laser desorption ionization (MILDI) combined with ion mobility-mass spectrometry for bio-surface analysis. J Proteome Res 4:540–545.

Thompson DA, Johar SS. 1979. Nonlinear sputtering effects in thin metal films. Appl Phys Lett 34:342–345.

Todd PJ, Schaaff TG. 2002. A secondary ion microprobe ion trap mass spectrometer. J Am Soc Mass Spectrom 13:1099–1107.

Todd PJ, Short RT, Grimm CC, Holland WM, Markey SP. 1992. Organic ion imaging using tandem mass spectrometry. Anal Chem 64:1871–1878.

Todd PJ, Schaaff TG, Chaurand P, Caprioli RM. 2001. Organic ion imaging of biological tissue with secondary ion mass spectrometry and matrix-assisted laser desorption/ionization. J Mass Spectrom 36:355–369.

Touboul D, Halgand F, Brunelle A, Kersting R, Tallarek E, Hagenhoff B, Laprévote O. 2004a. Tissue molecular ion imaging by gold cluster ion bombardment. Anal Chem 76:1550–1559.

Touboul D, Piednoël H, Voisin V, Porte SDL, Brunelle A, Halgand F, Laprévote O. 2004b. Changes in phospholipid composition within the dystrophic muscle by matrix-assisted laser desorption/ionization mass spectrometry and mass spectrometry imaging. Eur J Mass Spectrom 10:657–664.

Touboul D, Kollmer F, Niehuis E, Brunelle A, Laprévote O. 2005. Improvement of biological time-of-flight secondary ion mass spectrometry imaging with bismuth cluster ion source. J Am Soc Mass Spectrom 16:1608–1618.

Touboul D, Brunelle A, Laprévote O. 2006. Structural analysis of secondary ions by post-source decay in time-of-flight secondary ion mass spectrometry. Rapid Comm Mass Spectrom 20:703–709.

Townes JA, White AK, Wiggins EN, Krantzman KD, Garrison BJ, Winograd N. 1999. Mechanism for increased yield with $SF_5^+$ projectiles in organic SIMS: The substrate effect. J Phys Chem A 103:4587–4589.

Tyler BJ. 2001. ToF-SIMS image analysis. In: Vickerman JC, Briggs D, editors. ToF-SIMS: Surface analysis by mass spectrometry. Chichester: IM Publications. pp 475–493.

Tyler BJ. 2006. Multivariate statistical image processing for molecular specific imaging in organic and bio-systems. Appl Surf Sci 252:6875–6882.

Urbassek HM. 2001. Status of cascade theory. In: Vickerman JC, Briggs D, editors. ToF-SIMS: Surface analysis by mass spectrometry. Chichester: IM Publications. pp 139–160.

van Stipdonk MJ, Santiago V, Schweikert EA. 1999. Negative secondary ion emission from $NaBF_4$: Comparison of atomic and polyatomic projectiles at different impact energies. J Mass Spectrom 34:554–562.

van Vaeck L, Adriaens A, Gijbels R. 1999. Static secondary ion mass spectrometry: (S-SIMS) Part 1. Methodology and structural interpretation. Mass Spectom Rev 18:1–47.

Vertes A, Luo G, Ye L, Chen Y, Marginean I. 2004. Laser pulse length dependence of internal energy transfer in UV-MALDI-MS. Appl Phys A 79:823–825.

Veryovkin IV, Calaway WF, Moore JF, Pellin MJ, Burnett DS. 2004. A new time-of-flight instrument for quantitative surface analysis. Nucl Instr Meth Phys Res B 219-220:473–479.

Vestal ML, Juhasz P, Martin SA. 1995. Delayed extraction matrix-assisted laser desorption time-of-flight mass spectrometry. Rapid Commun Mass Spectrom 9:1044.

Vickerman JC. 2001. ToF-SIMS—An overview. In: Vickerman JC, Briggs D, editors. ToF-SIMS: Surface analysis by mass spectrometry. Chichester: IM Publications. pp 1–40.

Vickerman JC, Briggs D. 2001. ToF-SIMS: Surface analysis by mass spectrometry. Chichester: IM Publications.

Vickerman JC, Brown A, Reed NM. 1989. Secondary ion mass spectrometry. Oxford, New York: Oxford University Press.

Vickerman JC, Briggs D, Henderson A. 2002. The Static SIMS Library: Surface Spectra.

Videler H, Ilag LL, McKay ARC, Hanson CL, Robinson CV. 2005. Mass spectrometry of intact ribosomes. FEBS Lett 579:943–947.

Wagner MS. 2005. Molecular depth profiling of multilayer polymer films using time-of-flight secondary ion mass spectrometry. Anal Chem 77:911–922.

Wagner MS, Tyler BJ, Castner DG. 2002. Interpretation of static time-of-flight secondary ion mass spectra of adsorbed protein films by multivariate pattern recognition. Anal Chem 74:1824–1835.

Wagner MS, Graham DJ, Ratner BD, Castner DG. 2004. Maximizing information obtained from secondary ion mass spectra of organic thin films using multivariate analysis. Surf Sci 570:78–97.

Wagter ML, Clarke AH, Taylor KF, van der Heide PAW, McIntyre NS. 1997. Topographic correction of 3D SIMS images. Surf Interface Anal 25:788–789.

Wang T-CL, Cornio LJ, Markey SP. 1996. Liquid chromatography particle beam-mass spectrometry with massive cluster impact. J Am Soc Mass Spectrom 7:293–297.

Weibel D, Wong S, Lockyer N, Blenkinsopp P, Hill R, Vickerman JC. 2003. A $C_{60}$ primary ion beam system for time of flight secondary ion mass spectrometry: Its development and secondary ion yield characteristics. Anal Chem 75:1754–1764.

Weickhardt C, Moritz F, Grotemeyer J. 1996. Time-of-flight mass spectrometry: State-of-the-art in chemical analysis and molecular science. Mass Spectom Rev 15:139–162.

Weissleder R. 2006. Molecular imaging in cancer. Science 312:1168.

Wickes BT, Kim Y, Castner DG. 2003. Denoising and multivariate analysis of time-of-flight SIMS images. Surf Interface Anal 35:640–648.

Wittmaack K. 1979. Secondary-ion emission from silicon bombarded with atomic and molecular noble-gas ions. Surf Sci 90:557–563.

Wittmaack K. 2000a. Influence of the depth calibration procedure on the apparent shift of impurity depth profiles measured under conditions of long-term changes in erosion rate. J Vac Sci Technol B 18:1–6.

Wittmaack K, Szymczak W, Hoheisel G, Tuszynski W. 2000b. Time-of-flight secondary ion mass spectrometry of matrix-diluted oligon- and polypeptides bombarded with slow and fast projectiles: Positive and negative matrix and analyte ion yeilds, background signals, and sample aging. J Am Soc Mass Spectrom 11:553–563.

Wong SCC, Hill R, Blenkinsopp P, Lockyer NP, Weibel DE, Vickerman JC. 2003. Development of a $C_{60}^+$ ion gun for static SIMS and chemical imaging. Appl Surf Sci 203:219–222.

Wu KJ, Odom RW. 1996. Matrix-enhanced secondary ion mass spectrometry: A method for molecular analysis of solid surfaces. Anal Chem 68:873–882.

Wucher A. 2001. Laser post-ionisation: Fundamentals In: Vickerman JC, Briggs D, editors. ToF-SIMS: Surface analysis by mass spectrometry. Chichester: IM Publications. pp 347–373.

Wucher A, Sun S, Szakal C, Winograd N. 2004. Molecular depth profiling of histamine in ice using a buckminsterfullerene probe. Anal Chem 76:7234–7242.

Xu J, Szakal CW, Martin SE, Peterson BR, Winograd AW. 2004. Molecule-specific imaging with mass spectrometry and a buckminsterfullerene probe: Application to characterizing solid-phase synthesized combinatorial libraries. J Am Chem Soc 126:3902–3909.

Yamada I, Matsuo J, Toyoda N, Kirkpatrick A. 2001. Materials processing by gas cluster ion beams. Mat Sci Eng R 34:231–295.

Yanagisawa K, Shyr Y, Xu BJ, Massion PP, Larsen PH, White BC, Roberts JR, Edgerton M, Gonzalez A, Nadaf S, Moore JH, Caprioli RM, Carbone DP. 2003. Proteomic patterns of tumour subsets in non-small-cell lung cancer. The Lancet 362:433–439.

Zenobi R, Knochenmuss R. 1998. Ion formation in MALDI mass spectrometry. Mass Spectom Rev 17:337–366.

Zhang J, Campell RE, Ting AY, Tsien RY. 2002. Creating new flourescent probes for cell biology. Nature Rev 3:906–918.

Zhigilei LV, Garrison BJ. 2000. Microscopic mechanisms of laser ablation of organic solids in the thermal and stress confinement irradiation regimes. J Appl Phys 88:1281–1298.

Zhigilei LV, Leveugle E, Garrison BJ, Yingling YG, Zeifman MI. 2003a. Computer simulations of laser ablation of molecular substrates. Chem Rev 103:321–347.

Zhigilei LV, Yingling YG, Itina TE, Schoolcraft TA, Garrison BJ. 2003b. Molecular dynamics simulations of matrix-assisted laser desorption—Connections to experiment. Int J Mass Spectrom 226:85–106.

**Liam A. McDonnell** received his MCHEM from the University of Oxford, UK in 1997 and his Ph.D. in chemistry from the University of Warwick in 2001. His Ph.D. included aspects of reaction dynamics utilizing ion-imaging techniques but concentrated mostly on developing high-resolution, accurate mass capabilities for the characterization of complex polymeric systems. In 2002, he moved to the FOM Institute for Atomic and Molecular Physics where his major research area has been developing macromolecular desorption/ionization techniques and spatially resolved mass analyzers for fast, high mass, high sensitivity, high spatial resolution imaging mass spectrometry of biological systems. This has been complemented by continued research into fundamentals of desorption, ionization, and fragmentation of macromolecular ions.

**Ron M.A. Heeren** obtained a Ph.D. degree in technical physics in 1992 at the University of Amsterdam on plasma-surface interaction. After 2 years of post-doctoral work on FTICR mass spectrometry, he joined the MOLART research team at the FOM-Institute for Atomic and Molecular Physics as a project leader, heading the instrumental developments for paint cross-section analysis in early 1995. In 1999, he started a research group focusing on macromolecular ion physics with high resolution mass spectrometry and the development of imaging mass spectrometry at AMOLF. In 2001, he was appointed professor at the chemistry faculty of Utrecht University studying the physical aspects of biomolecular mass spectrometry. He is the 2002 recipient of the Dutch MS society award for distinguished contribution to mass spectrometry. His academic research focuses on fundamental studies of the energetics of macromolecular systems, conformational studies of non-covalently bound protein complexes, and the development and validation of new mass spectrometry-based molecular imaging techniques for the life sciences.